TRANSCRIPTIONAL MECHANISMS UNDERLYING NEURONAL ACTIVITY-DEPENDENT PLASTICITY

APPROVED BY SUPERVISORY COMMITTEE

Tae-Kyung Kim, Ph.D

Kimberly Huber, Ph.D

Jane Johnson, Ph.D

Carol Tamminga, M.D.

W. Lee Kraus, Ph.D

Dedicated to my parents, Frank and Theresa Schaukowitch,

for their continual love and support through this entire process,

and all of my friends and family who have been with me along the way.

ACKNOWLEDGEMENTS

I would like to first thank my mentor, Dr. Tae-Kyung Kim, for his guidance and support during my time in graduate school. I have learned so much from him, and I am a better scientist because of it. I would also like to thank the members of my thesis committee, Drs. Kimberly Huber, Carol Tamminga, Jane Johnson, and W. Lee Kraus for their thoughtful advice, constructive criticism, and for always providing a fresh perspective on my projects.

Life in lab would definitely not be as fun if it were not for the other members of the Kim Lab, both past and present. Many thanks to you all for creating such a wonderful environment to do research, especially Dr. Xihui Liu and Dr. Jae-Yeol Joo, who I learned a lot from over the years, and who were always up for answering my questions and discussing results, good or bad.

I am infinitely grateful for the friends that I have made in Dallas, both in graduate school as well as through the volleyball group. I truly appreciate the support and balance you have given me, and will value your friendship forever. To all of my friends from California, who came out to visit or hosted a visit home, it is always great to catch up and I appreciate being able to recharge when feeling burnt out.

Finally, I want to express my absolute gratitude and love for my amazing family. I am thankful for my cousin Jessica, who has come out to visit for multiple holidays, which helped make Dallas feel like home and who always encourages me to keep going, and my sister, Naomi, for her support and friendship. I cannot describe how amazing my parents are, and I definitely would not be here if it were not for my mom and dad, Theresa and Frank Schaukowitch. Thank you for your love and support, and for being my sounding board when times were hard, and my biggest cheerleaders when things went well. Thank you for everything.

TRANSCRIPTIONAL MECHANISMS UNDERLYING NEURONAL ACTIVITY-DEPENDENT PLASTICITY

by

KATIE MARIE SCHAUKOWITCH

DISSERTATION/THESIS

Presented to the Faculty of the Graduate School of Biomedical Sciences

The University of Texas Southwestern Medical Center at Dallas

In Partial Fulfillment of the Requirements

For the Degree of

DOCTOR OF PHILOSOPHY

The University of Texas Southwestern Medical Center

Dallas, Texas

December, 2016

TRANSCRIPTIONAL MECHANISMS UNDERLYING NEURONAL ACTIVITY-DEPENDENT TRANSCRIPTION

KATIE MARIE SCHAUKOWITCH

The University of Texas Southwestern Medical Center at Dallas, 2016

SUPERVISING P.I.: TAE-KYUNG KIM, Ph.D.

Impairment in learning and memory is a well-established cognitive symptom that is manifested in many psychiatric diseases including autism and schizophrenia. Studies have shown that long-lasting memory formation is mediated by rapid changes in nuclear gene expression in response to learning-induced sensory experience. Despite these findings, there is a significant gap in our knowledge as to how sensory information is precisely translated into specific transcriptional outputs. Recently, a class of long noncoding RNAs that are transcribed bidirectionally from the enhancers of activity-dependent genes in neurons (eRNAs) has been identified. My first project studied the function of eRNAs of two immediate early genes *Activity-regulated cytoskeletal protein* (*Arc*) and *Growth arrest and DNA-damage-inducible, beta* (*Gadd45b)*, which have been implicated in mediating synaptic plasticity. Using a knockdown

approach, we found that eRNAs are necessary for the full induction of their target genes in response to membrane depolarization. eRNAs specifically regulate the early elongation stage of transcription by allowing for efficient release of paused RNA polymerase II (RNAPII) from the promoters of activity-regulated genes. Knockdown of eRNAs results in the retention of an RNAPII pausing factor, Negative Elongation Factor (NELF), at the target gene promoter. eRNAs directly bind to NELF during stimulated conditions, suggesting that eRNAs interact with NELF to facilitate its release from the promoter, thus resulting in efficient and precisely timed gene activation. These data define a new role for the spatiotemporally controlled expression of regulatory RNAs in the experience-dependent gene expression network. My second project aimed to identify the transcriptional program activated when activity levels are suppressed. Homeostatic scaling allows neurons to maintain stable activity patterns by globally altering their synaptic strength in response to changing activity levels. Decreasing activity leads to an upregulation in synaptic strength, as seen by increases in AMPA mediated mEPSCs. It was previously shown that the increase in mEPSC amplitude could be blocked by a transcription inhibitor, suggesting that transcription is necessary for the scaling response. However, little is known about the genes directly regulated by activity suppression or the signaling mechanisms underlying the transcriptional control. Using RNA-Seq, we identified nearly 100 genes that were specifically upregulated in response to activity suppression. *Neuronal pentraxin-1* (*Nptx1*), previously shown to promote AMPAR clustering, was increased ~3 fold, and knockdown of this gene blocked the increase in mEPSC amplitudes. SRF is a key transcription factor in regulating *Nptx1* induction, which is calcium-dependent, indicating the existence of an active pathway to control transcription. Taken together, this study defines a novel transcriptional program that is able to sense the absence of activity and coordinate the global increase in synaptic strength.

TABLE OF CONTENTS

PRIOR PUBLICATIONS

1. **Schaukowitch, K.***, Reese, A.L.*, Kim, S.-K., Kilaru, G., Joo, J.-Y., Kavalali, E.T., Kim, T.-K. Ca2+ channel activity at rest drives a transcriptional program underlying synaptic scaling. (Manuscript in preparation) *equal contribution

2. Joo, J.-Y., **Schaukowitch, K.**, Farbiak, L., Kilaru, G., Kim, T.-K. Stimulus-specific combinatorial functionality of neuronal c-fos enhancers. *Nature Neuroscience* 19, 75-83 (2016).

3. **Schaukowitch, K.***, Joo, J.-Y.*, Liu, X., Watts., J.K., Martinez, C., Kim, T.-K. Enhancer RNA Facilitates NELF Release from Immediate Early Genes. *Molecular Cell* 56, 29-42 (2014). *equal contribution

4. **Schaukowitch, K.**, Kim, T.-K. Emerging epigenetic mechanisms of long-noncoding RNAs. Neuroscience 264, 25-38 (2014).

5. Zhou, X., Chen, Q., **Schaukowitch, K.**, Kelsoe, JR, Geyer, MA. Insoluble DISC1-Boymaw Fusion Proteins Generated by the DISC1 Translocation. Molecular Psychiatry 15, 670-672 (2010).

LIST OF FIGURES AND TABLES

LIST OF ABBREVIATIONS

ActD - Actinomycin D

Airn – Antisense to Igf2r RNA noncoding

AMPAR - α-amino-3-hydroxy-5-methyl-4-isoxazolepropionic acid receptor

Arc – Activity-regulated cytoskeletal protein

CaMK – calcium calmodulin kinase

CBP – CREB binding protein

CDK9 – cyclin dependent kinase 9

c-*fos* - FBJ osteosarcoma oncogene

CRE – cyclic AMP responsive element

CREB – CRE binding protein

CTCF – CCCTC-binding factor

Egr1 – Early growth response 1

ELK1 –Ets transcription factor 1

eRNA - enhancer RNA

Gadd45b – growth arrest and DNA damage inducible beta

H3K4me1/3 – histone H3 lysine 4 mono- or tri-methylated

IEG – immediate early gene

Igf2r – insulin-like growth factor 2 receptor

KCl – potassium chloride

lncRNA - long noncoding RNAs

LTD - Long-term depression

LTP - Long-term potentiaion

MeCP2 – methylated CpG binding protein 2

MEF2 – Myocyte enhancer factor 2

mRNA – messenger RNA

NELF – Negative Elongation Factor

NMDAR - *N*-methyl-D-aspartate receptor

PRC2 – polycomb repressive complex 2

p-TEFb – positive transcription elongation factor b

RNAPII – RNA polymerase II

RNA-Seq – RNA sequencing

Slc22a3 – solute carrier family 22 member 3

Slc22a2 – solute carrier family 22 member 2

SRF – Serum Response Factor

Tsix – *Xist*, opposite strand

TTX - Tetrodotoxin

VGCC – voltage gated calcium channel

XCI - X chromosome inactivation

Xic - X inactivation center

Xist – X inactive specific transcript

CHAPTER 1

Introduction

Neurons within the brain are responsible for processing sensory information and using this information to respond to the environment in an appropriate manner. This is critical for proper circuit formation during development, and throughout life, information can be stored in the brain through learning and memory behaviors, which allow an organism to make decisions based on past experiences. Different patterns of neuronal activity are able to encode information by making long lasting changes in synaptic strength, and these changes represent the synaptic plasticity that is thought to be the molecular correlate of learning and memory. Two common forms of synaptic plasticity are long-term potentiation (LTP) and long-term depression (LTD), where synaptic strength is either stably increased or decreased, respectively (Bear and Malenka, 1994; Luscher and Malenka, 2012).

Activity patterns encoding information are communicated between neurons, leading to the activation of specific gene programs that encode the information (Lyons and West, 2011). Upon synaptic activity, a first, rapid wave of transcription is induced, including immediate early genes (IEGs) such as *Actvity-regulated cytoskeletal protein* (*Arc*) and *FBJ osteosarcoma oncogene* (c-*Fos*), which are then responsible for coordinating the cell's actions to stabilize any resulting changes in synaptic strength. The regulation of these genes is tightly controlled, maintaining low levels under basal conditions, but allowing for rapid, robust induction upon activity. It has been shown that this transcription is necessary for the late stages of LTP as well as long-term memory formation (Kandel, 2001). Early studies identified many mRNAs that were induced in response to neuronal activity, for example, through seizure induction (Cole et al., 1990; Hevroni et al., 1998; Nedivi et al., 1993), and with the recent advances in genome-wide

sequencing, many more genes that are induced in response to depolarization with 55 mM KCl have been identified (Kim et al., 2010).

Many studies have aimed to dissect the upstream pathways that link synaptic activity to nuclear gene transcription. In response to the activation of postsynaptic receptors by the release of excitatory neurotransmitters such as glutamate, there is a depolarization of the postsynaptic neuron and an influx of Ca^{2+}, mainly through the NMDA receptor (NMDAR) or L-type voltage gated calcium channel (VGCC) (Dolmetsch et al., 2001). Ca^{2+} can act as a second messenger to activate Ca^{2+}/Calmodulin-dependent kinases (CaMKs), found at the synapse, which initiate signaling cascades of additional kinases, such as CaMKII or CaMKIV (Bading et al., 1993). These molecules are then responsible for transmitting the electrical stimulus at the synapse to the nucleus, oftentimes by phosphorylating transcription factors such as cAMP responsive element binding protein (CREB), Serum Response Factor (SRF), or Myocyte enhancing factor 2 (MEF2) (Figure 1.1) (Deisseroth et al., 1996). Specifically, phospohorylation of CREB at Serine 133 (Ser133) has been shown to facilitate association of CREB with the transcriptional co-activators, CREB binding protein (CBP) and p300, both of which have histone aceytltransferase (HAT) activity, resulting in transcriptional activation (Chrivia et al., 1993). SRF is necessary for synaptic plasticity in the hippocampus, and without SRF there is impaired induction of neuronal IEGs (Ramanan et al., 2005). While many genes have SRF prebound to their promoters, even under activity-suppressed conditions, SRF-dependent transcription seems to be regulated in part though the action of two families of co-factors, the Ternary complex factors (TCFs) and Myocardin related transcription factors (MRTFs) (Knoll and Nordheim, 2009). MEF2 is another transcription factor that has been implicated in the activity-dependent elimination of synapses

(Flavell et al., 2006), and can act as both an activator and repressor based on its interaction partners and phosphorylation status.

In addition to regulating the activity of transcription factors in response to neuronal stimuli, the accessibility of the chromatin surrounding the genes appears to play an important role in determining whether a gene is actively transcribed. DNA within the nucleus is wrapped tightly around proteins called histones, which have N-terminal tails that can undergo extensive posttranslational modifications, such as methylation (me) and acetylation (Ac). Specific modifications have been correlated with specific transcriptional states of genes (Strahl and Allis, 2000). For example, active gene promoters are associated with high levels of histone 3 trimethylated at lysine 4 (H3K4me3), while enhancer regions are associated with high levels of H3K4me1 and H3K27Ac and low levels of H3K4me3 (Heintzman et al., 2007). Repressed genes, on the other hand, display H3K27me3. It is thought that these modifications can affect how open or compact the chromatin is, which in turn regulates how accessible the DNA sequence is to specific transcription factors or RNA polymerase II (RNAPII) and the transcription machinery. Although many of these marks become established during development, it has also been shown that they can be inducible (Kaikkonen et al., 2013), and in particular, neurons depolarized with KCl showed dynamic activity-dependent changes in H3K27Ac (Malik et al., 2014).

While many studies have analyzed the mechanisms neurons use to dynamically regulate transcription in response to neuronal activity, neurons are also able to adapt to the absence of activity. Chronic periods of both activity and inactivity, lead to global changes in synaptic strength in a phenomenon called homeostatic plasticity (Turrigiano et al., 1998). In response to low activity levels, which can be modeled in culture using a sodium channel blocker tetrodotoxin (TTX) that blocks all of the action potentials within the culture, neurons increase their synaptic

strength. In the opposing way, in response to chronic high activity levels, neurons will decrease their synaptic strength. This allows neurons to maintain their own stable firing patterns, as well as stable activity levels within the network. This process is also thought to be critical for learning and memory, as this is a global mechanism that scales all the synapses multiplicatively, i.e. all increasing by two-fold. In this way, the relative weights of synaptic strength, that have been established by processes such as LTP and LTD, will be maintained, along with the information that those weights encoded. Deficits in scaling have also been identified in models of neuropsychiatric disorders such as autism and schizophrenia (Wondolowski and Dickman, 2013), suggesting that the tight control of network activity is crucial for proper neuronal function. Many studies have focused on the signal mechanisms regulating local translational control in this process, but a recent study found that activity-suppression induced scaling was sensitive to the transcription blocker, Actinomycin D (ActD) (Ibata et al., 2008), suggesting that there might be a specific transcriptional program that is activated in response to an absence of activity.

My studies have aimed to understand two specific mechanisms of regulating activity-dependent transcription, one in response to neuronal activity, and the other when activity is suppressed. My first project studied the role of a recently identified class of long noncoding RNAs (lncRNAs) expressed from the enhancers of activity-induced genes (eRNAs) in target gene induction in one case. In the second, I aimed to identify the specific gene set that was activated in response to activity-suppression, and understand the molecular components that actively transmitted the signal from the synapse to the nucleus to regulate gene transcription.

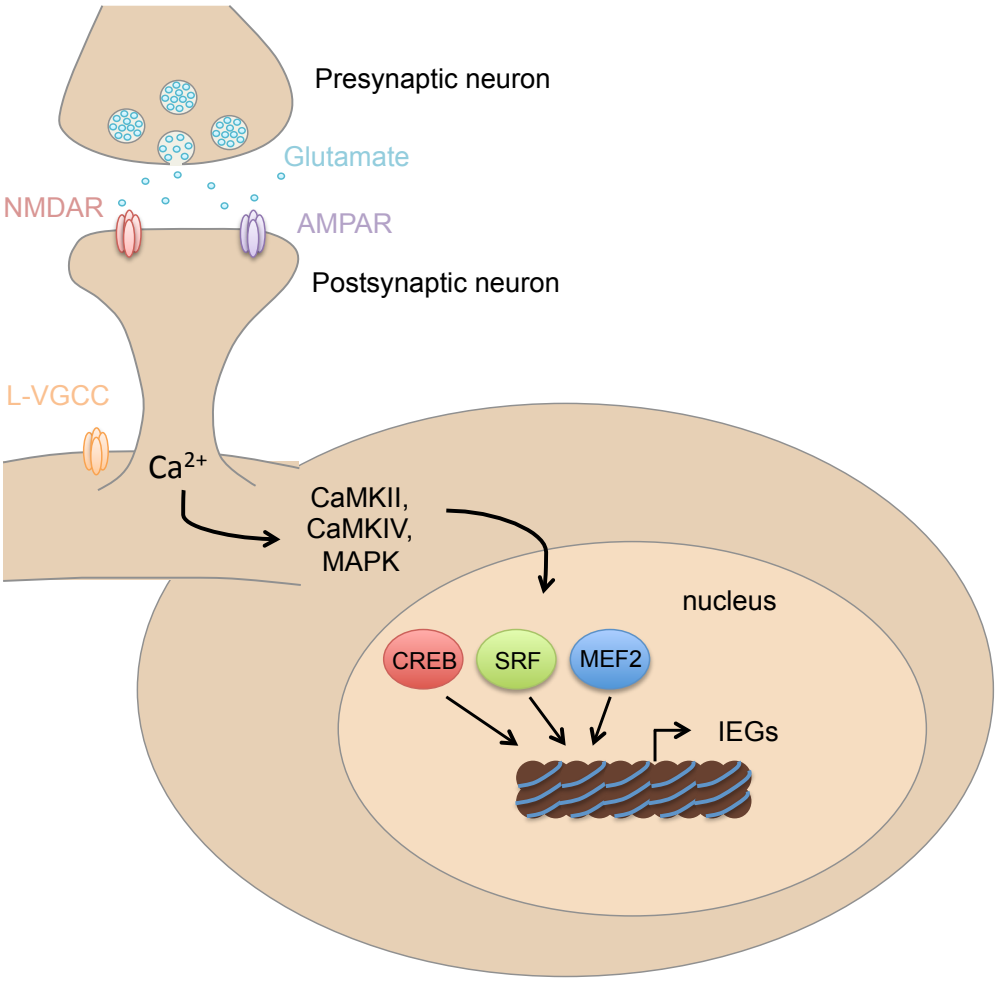

Figure 1.1 Neuronal activity upregulates immediate early genes. In response to an action potential at an excitatory synapse, the presynaptic neuron releases neurotransmitter such as glutamate, which activates postsynaptic receptors such as AMPA and NMDA receptors. In response to depolarization by AMPARs, Ca^{2+} enters the cell through NMDARs and L-VGCCs and activates signaling pathways that regulate the function of transcription factors such as CREB, SRF, and MEF2. A subset of genes, such as *Arc*, *c-fos*, and *Gadd45b*, are then induced, and are responsible for coordinating the cell's response to the stimulus, i.e. increasing synaptic strength during LTP.

CHAPTER 2

A role for eRNAs in regulating activity-dependent gene expression

2.1 Introduction

2.1.1 Enhancers express lncRNAs

In addition to the promoter region, many genes are regulated by enhancer regions, which are *cis* regulatory regions that act in an orientation- and distance-independent manner to influence gene expression in addition to the promoter alone. Enhancers tend to be cell-type and developmental stage-specific, ensuring that genes are only turned on in the right cell at the right time. These regions have been identified by specific chromatin signatures, including high levels of H3K27Ac, as well as high H3K4me1 and low H3K4me3. It had been known that enhancers contained binding sites for transcription factors and co-activators, such as CBP or p300, but it was recently shown, on a genome-wide scale, that enhancers could also recruit RNAPII and transcribe, in a bidirectional manner, lncRNAs, termed enhancers RNAs (eRNAs) (De Santa et al., 2010; Kim et al., 2010). In neurons depolarized with KCl, there were ~2000 enhancers identified that induced eRNA expression, and when compared to nearby protein coding genes, the induction of the eRNA was well correlated with the induction of the nearby mRNA (Kim et al., 2010), suggesting a potential regulatory function. Since their initial identification, eRNAs have been found in many different cell types, across species, suggesting this is a conserved feature of enhancers, and in fact eRNAs have been shown to be the most reliable marker of an active enhancer within a cell type (Wang et al., 2011a).

While eRNAs appear to be a common feature of active enhancers, their biological function within the cell is still an open question. It is possible that due to the chromosomal looping that occurs between promoters and enhancers, RNAPII could bind to the enhancers and

begin transcribing RNA from the adjacent regions, but this is simply spurious transcription and not functional. A second possibility could be that transcription *per se* through those regions is important for the activity of the enhancer, by establishing or maintaining an active chromosome conformation or maintaining the active histone modifications. Evidence for this has been provided in macrophages, where they showed that blocking transcription with transcription inhibitors reduced the levels of histone modifications such as H3K4me1/2 at induced enhancers (Kaikkonen et al., 2013). A third possibility, which is not mutually exclusive from the second scenario, would be that the transcripts themselves would have a function. A functional role for eRNAs has been demonstrated in certain cell types, such as human cancer cells (MCF-7), mouse macrophages, and mouse skeletal muscle cells (Lam et al., 2013; Li et al., 2013; Melo et al., 2013; Mousavi et al., 2013). Additionally, lncRNAs with enhancer-like function were identified to have an activating function for nearby protein coding genes, termed activating ncRNAs (ncRNA-a) (Lai et al., 2013; Orom et al., 2010). In breast cancer cells, eRNAs were shown to be necessary for proper looping of the enhancer to the promoter region, as determined by Chromosome conformation capture (3C) and binding of a subunit of the cohesion complex (RAD21), which is critical for looping (Li et al., 2013). ncRNA-a's were also shown to bind to one of the subunits of Mediator, (Med12), another critical complex in looping, and be necessary for looping (Kagey et al., 2010; Lai et al., 2013). However, in another study of breast cancer cells, reducing eRNA expression with transcription inhibitors had no effect on chromosomal looping, and in muscle cells, eRNA knockdown had no effect on RAD21 binding, but it did lead to a decreasing in RNAPII binding at the promoter (Hah et al., 2013; Mousavi et al., 2013).

2.1.2 Functional lncRNAs

With the increasing prevalence of genome-wide sequencing techniques, it has been discovered that a large portion of the genome is actively transcribed (Djebali et al., 2012; Guttman et al., 2009). There have been many examples of these transcripts playing a role in regulating gene expression through various targeting mechanisms (Figure 2.1). One of the best-characterized examples of a functional lncRNA acting in *cis* is *Xist*. X chromosome inactivation (XCI) is the process by which mammalian cells will inactivate one of the X chromosomes in female to achieve dosage compensation (Lyon, 1961). The X-inactivation center (*Xic*) is a region present on the X chromosome that expresses the genes necessary for this process including multiple lncRNAs such as *Xist*, *Tsix*, and *Jpx*. While *Xist* might be considered the main regulator of XCI, as it has been shown to coat the chromosome to be inactivated and recruit Polycomb Repressive Complex 2 (PRC2) through a direct interaction which then results in gene silencing (Zhao et al., 2008). *Xist* expression itself, however, is also regulated opposing interactions of RNA-protein complexes. The expression of *Tsix*, which is transcribed in an anti-sense direction from *Xist*, another example of *cis* regulation, downregulates *Xist* expression, while also interfering with the interaction between *Xist* and PRC2. In the opposite way, the RNA *Jpx* activates *Xist* expression by binding to the CTCF that is found at the *Xist* promoter and titrating the complex away to induce *Xist* as differentiation progresses (Sun et al., 2013; Tian et al., 2010). This single locus provides evidence of the complex interactions between lncRNAs and proteins used to fine-tune gene expression within the cell.

Airn (*antisense Igf2r RNA noncoding*) is another example of a lncRNA acting in *cis*, this time in imprinting, where a set of genes from the paternal allele are silenced (Sleutels et al., 2002). This lncRNA, also expressed from the paternal allele, is responsible for silencing three

genes, *Igf2r*, *Slc22a3*, and *Slc22a2*, but it appears to silence them using different mechanisms. To silence *Slc22a3*, the *Airn* transcript recruits the EHMT2 methyltransferase, but silencing *Igf2r* relies on transcription interference, which only requires the overlap of transcription of *Airn* through the *Igf2r* promoter region (Latos et al., 2012; Nagano et al., 2008).

lncRNAs can also work in *trans*. Initial analysis of HOTAIR expressed from the HOXC locus showed that it mediates transcriptional repression of the HOXD locus located on a different chromosome via PRC2 recruitment (Rinn et al., 2007). Subsequent genome-wide analysis of HOTAIR occupancy revealed 832 HOTAIR occupancy sites across the genome in MDA-MB-231 breast cancer cells occurring on multiple chromosomes in addition to the HOXD locus. Supporting its role in *trans*, over-expression of HOTAIR in epithelial cancer cells induced genome-wide re-targeting of PRC2, leading to altered H3K27me3, gene expression, and increased cancer invasiveness and metastasis in a manner dependent on PRC2 (Gupta et al., 2010).

HOTTIP is a well-characterized lncRNA transcribed in an antisense direction to the 5' end of the developmentally regulated gene locus, HOXA, and provides an example of how transcripts can work in a *cis*-like manner to regulate genes at a location physically close to their own transcription site through choromosomal looping. Transcription of HOTTIP leads to activation of the cluster of HOXA genes through binding to WDR5 and promotion of chromosome looping (Wang et al., 2011c; Wysocka et al., 2005). It is able to regulate many genes through the chromosomal looping that brings these genes into close proximity, where HOTTIP then recruits Mixed Lineage Leukemia 1 (MLL1), which is a methyltransferase that is responsible for producing the activating histone modification, H3K4me3, and this results in upregulation of this gene set (Wysocka et al., 2005).

2.1.3 *Arc* and *Gadd45b* are important neuronal IEGs

Many of the neuronal IEGs are transcription factors, such as *c-fos*, *Egr1*, and *Nr4a1*, which are able to initiate later waves of transcription to coordinate the cell's response to a specific stimulus. However, *Arc* and *Gadd45b* are not classical transcription factors. *Arc* is a synaptic localized protein that regulates the endocytosis rate of AMPARs to control the surface levels of the receptor, while *Gadd45b* is necessary for the demethylation of DNA at the promoters of specific genes, such as *Bdnf*. *Arc* has been shown to be necessary for LTP and long-term memory formation, while *Gadd45b* knockout mice show enhanced LTP and long-term memory formation (Guzowski et al., 2000; Ma et al., 2009; Ploski et al., 2008; Sultan et al., 2012). Both genes also have eRNAs expressed from potential enhancer regions. The enhancer for *Arc* has been well characterized. Named the synaptic-activity responsive element (SARE), this site was found to be the minimal region necessary for enhancer activity in a luciferase assay (Kawashima et al., 2009). Binding sites for transcription factors such as SRF have been identified in the SARE as well. This region displays bidirectional transcription of eRNAs, while the potential enhancer for *Gadd45b* appears to mainly express eRNAs from the *plus* strand (Figure 2.2).

2.1.4 RNAPII pausing regulates neuronal IEG induction

Neuronal IEGs, including *Arc* were recently shown to be regulated by the mechanism of RNAPII pausing (Saha et al., 2011). This is a regulatory mechanism found across metazoans, at about 30% of genes, that allows for a coordinated and synchronous response to specific stimuli (Adelman and Lis, 2012). RNAPII is recruited to promoters of certain genes, and begins transcribing 20-60 bp into the gene before it becomes paused by the binding of pausing factors,

Negative Elongation Factor (NELF) and DRB-sensitivity-inducing Factor (DSIF), where it remains paused until the cell receives the proper signal. pTEF-b is then recruited, and it phosphorylates RNAPII, DSIF, and possibly NELF, NELF is released, and RNAPII enters into productive elongation (Rougvie and Lis, 1988). Bound RNAPII was found at the promoters of rapidly induced genes in neurons, along with the pausing factor NELF (Saha et al., 2011). NELF binding was decreased when TTX was washed out, suggesting that NELF was released in response to an increase in neuronal activity. Reducing levels of NELF led to a decrease in the induction of these IEGs at early time points after TTX washout, as well as a decrease in Ser5p induction and active histone modifications, such as H3K3me3, at the *Arc* promoter. These data fit with one of the proposed functions of pausing, which is to maintain a permissive chromatin state. While NELF is able to act as a pausing factor, repressing transcription until it is released, studies have found that knocking down NELF actually leads to a decrease in many genes, which at first seems counterintuitive (Adelman et al., 2009). However, the paused polymerase at the promoter is able to compete with nucleosomes for binding to the region, thus allowing the promoter to maintain an open conformation where other transcription factors can bind (Core et al., 2012; Gilchrist et al., 2010).

2.2 Results

2.2.1 eRNAs are necessary for target gene induction

In our initial effort to characterize the function of eRNAs, we performed a time course measurement of the eRNAs that are expressed from the enhancer for *Arc,* an IEG important for brain development and function (Korb and Finkbeiner, 2011) (Figure 2.3 A and B). Neuronal activity was first suppressed by tetrodotoxin (TTX), a sodium channel blocker that prevents neuronal action potentials, and then expression levels of *Arc* eRNA, pre-mRNA, and mRNA

were monitored for various times following KCl-mediated membrane depolarization. We observed that the bi-directional synthesis of *Arc* eRNA was induced by membrane depolarization but peaked earlier than *Arc* pre-mRNA and mRNA (Figure 2.3 B). The difference in peak times between eRNA and pre-mRNA is not due to a significant difference in decay times between the transcripts as both transcripts show a similar decay rate (approximate half-life $\leq$ 7.5 min) upon addition of a transcription inhibitor, ActD following 30 min of KCl-mediated depolarization (Figure 2.4). This result could suggest that eRNA synthesis is not merely a byproduct of promoter-driven transcription activity, but instead an independently regulated process.

Arc eRNA was also induced by the $GABA_A$ receptor antagonist bicuculline, which more closely resembles the physiological activation of synapses (Figure 2.5 A) (Hardingham et al., 2001). By blocking the major inhibitory input in neurons, bicuculline triggers a synchronous burst of action potentials and induces both *Arc* eRNA and mRNA. Notably, the minus strand of *Arc* eRNA was predominantly induced in response to bicuculline, suggesting that synaptic activity-driven eRNA induction may occur in a strand-specific manner. When the minus strand of *Arc* eRNA was sequenced using an RNA circularization method, we found that while there was a distinct 5' end of the transcript, the 3'ends were degenerate without noticeable polyadenylation (Figure 2.5 B), although we cannot rule out the possibility that a minor population of the eRNAs could be polyadenylated. We also found that *Arc* eRNA can be induced by serum stimulation in NIH3T3 cells, but remain localized in the nucleus after their synthesis whereas *Arc* mRNA is present in both the nucleus and the cytoplasm (Figure 2.5 C). These properties of *Arc* eRNAs are in good agreement with the latest ENCODE consortium analysis of eRNAs in human cell lines showing that eRNAs are prevalent in the nuclear non-polyadenylated RNA fraction (Djebali et al., 2012).

To test the functionality of eRNAs in activity-induced neuronal gene expression more directly, lentiviral constructs containing short-hairpin RNAs (shRNAs) against the minus strand of *Arc* eRNA were designed to knockdown the eRNAs and assess the effect on *Arc* mRNA induction in response to membrane depolarization. Knockdown of *Arc* eRNAs reproducibly led to a decrease in the level of *Arc* mRNA induction when compared to a scrambled control shRNA, suggesting that *Arc* eRNAs are functionally important for neuronal activity-dependent transcriptional induction of the *Arc* gene (Figure 2.3 C). *Arc* eRNA appears to specifically regulate *Arc* gene expression since the expression levels of other neuronal IEGs (*e.g.*, *c-fos*, *Egr-1*, *Gadd45b*) were not affected by the *Arc* eRNA knockdown. To further evaluate the specificity of eRNA action, we examined the knockdown effect of the eRNAs expressed from an enhancer located nearby the *Gadd45b* gene (Figure 2.3 D and E). Although expressed from a well-defined enhancer region, the plus strand of *Gadd45b* eRNAs is predominantly transcribed upon membrane depolarization and peaks ~50 min after KCl treatment (Figuress 2.2 and 2.3 E), which is later than the *Arc* eRNA peak time. Knockdown of the *Gadd45b* eRNA plus strand specifically reduces the induction level of *Gadd45b* mRNA but not other IEGs upon KCl-mediated membrane depolarization of neurons (Figure 2.3 F). We also observed that the impairment in the activity-dependent induction of *Arc* and *Gadd45b* transcription caused by the knockdown of corresponding eRNAs leads to a decrease in the levels of ARC and GADD45B proteins (Figure 2.5 D). Taken together, these results suggest that eRNAs can act locally at their specific target genes, which is consistent with recent functional analyses of eRNAs in non-neuronal cells (Hsieh et al., 2014; IIott et al., 2014; Lam et al., 2013; Li et al., 2013; Melo et al., 2013; Mousavi et al., 2013) (see also Figure 2.9 A).

2.2.2 Enhancer-promoter interactions are not dependent on eRNA

Promoters and distal enhancers can be physically juxtaposed with each other through chromosomal looping as part of a gene regulatory mechanism (Smallwood and Ren, 2013). We reasoned that the target specificity of eRNAs could be mediated by enhancer-promoter looping. In order to see if the interaction between the *Arc* promoter and enhancer occurs constitutively or in a stimulus-dependent manner (*i.e.*, membrane depolarization of neurons), we performed Chromatin Conformation Capture (3C) to quantitatively measure the chromosomal interactions in the regions surrounding the *Arc* gene (Figure 2.6 A). As expected, the eRNA-producing *Arc* enhancer was the most prominent genomic locus that interacts with the *Arc* promoter in an activity-dependent manner. The 3C analysis also found another interaction site (B4) that had not been previously identified, but its interaction with the *Arc* gene locus was constitutive. Some lncRNAs and eRNAs have been shown to promote target gene expression by facilitating chromosomal looping between the enhancer and promoter (Lai et al., 2013; Li et al., 2013). Therefore we tested if *Arc* eRNA can also mediate the interaction between the *Arc* promoter and enhancer (Figure 2.6 A). We found no significant change in the chromosomal interaction between the *Arc* enhancer and promoter. This was also the case with the *Gadd45b* locus, as we identified a strong activity-dependent interaction between the *Gadd45b* promoter and enhancer that was unaffected by *Gadd45b* eRNA knockdown (Figures 2.6 B).

To corroborate our findings from 3C analysis, we next examined the effect of eRNA knockdown on the binding levels of the Mediator and cohesin complexes at both the *Arc* and *Gadd45b* enhancers as well as promoters (Figures 2.6 C and D). The Mediator-cohesin complex co-occupies enhancers and promoters to facilitate enhancer–promoter DNA looping, and recent studies have implicated ncRNA-a and eRNAs in chromosomal looping through interactions with

Mediator and the cohesion complex, respectively (Lai et al., 2013; Li et al., 2013). Chromatin immunoprecipitation (ChIP) analysis of a common Mediator complex subunit Med1 and a cohesin subunit RAD21 shows that both the promoters and enhancers of *Arc* and *Gadd45b* genes are inducibly occupied by the Mediator/cohesin complex upon membrane depolarization, but eRNA knockdown has no effect on their occupancy. Together with the 3C analysis, these results collectively argue that at least for neuronal IEG expression, eRNAs are not required for the enhancer-promoter interaction. Our finding is consistent with other reports showing that eRNA transcription is not necessary for enhancer-promoter looping in human breast cancer cells and that eRNA knockdown has no effect on cohesin complex loading in mouse skeletal muscle (Hah et al., 2013; Mousavi et al., 2013).

2.2.3 Knockdown of eRNAs causes NELF to remain bound to target gene promoters

Recent genome-wide studies unambiguously argue that proximal-promoter pausing of RNAPII is a widespread mechanism of transcriptional regulation for controlling expression of stimulus-responsive genes in higher eukaryotes (Adelman and Lis, 2012; Gilchrist et al., 2012). Because of the rapid induction kinetics of eRNAs (Figure 2.3 B and E), we investigated whether eRNAs play a role in the early transcription elongation step that involves RNAPII pausing and release. Analyses of RNAPII elongation complexes using a native electrophoretic mobility shift assay have demonstrated that DSIF and NELF complexes are stably associated with paused RNAPII through interactions with both RNAPII and nascent transcripts (Cheng and Price, 2008; Missra and Gilmour, 2010). Therefore, we hypothesized that during target gene activation, eRNAs might destabilize the DSIF/NELF association with RNAPII by mimicking nascent transcripts and thereby facilitate the RNAPII transition from pausing to productive elongation.

Expression of neuronal IEGs was also shown to be subject to this RNAPII pausing mechanism (Saha et al., 2011). Consistently we found that NELF binds specifically to the *Arc* promoter, but not to the *Arc* enhancer when neuronal gene expression is suppressed by TTX (Figure 2.7 A). NELF is then released from the *Arc* promoter upon activation of neuronal gene expression by KCl-mediated membrane depolarization. NELF release appears to occur within a narrow time window and to be gene-specific, as NELF occupancy at the promoters of *Arc* and *c-fos* was transiently decreased at 30 min after KCl stimulation whereas NELF complexes bound at *Gadd45b* and *Egr1* promoters were released at 1 h (Figures 2.8 A and B). Transient release of NELF during transcription activation was also observed in a previous study where NELF occupancy at the TNFα proximal promoter in macrophages was temporarily decreased at 30 min after lipopolysaccharide (LPS) treatment (Adelman et al., 2009). Interestingly, shRNA-mediated knockdown of *Arc* and *Gadd45b* eRNAs blocked the NELF release from their corresponding promoters even during membrane depolarization (Figures 2.8 A and B). A subunit of P-TEFb, CDK9 was also inducibly recruited to the *Arc* promoter at 30 min after membrane depolarization (Figure 2.7 B), but its recruitment was unaffected by eRNA knockdown (Figure 2.8 C). This result strongly suggests that eRNAs facilitate transient release of NELF during gene activation.

To further validate our findings, we applied a Locked Nucleic Acid antisense-oligonucleotide (LNA) method to see if we would observe the same result when the level of eRNA is reduced by another independent knockdown method. LNAs can induce degradation of the complementary target RNA by recruiting RNase H without involving the cell's RNAi machinery (Watts and Corey, 2012). Due to the low efficiency of LNA transfection in neurons, we tested the effect of LNA-mediated knockdown of *Arc* eRNA in NIH3T3 cells, in which both *Arc* eRNA and mRNA are induced by serum stimulation (Figure 2.9 A). As seen by shRNA-

mediated knockdown of *Arc* eRNA in neurons, an LNA designed to target *Arc* eRNA was able to reduce both *Arc* eRNA and mRNA levels during serum stimulation, without affecting other IEGs induced by serum (compare Figures 2.3 C and 2.9 A). The *Gadd45b* gene was not induced by serum stimulation in NIH3T3 cells, thus not analyzed in this experiment. Having verified the effect of *Arc* eRNA by two independent knockdown methods, we then asked if the LNA-mediated knockdown of *Arc* eRNA would also block NELF release from the *Arc* promoter during serum stimulation (Figure 2.9 B). In NIH3T3 cells, NELF was transiently released from the promoters of *Arc*, *c-fos*, and *Egr1* at 30 min after serum stimulation. However, knockdown of *Arc* eRNA by LNA caused the retention of NELF only at the *Arc* promoter during serum stimulation, which is consistent with the results from the shRNA-mediated knockdown experiment (compare Figures 2.8 A and 2.9 B). The consistent results obtained by two independent knockdown methods in two different cell types strongly suggest that the effects of *Arc* eRNA knockdown on NELF release as well as target gene induction are unlikely an artifact or indirect consequence that is associated with a particular knockdown method.

2.2.4 eRNAs facilitate the transition of paused RNAPII to elongation

The NELF/DSIF complex pauses RNAPII during the early elongation stage of the transcription cycle (after transcribing 20 - 60 nucleotides of nascent transcript) (Adelman and Lis, 2012; Rasmussen and Lis, 1993; Rougvie and Lis, 1988). If eRNA contributes to the efficient release of NELF from paused RNAPII, thereby facilitating the RNAPII transition to productive elongation, then eRNA knockdown would specifically reduce the level of RNAPII at the elongation stage but not at the initiation and pre-initiation stages. The C-terminal domain (CTD) of RNAPII is subject to sequential phosphorylation events during the transcription cycle (Egloff

et al., 2012). Only the unphosphorylated form of RNAPII can be assembled into the pre-initiation complex at the promoter. During the promoter escape and early elongation stage, the serine 5 (Ser-5) residue of the CTD is phosphorylated by the CDK7 kinase subunit of TFIIH. The serine 2 (Ser-2) residue of the CTD is then gradually phosphorylated by the CDK9 subunit of P-TEFb as RNAPII stably elongates toward the 3' end of the gene. To test whether eRNAs selectively regulate the RNAPII transition to productive elongation, we examined the effect of *Arc* eRNA knockdown on RNAPII levels along the *Arc* gene by ChIP experiments with antibodies recognizing different forms of RNAPII: unphosphorylated RNAPII (8WG16), RNAPII-Ser5P, and Pan RNAPII. We found that when *Arc* eRNA levels were reduced using shRNAs targeting the *Arc* minus strand, there was no change in the level of unphosphorylated RNAPII at the *Arc* promoter detected by the 8WG16 antibody (Jones et al., 2004) (Figure 2.10 B, top). Since only the unphosphorylated form of RNAPII can enter into the pre-initiation complex, this suggests that recruitment of RNAPII to the promoter is unaffected by the eRNA knockdown. However, the level of RNAPII phosphorylated at Ser-5 (Ser-5P) was significantly decreased at the promoter as well as the 3' end of the *Arc* gene during KCl stimulated conditions (Figure 2.10 B, middle). The Pan RNAPII antibody also detected a significant reduction in total RNAPII levels at the *Arc* promoter region during stimulation, and RNAPII levels along the coding region showed a trend toward a decrease, as well, although weak (Figure 2.10 B, bottom). Since the Pan RNAPII antibody cannot distinguish between the different forms of RNAPII, it detects the sum of the levels of RNAPIIs present in different stages of transcription. As the unphosphorylated form of RNAPII is unchanged, the decrease seen in the Pan RNAPII ChIP is likely due to a decrease in the phosphorylated, elongating RNAPII, as is seen with the Ser5P antibody, although we cannot completely rule out a possibility that recruitment of RNAPII is also affected. These

results indicate that upon KCl-depolarization, eRNAs play an important role in facilitating the transition of paused RNAPII to elongating RNAPII, as the level of elongating forms of RNAPII is specifically decreased when the *Arc* eRNA level is lowered.

To correlate the RNAPII ChIP results with transcription, we then selectively compared the levels of various regions of nascent *Arc* transcripts induced by KCl treatment with or without shRNA-mediated eRNA knockdown (Figures 2.10 A and C). The transcript level immediately downstream of the transcription start site (TSS; detected by primer set A) in the nascent RNA sample was not reduced when compared to the scrambled control, whereas all other regions (detected by primer sets B-E) were lower. In contrast, knockdown of *Arc* eRNA resulted in a uniform decrease in the steady state level of *Arc* mRNA. Retention of similar or even higher levels of nascent transcription specifically near the 5' end of the *Arc* gene after *Arc* eRNA knockdown is consistent with the RNAPII ChIP results and further supports a role of eRNA in the transition of paused RNAPII to productive elongation.

2.2.5 eRNAs interact with NELF-E in an RRM-dependent manner

The observed effect of eRNA knockdown on NELF release suggests a possibility that the NELF complex and eRNAs might directly interact with each other. The NELF-E subunit contains an RNA recognition motif (RRM) that mediates direct interactions with various RNA sequences with little or no apparent sequence or structural constraint, which is suitable for binding to nascent RNAs derived from many genes (Rao et al., 2006; Yamaguchi et al., 2002). The RRM of NELF-E was also shown to be critical for the RNAPII pausing activity of NELF in an *in vitro* transcription assay (Yamaguchi et al., 2002). We postulate that when eRNAs are rapidly induced in neurons by KCl-depolarization, they might compete with the nascent RNA

attached to paused RNAPII for binding to NELF, thereby facilitating the release of the NELF complex. To test this idea, we performed UV-RNA Immunopreciptation (UV-RIP) with an antibody directed against the NELF-E subunit that contains the RRM in order to see if eRNAs can directly bind to the NELF-E subunit (Yamaguchi et al., 2002) (Figure 2.11 A). We found that the proportions of *Arc, Gadd45b,* and *c-fos* eRNAs brought down with NELF-E at 30 min following membrane depolarization were significantly higher than those with the IgG control, whereas there was no such enrichment of target gene mRNAs or the constitutively expressed *TBP* mRNA. We also performed eRNA pull-down experiments using biotinylated full-length *Arc* eRNA transcribed *in vitro* and lysates from HEK293T cells that overexpress either a FLAG-tagged wild-type (WT) or RRM-deletion mutant (ΔRRM) of the NELF-E protein. When biotinylated *Arc* eRNAs were pulled down by streptavidin beads under two different salt washing conditions, we reproducibly observed a higher level of WT NELF-E protein co-precipitated than the ΔRRM NELF-E protein (Figure 2.11 B). This data not only provides additional evidence supporting the conclusion that eRNAs are able to interact with NELF-E, but also demonstrates that the interaction is dependent on the RRM.

2.2.6 The RRM of the NELF-E subunit is critical for IEG induction in neurons

Having found an interaction between the eRNA and the NELF-E RRM, we next examined how critical the RRM domain is for NELF function for IEG expression in neurons. To do this, we co-infected neurons with two different lentiviruses that express an shRNA against the 3' UTR of endogenous NELF-E mRNA, and the shRNA-resistant forms of FLAG-tagged WT or ΔRRM NELF-E protein, which lack both the 5' and 3' UTRs. In this replacement experiment, we titrated the amount of NELF-E protein variants to be similar to the level of endogenous

NELF-E protein before knockdown, to avoid any complication resulting from excessive expression of exogenous protein in neurons (Figure 2.11 C). We observed in KCl-depolarized neurons that the induction of both *Arc* and *Gadd45b* mRNAs was similar to the scrambled control levels when endogenous NELF-E protein was replaced by the FLAG-tagged version of WT NELF-E, but replacement with the FLAG-ΔRRM NELF-E protein led to a significant decrease in the induction levels of *Arc* and *Gadd45b* mRNAs compared to the scrambled control or WT NELF-E (Figures 2.11 C and D).

We also measured the binding levels of NELF complexes assembled with exogenously expressed NELF-E variants at various IEG promoters. NELF complexes formed with either endogenous NELF-E (scrambled condition) or the WT NELF-E variant showed similar levels of occupancy at the promoters of *Arc, Gadd45b, c-fos* and *Egr1* when neuronal activity was suppressed by TTX. However, the NELF complex assembled with the FLAG-ΔRRM NELF-E protein showed a much lower level of binding at the IEG promoters, suggesting that the RRM interaction with nascent RNA emerging from initiating RNAPII is important for NELF to stably associate with RNAPII to mediate pausing in quiescent neurons (Figure 2.11 E). A previous study in neurons showed that NELF-dependent RNAPII pausing allows rapid induction of neuronal IEG expression (Saha et al., 2011). Reduction of RNAPII pausing by knockdown of *Nelf-a* or *Nelf-e* prevented rapid *Arc* transcription, resulting in a lower level of pre-*Arc* mRNA induction than a scrambled control upon neuronal activity increase. Our results would further suggest that the interactions with various RNAs via the NELF-E RRM might be a critical mechanism for NELF to regulate IEG induction in neurons. Deletion of the RRM in NELF-E disrupted NELF binding at the promoters of these IEGs (Figure 2.11 E), which we propose

causes a reduction of RNAPII pausing, and in turn impairs rapid and synchronous induction of neuronal IEGs such as *Arc* and *Gadd45b* (Figure 2.11 D).

2.3 Conclusions

These results together define a new function for eRNAs in target gene activation through regulating the transition of paused RNAPII to productive elongation. The *Arc* and *Gadd45b* eRNAs were necessary for proper induction of both of their respective target genes, at the level of RNA as well as protein, suggesting that the regulation provided by these eRNA transcripts might be important for the downstream biological function of these proteins in neuronal function. The induction kinetics of the eRNAs peaked earlier than the target gene, suggesting that the eRNAs could be playing a role early in transcription activation. This also suggests, since the eRNA transcription is initiated and then begins turning off before the target gene has peaked, that the eRNAs are independently regulated and not just a byproduct of transcription from the promoter. This appears to be a common feature of enhancer-derived transcripts, as a recent study by the FANTOM Consortium analyzed thousands of samples and found that eRNA transcription was in fact the earliest stage of any transition in different cell types (Arner et al., 2015). The fact that this is a common feature of enhancers further supports the idea that they have an important regulatory role.

In looking for an early step in transcription that the eRNAs could be acting, we first looked at chromosomal looping, but 3C experiments and ChIP results of looping factors suggested that neuronal eRNAs do not affect looping between the promoter and enhancer. Instead, eRNAs are necessary for the proper release of the pausing factor NELF from the promoter of the target genes. The *Arc* eRNA directly interacts with NELF-E, in a manner that is

dependent on the protein's RNA binding domain, the RRM. When the eRNAs are knocked down, there is less elongating polymerase, and a decrease in nascent transcripts downstream of the TSS. In our model, in response to depolarization, the *Arc* enhancer is brought into close proximity of the *Arc* promoter, and it is the high levels of these transcripts expressed in the local area of the promoter, that allows them to compete with the nascent *Arc* transcript for binding to NELF. NELF can then be efficiently released from the promoter, and RNAPII can enter into productive elongation and achieve induction of the target gene (Figure 2.12). While eRNAs are necessary for efficient release of NELF, we envision that eRNAs play more of a modulatory role, fine-tuning the process of transcriptional activation. Other factors, such as phosphorylation by pTEF-b might also be important as well.

A recent study examining eRNAs produced from androgen receptor-regulated enhancers (AR-eRNAs) demonstrated a role for these eRNAs in regulating transcription elongation through an interaction with the CyclinT1 subunit of pTEF-b which results in higher activation of p-TEFb and higher levels of RNAPII-Ser2p (Zhao et al., 2016). In addition to affecting the target gene, *PSA*, the effect of the *PSA* eRNA on the activation of p-TEFb was also able to work in *trans* affecting other gene targets as well. While the proposed mechanism of these AR-eRNAs works through p-TEFb rather than an interaction with NELF, this study provides further evidence that eRNAs play an important role in facilitating productive elongation of RNAPII. One possible reason for the differences between the studies could be due to the fact that many enhancers are cell-type specific, and it is possible that different cell types could have evolved different mechanisms to fine-tune the transition of paused RNAPII into productive elongation. It is also possible that in addition to binding to NELF, the neuronal eRNAs could also affect the activity of p-TEFb, which would contribute to the release of NELF and more efficient elongation. Our

study did not test the activity of p-TEFb once recruited to the promoter, and this would be an important experiment to do in the future to reconcile the two studies. While it may seem simply convenient to suggest that the eRNAs could be interacting with multiple different protein complexes at the promoter, as new classes of ncRNAs are constantly being discovered, it may not be unreasonable to think that protein complexes would have evolved to work in the presence of RNA molecules, and RNA is doing a lot more than previously thought. When an abundance of RNA molecules are transcribed in response to enhancer activation, it could be possible to affect multiple complexes that are all present at the promoter to facilitate the same response, i.e. activation of p-TEFb and release of NELF.

Another important concern to keep in mind is to continue to work towards differentiating the role of the RNA transcript, the role of transcription through the region, and the underlying DNA sequence that makes up the potential *cis* regulatory element, as exemplified by a recent study looking at the *Lockd* lncRNA (Paralkar et al., 2016). *Lockd* was previously identified as a polyadenylated, spliced, promoter driven (high levels of H3K4me3) lncRNA that is highly expressed in erythroid cells (Paralkar et al., 2014). Although many of these characteristics would result in excluding this transcript from the category of eRNA, it was eventually determined that the RNA from this region was probably transcribed from an enhancer. While deletion of the entire 25 kb region that was transcribed to form the 434-nt, 2 exon transcript led to a decrease in the expression of the neighboring *Cdkn1b* gene*,* insertion of a polyadenylation cassette 80 bp downstream of the TSS significantly decreased *Lockd* expression without affecting *Cdkn1b* expression, suggesting that there was a *cis* regulatory region within the region that was deleted. This was further supported by the fact that the 5' region of the *Lockd* transcript interacted with the promoter of *Cdkn1b* by next-generation Capture-C, suggesting that this region is actually an

enhancer that could contain important binding sites for necessary transcription factors. While more investigation might be necessary to fully understand the role of the different components at this locus, it demonstrates the importance of using different, complementary methods to understand the role of lncRNAs within the cell. Simply deleting the entire region would suggest a role for the transcript, but depletion of the transcript by insertion of a polyadenylation signal suggested the opposite. However, without accurate knowledge of the important regions of the transcript, it may still be easy to jump to conclusions. If transcription of only the first ~80 nucleotides is sufficient to bind complexes at that region, it could be possible that you would see no effect with a polyadenylation signal inserted 80 bp into the gene. As always, more studies will be needed to answer these questions fully.

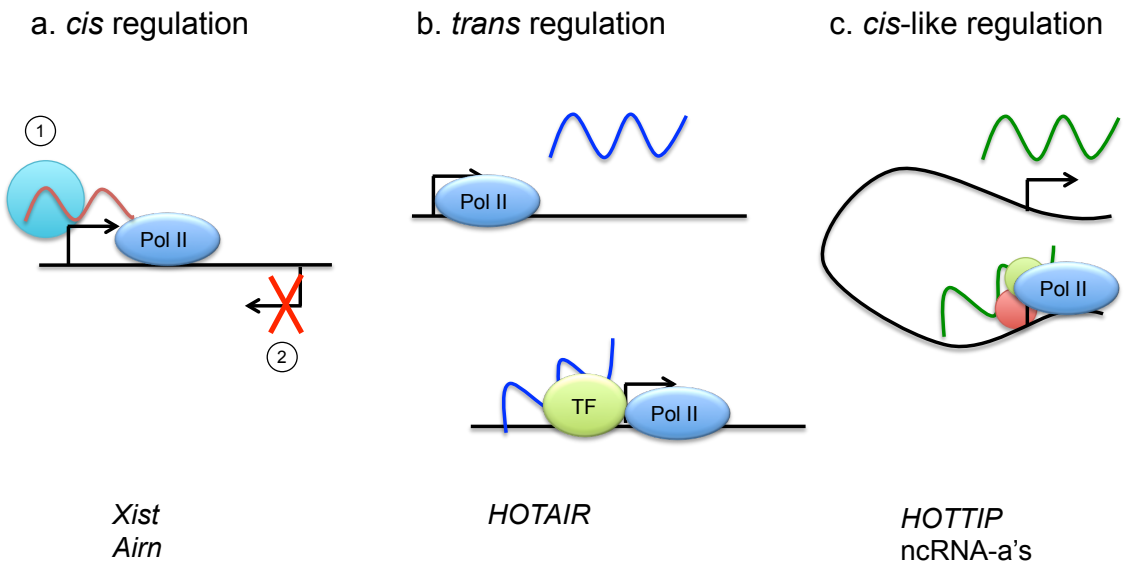

Figure 2.1 Targeting mechanisms of lncRNA action. (a) lncRNAs can act in *cis*, in which the lncRNA plays its role at the location where it is transcribed. This can occur by recruiting protein complexes to act at that location, as in the example of *Xist* in XCI, or through transcriptional interference, as in the example of *Airn* during imprinting of *Igr2f*. **(b)** lncRNAs can work in trans when they are transcribed at one location but are targeted to other locations to regulate genes throughout the genome, such as *HOTAIR* in cancer progression. **(c)** *cis*-like regulation occurs when chromosomal looping brings regions that may be linearly far away from each other into close physical proximity, so that lncRNAs are expressed close to the genes they will regulate. Examples of *cis*-like regulation include the action of *HOTTIP* at the HoxA locus and some ncRNA-a's.

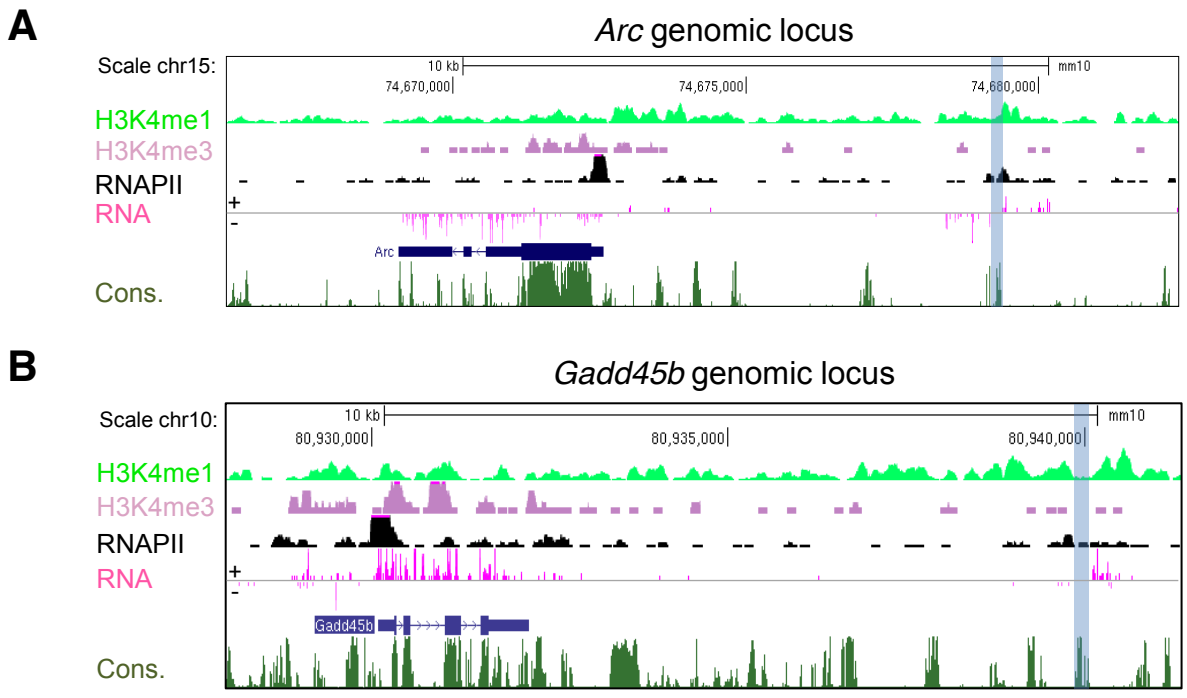

Figure 2.2 Arc and Gadd45b are neuronal IEGs that express eRNAs from enhancer regions. **(A)** A UCSC genome browser view of the *Arc* genomic locus with RNA-seq data from Kim et al., 2010 aligned with binding profiles of H3K4 mono-methylation, H3K4 tri- methylation, RNAPII, as well as the evolutionary conservation. **(B)** A UCSC genome browser view of the *Gadd45b* genomic locus. Blue bars represent the location of the enhancer regions.

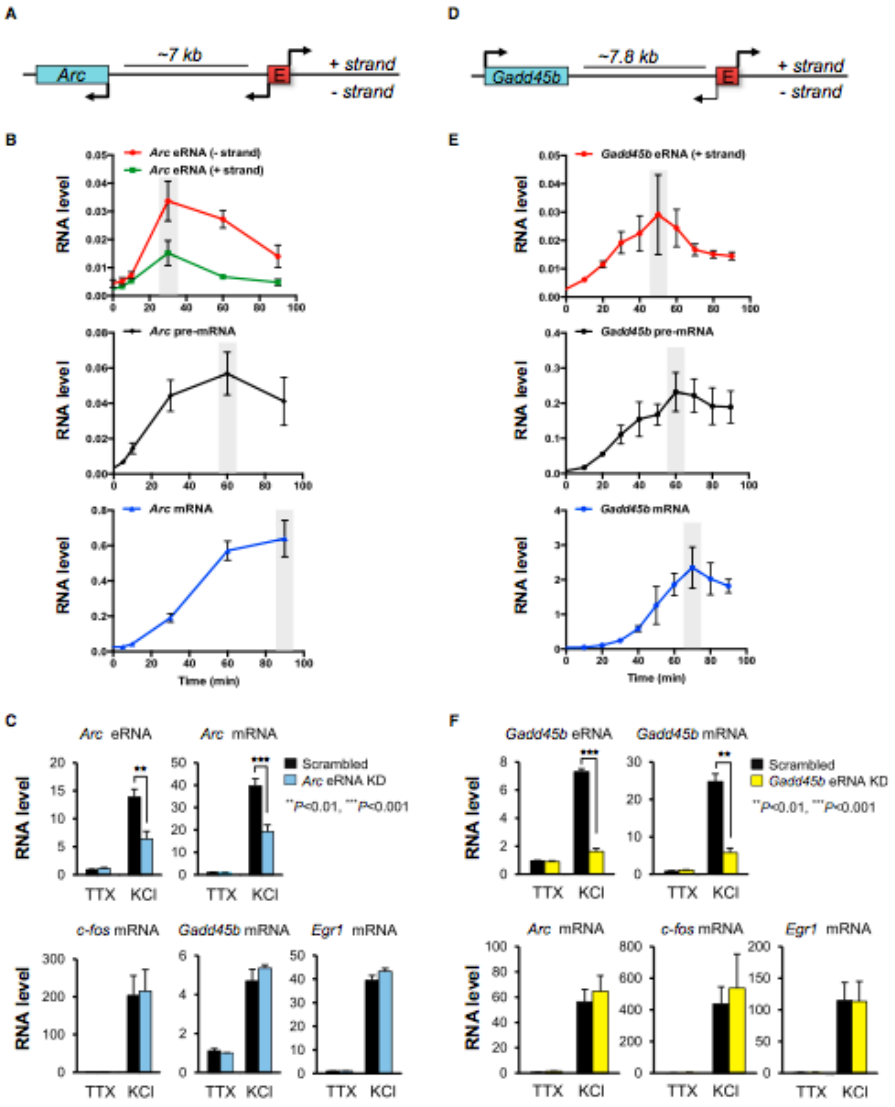

Figure 2.3 Characterization of *Arc* and *Gadd45b* eRNA. (A) Schematic diagram of the *Arc* genomic locus. **(B)** Cortical neurons were depolarized at DIV 6 with 55 mM KCl for various time points, and expression levels of *Arc* eRNAs, pre-mRNA, and mRNA were measured using qRT-PCR and normalized to the level of TBP mRNA (n = 4 biological replicates). **(C)** qRT-PCR analysis of *Arc* eRNA and mRNA expression after knockdown of *Arc* eRNA (- strand) or infection with a scrambled control in cortical neurons. Levels of indicated RNAs were measured after 30 min KCl or TTX treatment in cortical neurons and normalized to the level of TBP mRNA (n = 3 biological replicates). **(D)** Schematic diagram of the *Gadd45b* genomic locus. **(E)** Cortical neurons were depolarized at DIV 6 with 55 mM KCl for various time points, and expression levels of *Gadd45b* eRNA, pre-mRNA, and mRNA were measured using qRT-PCR and normalized to the level of TBP mRNA (n = 4 biological replicates, *Gadd45b* pre-mRNA: n=3 biological replicates) **(F)** qRT-PCR analysis of *Gadd45b* eRNA and mRNA expression after knockdown of *Gadd45b* eRNA (+ strand) in cortical neurons. Levels of indicated RNAs were measured after 60 min KCl or TTX treatment in cortical neurons and normalized to the level of TBP mRNA (n = 3 biological replicates). Error bars indicate SEM. *P*-value from two-tailed *t*-test.

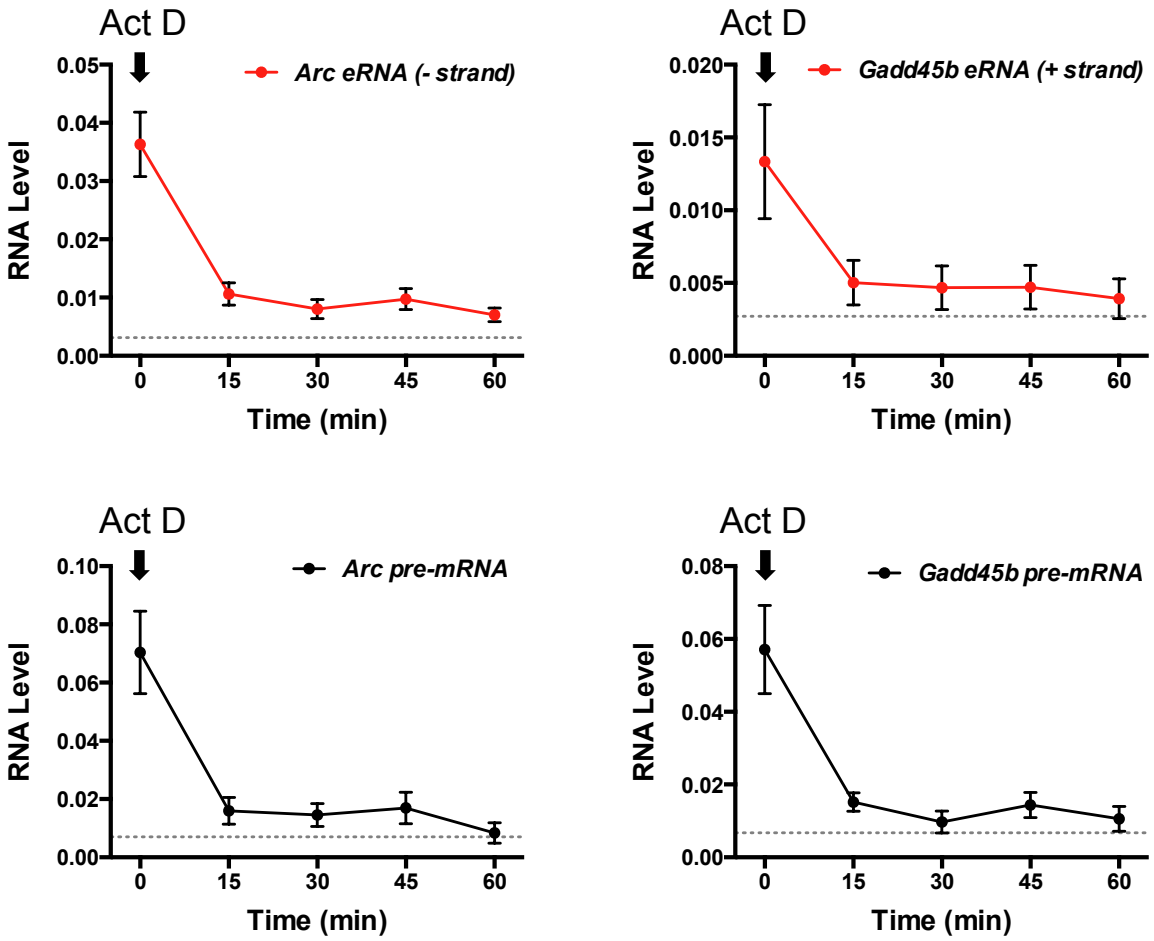

Figure 2.4 Stability of eRNA and pre-mRNA transcripts. Cortical neurons were depolarized with 55 mM KCl at DIV 6. After 30 min of stimulation, Actinomycin D was added (black arrow). Expression levels of Arc and Gadd45b eRNA and pre- mRNA were measured at the indicated time points using qRT-PCR and normalized to Tbp mRNA. The grey dotted line represents the average baseline, during TTX conditions, for each RNA (n = 3 biological replicates). Error bars represent SEM.

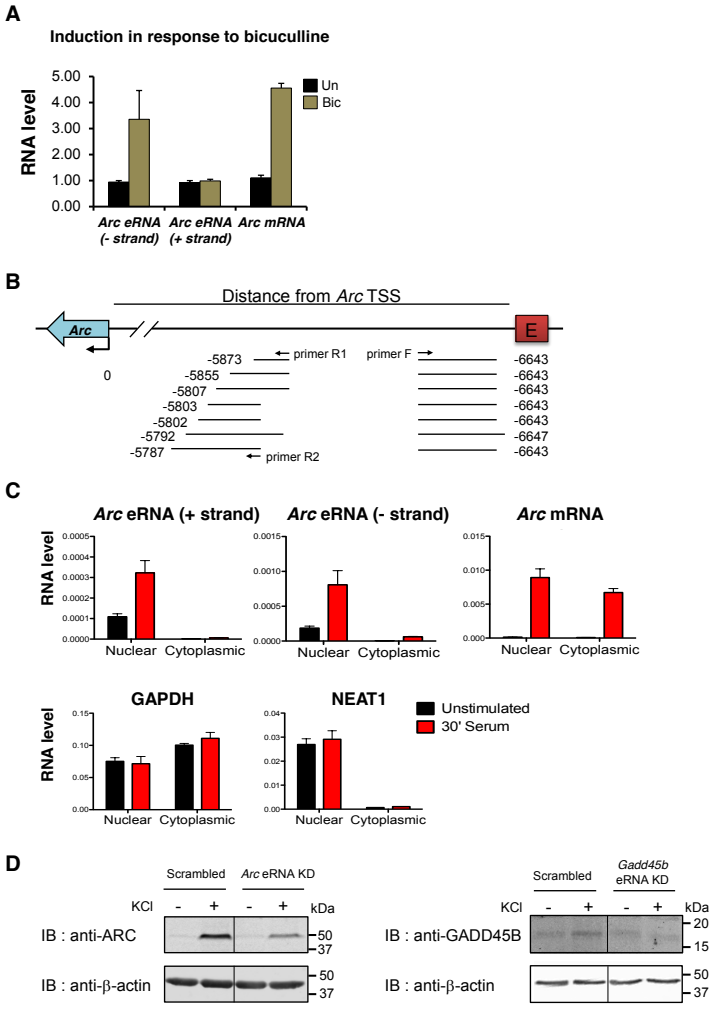

Figure 2.5 Characterization of eRNAs. (A) Cortical neurons at DIV 12-14 were treated with 50 μM bicuculline for 30 min, and expression levels of *Arc* eRNAs (plus and minus strand) and mRNA were measured using qRT-PCR and normalized to the level of *Tbp* mRNA (n = 2 biological replicates). **(B)** Mapping the 5' and 3' ends of the minus strand of the *Arc* eRNA transcript by RNA circularization. Black arrows represent the primers used during nested PCR. Values given are relative to the Arc TSS. **(C)** NIH3T3 cells were stimulated with 20% serum for 30 min. RNA from nuclear and cytoplasmic fractions was extracted and quantified with qRT-PCR. Both strands of *Arc* eRNAs and *Arc* mRNA were examined for their relative abundance in the nuclear and cytoplasmic fractions. *NEAT1* lncRNA was used as a positive control for nuclear-localized RNA. **(D)** Cortical neurons infected with lentivirus encoding either a scrambled control shRNA or shRNA against *Arc* eRNA (- strand) or Gadd45b eRNA (+ strand) were lysed and the levels of ARC and GADD45B proteins were analyzed by western blotting. Beta (β)-actin protein was also blotted as a loading control. Extra lanes were removed from the GADD45B western blot image for clarity, and the lines indicate the position of the deletion. Error bars represent SEM.

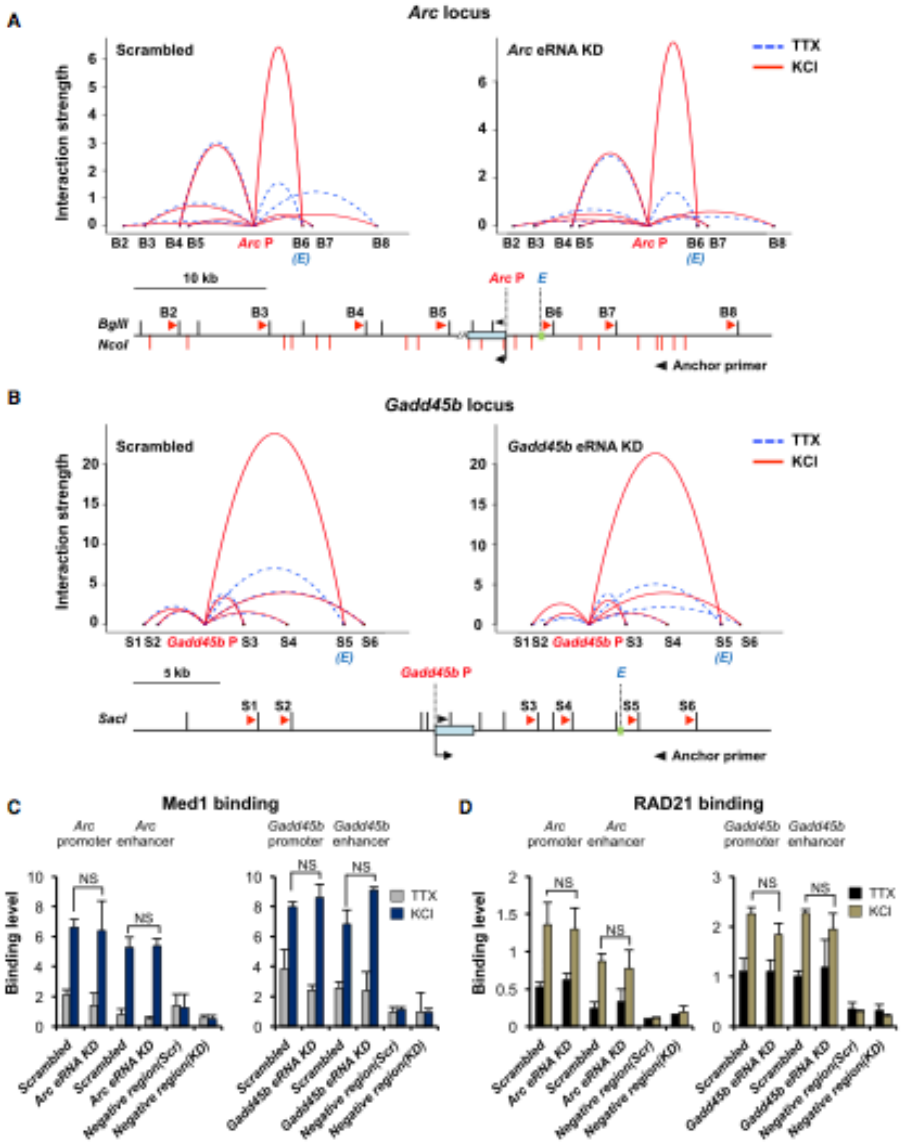

Figure 2.6 Activity-induced interactions between enhancers and promoters. (A and **B)** 3C analysis to examine the effect of eRNA knockdown in enhancer-promoter looping. Chromosomal interactions between the *Arc* or *Gadd45b* promoter and surrounding genomic loci were measured by q-PCR using the primers indicated in the schematic diagram. *Arc* P or *Gadd45b* P indicates the promoter and *E* indicates the enhancer. The black arrowhead near the *Arc* P and *Gadd45b* P indicates the anchor primer. The restriction enzyme sites (vertical lines) and primers used for q-PCR together with the anchor primer (arrowheads) are also shown (n = 3 biological replicates). **(C and D)** Binding levels of Med1 and RAD21 at the *Arc* and *Gadd45b* promoters, and corresponding enhancers determined by ChIP-qPCR in neurons infected with a scrambled control or eRNA knockdown lentivirus in quiescent (TTX) and KCl stimulated conditions (n = 2 biological replicates). Error bars indicate SEM. *P*-value from two-tailed *t*-test.
Note: The 3C and ChIP experiments were performed by Jae-Yeol Joo.

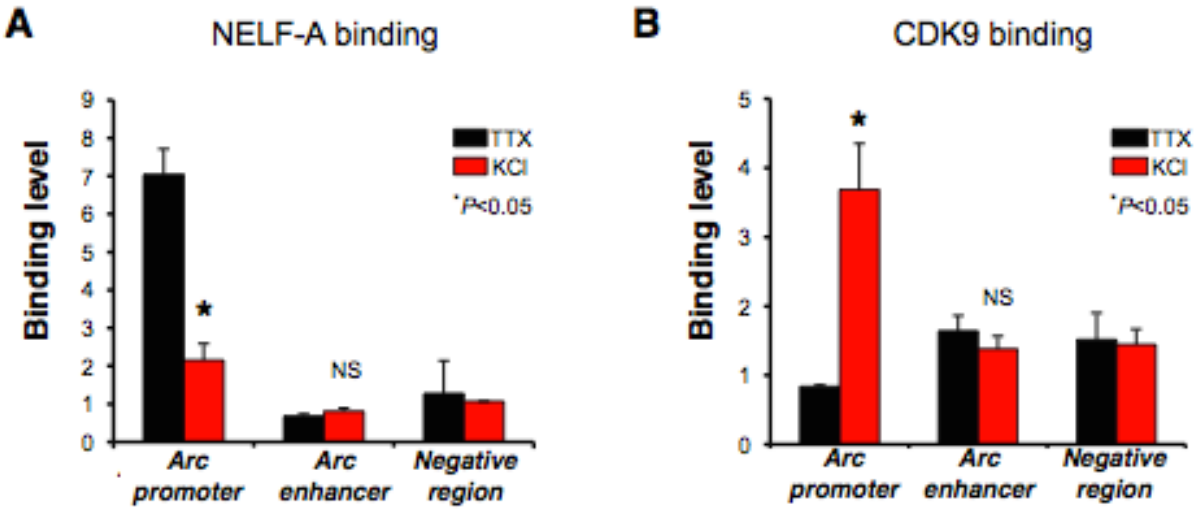

Figure 2.7 Reciprocal binding pattern of NELF and CDK9 at the *Arc* promoter and enhancer. (A) NELF-A binding profile at the *Arc* promoter and enhancer in quiescent and 30 min KCl stimulation conditions (n = 3 biological replicates). **(B)** CDK9 binding profile at the *Arc* promoter and enhancer in quiescent and 30 min KCl stimulation conditions (n = 3 biological replicates). Error bars indicate SEM. P-value from two-tailed t-test. NS, not significant.

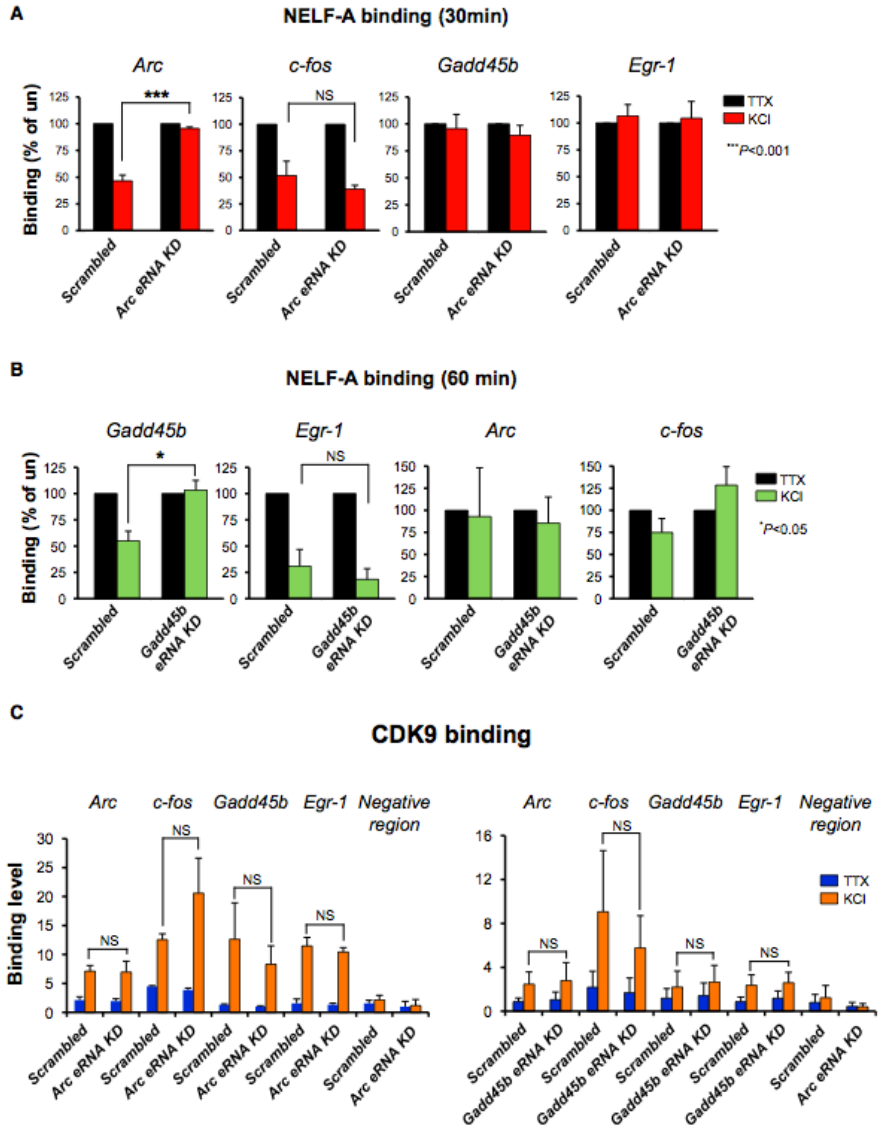

Figure 2.8 eRNAs function to facilitate the release of the NELF complex from paused RNAPII. (A) Effect of *Arc* eRNA knockdown on NELF-A binding at the *Arc*, *c-fos, Gadd45b* and *Egr-1* promoters (n = 2 biological replicates). **(B)** Effect of *Gadd45b* eRNA knockdown on NELF-A binding at the *Arc*, *c-fos, Gadd45b* and *Egr-1* promoters (n = 2 biological replicates). (C) Effect of *Arc* eRNA and *Gadd45b* eRNA knockdown on CDK9 binding at the *Arc*, *c-fos*, *Gadd45b* and *Egr-1* promoters (n = 2 biological replicates). Error bars indicate SEM. *P*-value from two-tailed *t*-test. NS, not significant.

Note: The NELF ChIP and CDK9, Arc eRNA KD ChIP were performed by Jae-Yeol Joo

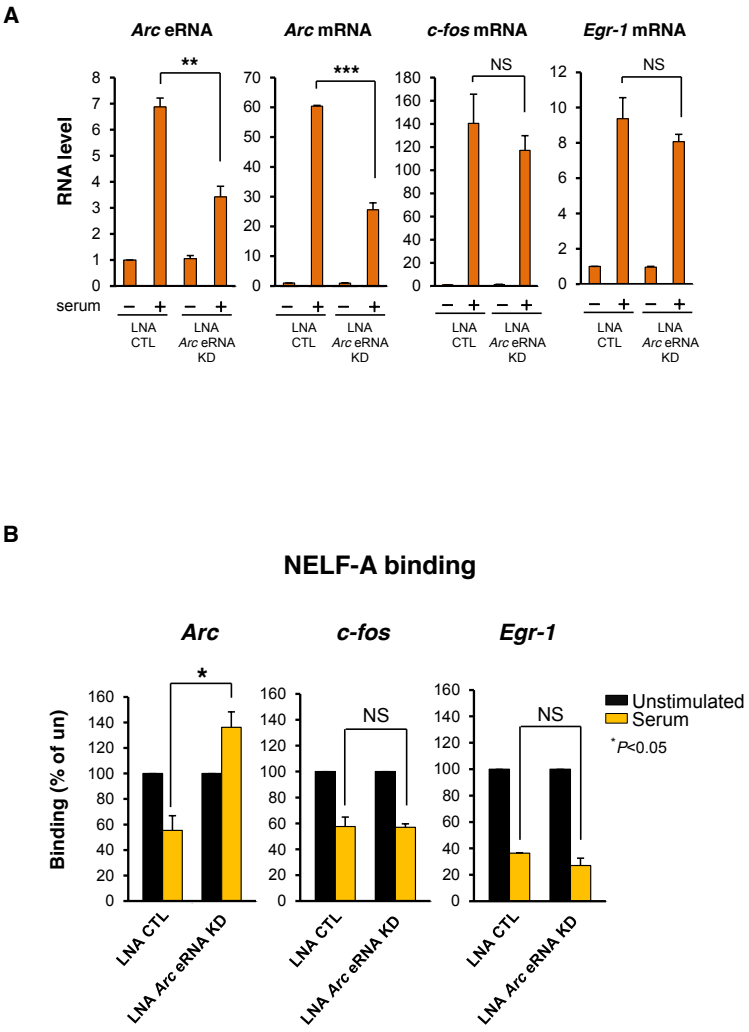

Figure 2.9 Reduction of eRNA expression inhibits the release of the NELF complex in NIH3T3 cells. (A) Knockdown of Arc eRNA using LNA decreased the induction levels of *Arc* eRNA and mRNA, but not *c-fos* and *Egr-1* mRNA expression levels. *Gadd45b* mRNA was not induced in the 3T3 cells. Levels of indicated RNAs were measured for LNA control and *Arc* eRNA knockdown (- strand) conditions after 30 min serum or unstimulated in NIH3T3 cells and normalized to the level of *Tbp* mRNA (n = 3 biological replicates). **(B)** Effect of *Arc* eRNA knockdown on NELF-A binding at the *Arc*, *c-fos* and *Egr-1* promoters (n = 2 biological replicates). Error bars indicate SEM. *P*-value from two-tailed t-test. NS, not significant.
Note: ChIP experiments performed by Jae-Yeol Joo.

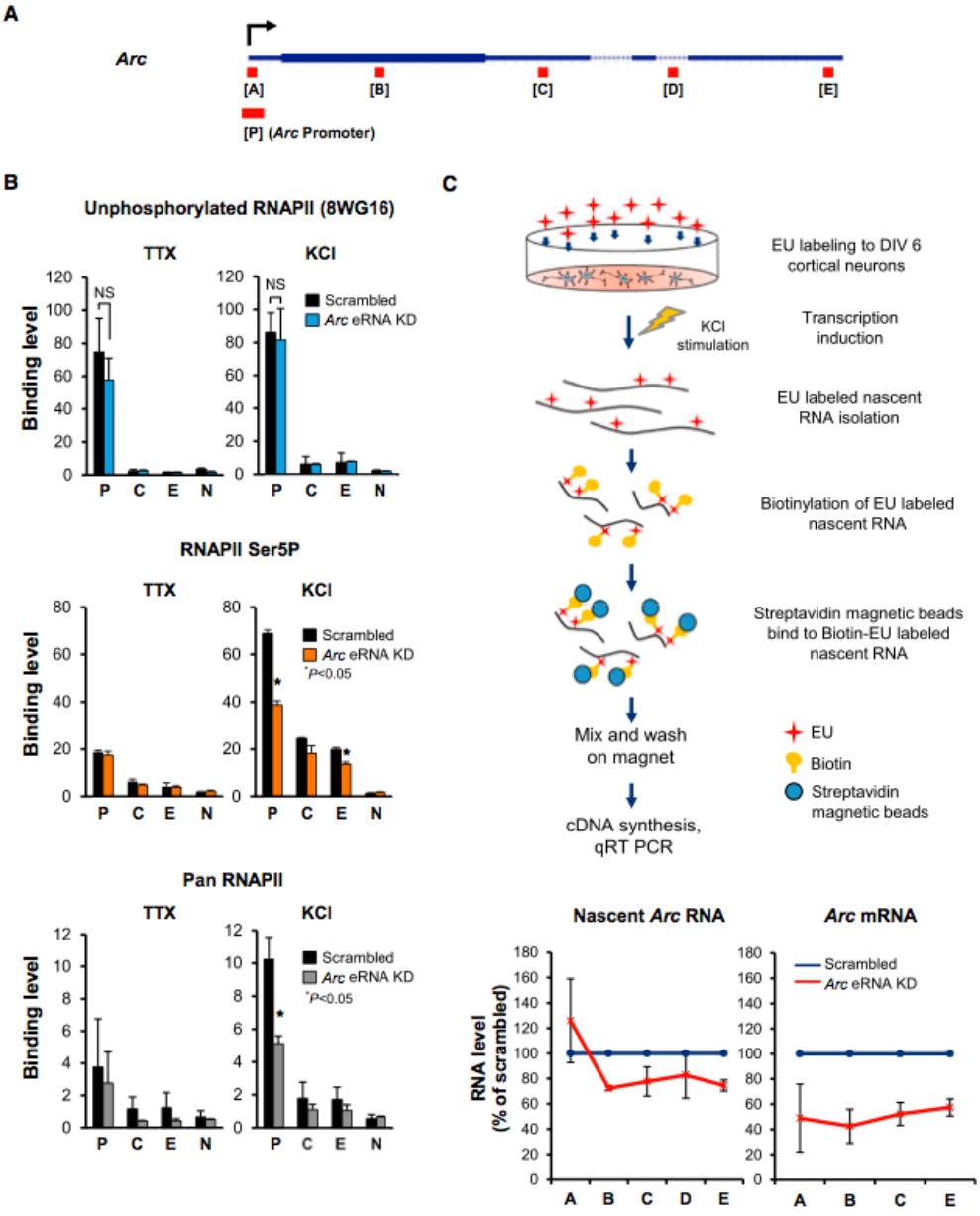

Figure 2.10 ***Arc*** **eRNAs promote efficient transition of RNAPII into productive elongation.** **(A)** Schematic diagram of primer sets used to measure binding levels (B) or RNA levels (C) at various locations along the *Arc* gene. **(B)** Effect of *Arc* eRNA knockdown on binding of unphosphorylated RNAPII (8WG16), RNAPII phosphorylated at Ser5 (Ser5P), and total levels of RNAPII (Pan RNAPII) (n = 2 biological replicates). Binding was determined at the following locations along the *Arc* gene: *Arc* Promoter [P], middle [C], 3' end [E], or a Negative control region [N]. **(C)** Schematic diagram of nascent RNA detection using a nascent RNA capture kit (top). RNA levels at various points along the transcript (primer sets A-E) are quantified using qRT-PCR (bottom) (n = 2 biological replicates). Error bars indicate SEM. *P*-value from two-tailed *t*-test. NS, not significant.

Note: The ChIP and nascent RNA experiments were performed by Jae-Yeol Joo.

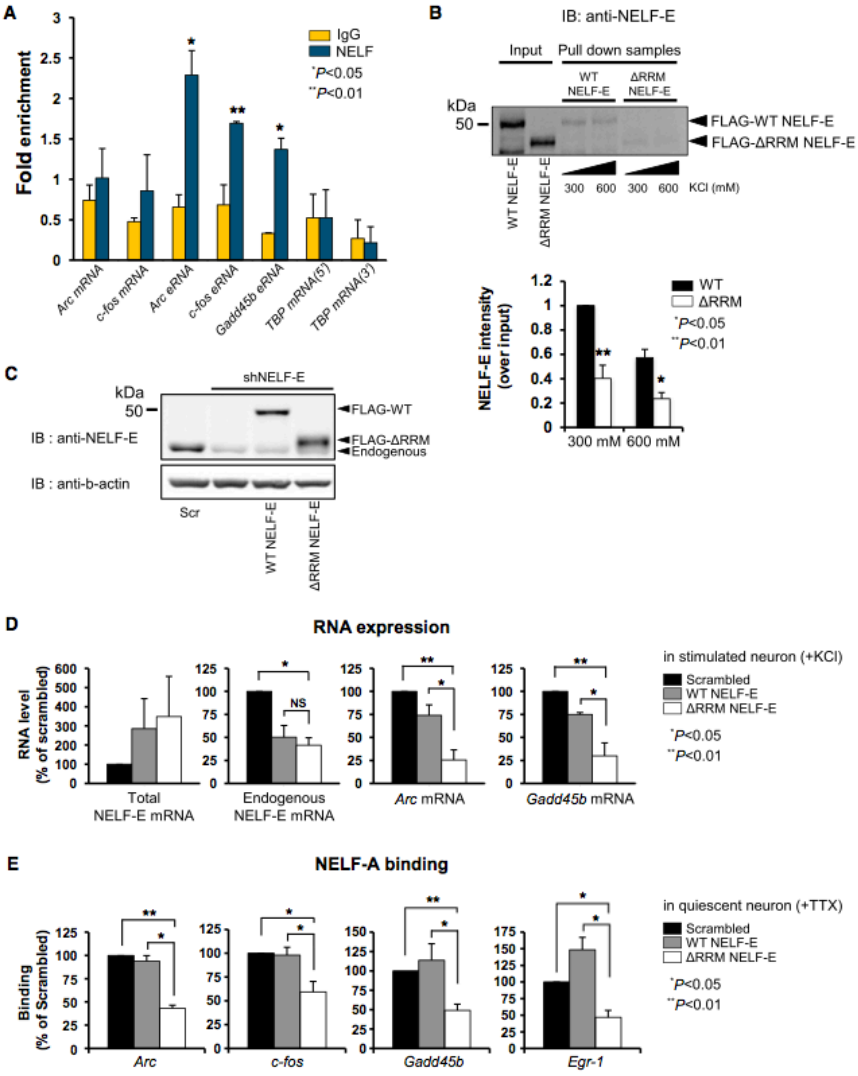

Figure 2.11 NELF-E directly interacts with eRNAs. (A) Ultraviolet-crosslinking RNA immunoprecipitation using KCl depolarized cultured cortical neuron lysates. Fold enrichment indicates the amount of RNA normalized to its respective input (n = 3 biological replicates). **(B)** Pull-down of FLAG-tagged wildtype (WT) or an RRM-deletion mutant (ΔRRM) of NELF-E overexpressed in HEK293T cells by *in vitro* transcribed biotinylated *Arc* eRNA. The top panel shows a representative western blot probed with anti-NELF-E. The bottom panel shows the quantification of the results, normalizing each lane to the corresponding input (n = 3 biological replicates). **(C)** Representative western blot showing the knockdown of NELF-E compared to a scrambled control shRNA and overexpression of either WT or ΔRRM NELF-E in cortical cultures. β-actin was used as a loading control. **(D)** Effect of replacement of endogenous NELF-E with FLAG-WT or FLAG-ΔRRM NELF-E on RNA levels during KCl depolarized conditions for total *Nelf-e* mRNA, endogenous *Nelf-e* mRNA, *Arc* mRNA, and *Gadd45b* mRNA. (n = 3 biological replicates). **(D)** Effect of replacement of endogenous NELF-E with FLAG-WT or FLAG-ΔRRM NELF-E on NELF-A binding during unstimulated conditions (n = 3 biological replicates, except *Arc* which has n = 2 biological replicates). Error bars indicate SEM. *P*-value from two-tailed *t*-test.

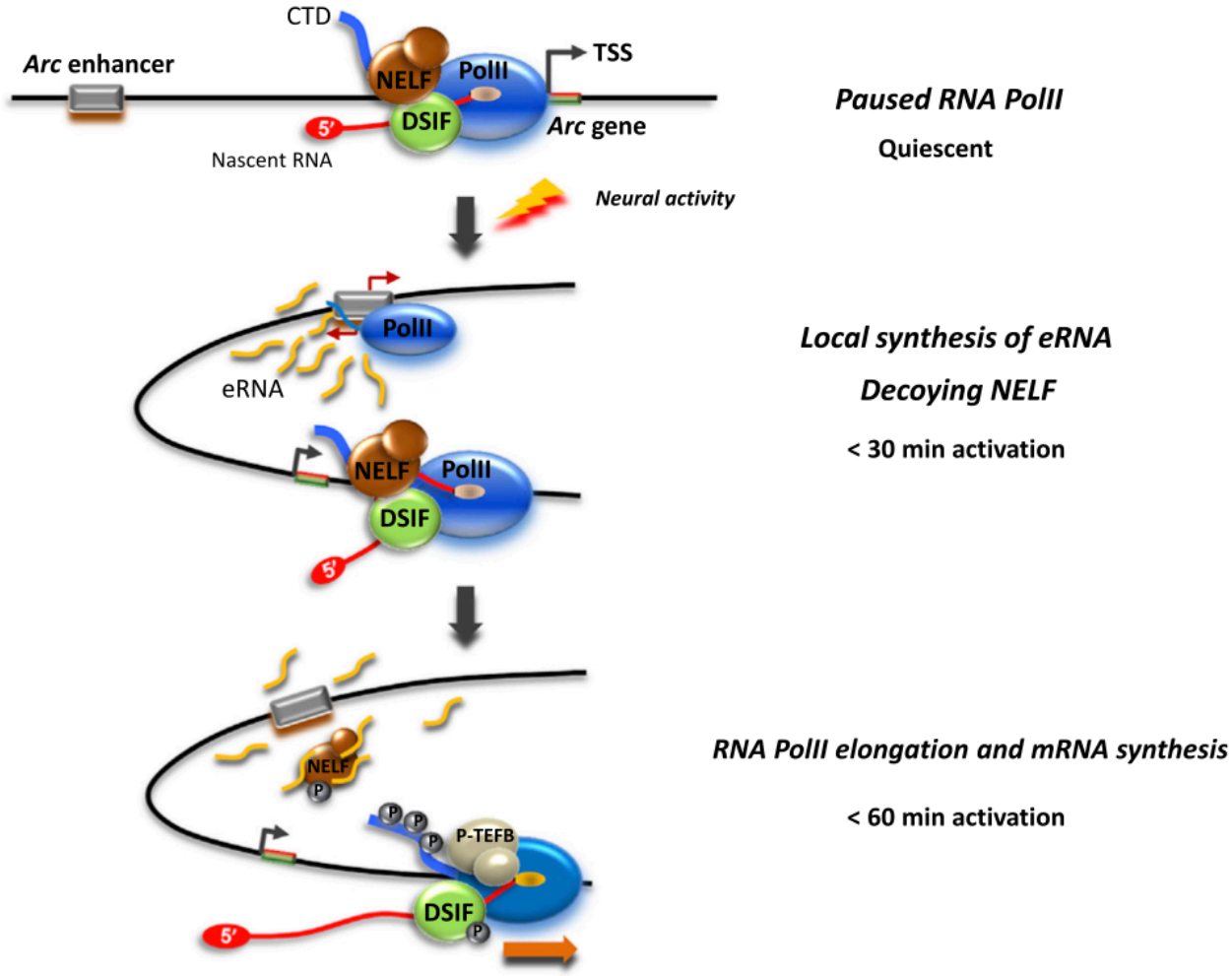

Figure 2.12 A model for *Arc* eRNA action during early transcription elongation. In response to neuronal activity, the enhancer of *Arc* is brought into close proximity with the promoter. The rapid local rise of *Arc* eRNA facilitates the dissociation of the NELF complex from paused RNAPII by competing with the nascent *Arc* mRNA emerging from paused RNAPII for NELF-E binding. P-TEFb is also recruited and phosphorylates RNAPII, DSIF, and NELF. The *Arc* eRNA is degraded before diffusing out, thus its effect is confined to the *Arc* gene. RNAPII is able to enter into productive elongation and *Arc* mRNA induction occurs.

2.4 Materials and Methods

Cell culture, stimulation, transfections, and retroviral infections. Primary mouse cortical neurons were dissected at embryonic day 16.5 (E16.5), and cultured in Neurobasal (NB) media supplemented with B-27 and Glutamax. For KCl mediated membrane depolarization, at days in vitro (DIV) 5 neurons were made quiescent by incubating with 1 μM TTX (Tocris) overnight, and then treated with 55 mM KCl to stimulate gene expression. For the bicuculline experiment, neurons at DIV 12-14 were treated with 50 μM bicuculline for 30 min. To generate lentiviruses, HEK293T cells were transfected using Fugene-HD (Promega) with a lentiviral construct containing the shRNA, along with the helper plasmids Δ8.9 and VsVg, and allowed to incubate for 48-72 h. For experiments with KCl mediated membrane depolarization, cells were infected with the lentiviral supernatant at DIV 3 and harvested at DIV 6-7.

LNA transfection of NIH3T3 cells. NIH 3T3 cells were transfected using Lipofectamine RNAiMAX (Invitrogen). 50nM of scrambled or *Arc* eRNA KD LNA were mixed with transfection reagent and incubated for 20 min at room temperature and then added into the cells. Cells were incubated with the transfection mixture overnight at 37℃, then the media was replaced with DMEM (Dulbecco's Modification of Eagle's Medium) with 10% fetal bovine serum (FBS) for 24 hours. The cells were then serum starved (in DMEM containing 0.5% FBS) for 24 h, after which the cells were stimulated (in DMEM containing 20% FBS) for 30 min, followed by immediate harvest with Trizol reagent (Invitrogen). The *Arc* minus strand targeting sequence is 5'–TGTGCAACCATATATG–3', with LNA nucleotides underlined.

RNA Circularization. Cultured cortical neurons were treated overnight with 1 μM TTX before being stimulated for 30 min with 55 mM KCl. Circularization was performed as previously described in (Kim et al., 2010). Briefly, RNA was extracted using Trizol (Invitrogen) as above, and treated with DNase I (Invitrogen) for 30 min in 1X DNase I buffer. DNase I was inactivated using 100 ul 25 mM EDTA and incubating at 75℃ for 10 min. RNA was extracted using Phenol/Chloroform and precipitated with ethanol. 10 ug of RNA was decapped using 25 U Tobacco Acid Pyrophosphatase (TAP, Epicentre Biotechnologies) for 1 h at 37℃, followed by Phenol/Chloroform extraction and ethanol precipitation. RNA was then circularized with T4 RNA ligase in the following reaction: 8 ug RNA, 50 mM Tris-HCl (pH 7.6), 10 mM $MgCl_2$, 1 mM ATP, 5% PEG-8000, 20 U T4 RNA Ligase, with a final volume of 2 ml. The reaction was incubated at 37℃ for 18 h, followed by 10 min at 65℃. Phenol/Chloroform extraction and ethanol precipitation were again performed. 1 ug of circularized RNA was reverse transcribed using the High-Capacity reverse transcription kit (Applied Biosystems). The cDNA was used in nested PCR, using Phusion High Fidelity polymerase in the HF buffer (NEB) according to the manufacturer's instructions, with the following primers: LeftCirc1 forward 5'-GATTTGGTGGCTGGTGTTCT-3', reverse 5'-AAAGCTAAAGGGGGCTACGA-3'; LeftCirc2 forward 5'-GGCAGAGTTACGAACCAGGA-3', reverse 5'-CCAGACCTGTGCAGATACCA-3'. PCR products were cloned using the TOPO TA cloning kit for sequencing (Invitrogen).

Chromosome Conformation Capture (3C). 3C analysis was performed as described (Tolhuis et al., 2002). Briefly, cultured neurons were harvested and cross-linked with 1% formaldehyde. Cross-linked cells were lysed with ice-cold lysis buffer (10 mM Tris, pH 8.0, 10 mM NaCl, 0.2% NP-40) containing protease inhibitor (Roche) for 15 min at 4℃ using rotating wheel. Nuclei

were resuspended in the 1X NEB buffer 3 containing 0.1% SDS and incubated for 10 min at 65℃. TritonX-100 was added to 1% and samples were then digested with BglII and NcoI or SacI restriction enzymes overnight at 37℃. SDS was added to 1.6% in order to inactivate the restriction enzyme for 25 min at 65℃. Triton X-100 was added to final concentration 1% and then samples were incubated at 37℃ for 1 hr, mixing occasionally. DNA was ligated using T4 ligase for 4 hr at 16℃ and 30 min at room temperature. Subsequently, 200 ug of protease K was added in order to remove the protein and then incubated overnight at 65℃ to reverse cross-link. The next day, samples were incubated with RNase (1 ug/ml) for 1 hr at 37℃, and the DNA was purified by phenol chloroform extraction and ethanol precipitation. The purified DNA was used as a qPCR template. Primers employed were: BglII *Arc* pro-rev anchor primer, 5′-AGTCAGTTGAGGCTCAGCAA-3′; BglII *Arc*-B2 primer, 5′-CTTTTTGCCCTGCATTAGAGT-3′; BglII *Arc*-B3 primer, 5′-GGCTCAGGAATTTGTCTCTC-3′; BglII *Arc*-B4 primer, 5′-GAGGTCTTGTATCCTGGCTG-3′; BglII *Arc*-B5 primer, 5′-CACACCAAATCTGCAGAGATT-3′; BglII *Arc*-B6 primer, 5′-GGCTGGAGACTGGTGACATT-3′; BglII *Arc*-B7 primer, 5′-CAGGTCCTGTCTATGCTCTT-3′; BglII *Arc*-B8 primer, 5′-GCATAAAGGCAGGCAACACA-3′; SacI *Gadd45b* pro-anchor primer, 5′-CGTGCAGTACTGCGGCTG-3′; SacI *Gadd45b*-S1 primer, 5′-CAGCAGGGCAAGGAGATAC-3′; SacI *Gadd45b*-S2 primer, 5′-GGCTACATGAGATTCAGTCTC-3′; SacI *Gadd45b*-S3 primer, 5′-CAGGTGTATGTTCACGCAGA-3′; SacI *Gadd45b*-S4 primer, 5′-

CTACACACCGCACCTACTG-3′; SacI *Gadd45b*-S5 primer, 5′-CAGGCACCCAGTGCTGAAG-3′; SacI *Gadd45b*-S6 primer, 5′-GAGCAGGGTTCAGAAAAGGG-3′. A bacterial artificial chromosome (BAC) clone containing the *Arc* or *Gadd45b* genes were used as a control template. The BAC plasmid was digested with BglII, NcoI or SacI restriction enzymes overnight at 37℃ and then ligated by T4 DNA ligase for 4 hr at 16℃. Subsequently, ligated DNA was purified by phenol/chloroform extraction and ethanol precipitation.

qRT-PCR. Total RNA was prepared from DIV6 cortical neurons using Trizol reagent (Invitrogen) according to the manufacturer protocols. Subsequently, RNA samples were reverse transcribed into cDNA using a High-Capacity reverse transcription kit (Applied Biosystems). Primers employed were: *Arc* promoter forward, 5′ -CGGTCAACAGATGCCGGTGGG-3′ , reverse, 5 ′ -GCCGGCCGCCAAACCCAAT-3 ′ ; *Arc* enhancer forward, 5 ′ -GGCTGGAGACTGGTGACATT-3′ , reverse, 5′ -CCATCTGCTTTCTCCTGGAA-3′ ; *c-fos* promoter forward, 5 ′ -GCCCAGTGACGTAGGAAGTC-3 ′ , reverse, 5 ′ -GTCGCGGTTGGAGTAGTAGG-3 ′ ; *Gadd45b* promoter forward, 5 ′ -CAATCTCAGCGCGGGATACT-3′ , reverse, 5′ -CAATCTCAGCGCGGGATACT-3′ ; *Gadd45b* enhancer forward, 5′-CTGAGTTCTCTCCCCAGCAC-3′, reverse, 5′-CTCACAGCAATCCTGCTTCA-3′; *Egr-1* promoter forward, 5′-CTCTTGGATGGGAGGGCTTC-3′ , reverse, 5′ -TCAAGGGTCTGGAACAGCAC-3′ ; Negative region forward, 5′ -ACCTGAAACTGTGGGGACAC-3′ , reverse, 5′ -ATGCCCTTTTGTCAACTTGG-3 ′ ; *Arc* enhancer (Left) forward, 5 ′ -

GAGATGATTTGGTGGCTGGT-3′, reverse, 5′-GAGATGATTTGGTGGCTGGT-3′; *Arc* coding forward, 5′-GTGAAGACAAGCCAGCATGA-3′, reverse, 5′-CCAAGAGGACCAAGGGTACA-3′; *c-fos* coding forward, 5′-ATCCTTGGAGCCAGTCAAGA-3′, reverse, 5′-ATGATGCCGGAAACAAGAAG-3′; *Gadd45b* enhancer forward, 5′-CTGAGTTCTCTCCCCAGCAC-3′, reverse, 5′-CTCACAGCAATCCTGCTTCA-3′; *Gadd45b* coding forward, 5′-GTTCTGCTGCGACAATGACA-3′, reverse, 5′-TTGGCTTTTCCAGGAATCTG-3′; *Egr-1* coding forward, 5′-AACACTTTGTGGCCTGAACC-3′, reverse, 5′-AGGCAGAGGAAGACGATGAA-3′; TBP forward, 5′-TGACTCCTGGAATTCCCATC-3′, reverse, 5′-TTGCTGCTGCTGTCTTTGTT-3′; GAPDH forward, 5′-AGGTCGGTGTGAACGGATTTG-3′, reverse, 5′-TGTAGACCATGTAGTTGAGGTCA-3′, *NEAT1* forward, 5′-TTGGGACAGTGGACGTGTGG-3′, reverse, 5′-TCAAGTGCCAGCAGACAGCA-3′; *Nelf-e* coding forward, 5' –TCAAACGTTCTCGGACCCTG-3', reverse, 5' -CTCTGGAACGGCTGGAAAGT-3'; *Nelf-e* 3' UTR forward, 5'-AGCTGGATTCCTTGTGCCTC-3', reverse, 5'-GAGGCTGACGGAGGTGAAAA-3'. PCR amplification conditions have been described (Kim et al., 2010). Statistical significance was evaluated by a paired two-tailed Student's *t*-test.

Chromatin Immunoprecipitation (ChIP). Cultured cortical neurons were treated overnight with 1 μM TTX. Next day, they were incubated with 55mM KCl for 30 min and then fixed with 1% formaldehyde for 10 min. ChIP was performed as described (Flavell et al., 2008; Kim et al., 2010). Briefly, cell lysate was incubated overnight with anti-NELF-A (A-20; SantaCruz), anti-

Cdk9 (ab6544; abcam), anti-Ser5P Pol II (ab5131; abcam), anti-8WG16 Pol II (COVANCE), anti- Pol II (N-20; SantaCruz), anti-RAD21 (ab992; abcam) or anti-Med1 (A300-793A; Bethyl labs) and then the lysate was incubated with Protein A/G agarose beads (Santa Cruz) for 2 h at 4℃. Subsequently, the agarose beads were washed with Low (150 mM NaCl, 20 mM Tris-HCl, 2 mM EDTA, 1% TritonX-100 and 0.1% SDS) and High (500 mM NaCl, 20 mM Tris-HCl, 2 mM EDTA, 1% TritonX-100 and 0.1% SDS) salt solutions, then agarose beads were washed using LiCl solution (250 mM LiCl, 10 mM Tris-HCl, 1 mM EDTA, 1% deoxycholic acid and 1% NP-40). Bound proteins were eluted by ChIP elution buffer (10 mM Tris-HCl, 1 mM EDTA and 1% SDS) for 10 min at 65℃. Samples were treated with RNase A (Qiagen) and Proteinase K (NEB) for post-immunoprecipitation and then the DNA was purified using a commercial DNA purification kit (Qiagen).

Analysis of EU-labeled nascent transcripts. The EU-labeled transcription experiment was performed with the Click-it Nascent RNA Capture kit (Invitrogen) protocol. Briefly, cultured cortical neurons were pulsed with 0.5 mM EU for 1 h at 37℃ and then total RNA was isolated. EU-labeled RNA was biotinylated with azide-modified biotin. Biotin-EU-labeled nascent RNA was captured on streptavidin T1 magnetic beads (Invitrogen) and then cDNA was synthesized using the High-Capacity reverse transcription kit and analyzed by qRT-PCR. Primers employed were: [A] forward, 5′-CAGGCTCGTCGCCGCTGAA-3′, reverse, 5′-GCAGAGCTCAAGCGAGTTCTC-3′; [B] forward, 5′-CTGCTTGAACTCCCACCACTT-3′, reverse, 5′-CCTGAGCCACCTGGAAGAGT-3′; [C] forward, 5′-CTTTAGCATCTGCCCTAGGAT-3′, reverse, 5′-TCATTCTGCTCCAGTGTCCAG-3′; [D] forward, 5′-GTGAGAGAACTGCTCACCAC-3′, reverse, 5′-CTATCCTGACCAAGCCTCAG-

3′; [E] forward, 5′-AGATGGTATGGGCAGACAGC-3′, reverse, 5′-GGACTAGGGAGACCCTGGAG-3′

Ultraviolet-crosslinking RNA Immunoprecipitation (UV-RIP). Cultured cortical neurons (1 x 10^8 millions) were harvested and UV-crosslinked at 400 nm (400 mJ/cm^2) in 10 ml ice-cold PBS with protease inhibitors. Neurons were incubated with ice-cold Low-salt lysis buffer (50 mM Hepes KOH, pH 7.5, 10 mM NaCl, 1 mM EDTA, pH 8.0, 10% Glycerol, 0.2% NP-40, 1% Triton X-100) containing protease inhibitor and RNase inhibitor (Promega) for 10 min at 4℃ using rotating wheel. Nuclei were resuspended in the ice-cold High-salt buffer (1 mM EDTA, pH 8.0, 0.5 mM EGTA, pH 8.0, 10 mM Tris, pH 8.0, 600 mM NaCl, 1% Triton X-100, 0.1% DOC) containing protease inhibitor and RNase inhibitor for 1 h at 4℃ using rotating wheel. After centrifugation, supernatants were diluted with Immunoprecipitation buffer (1 mM EDTA, pH 8.0, 0.5 mM EGTA, pH 8.0, 10 mM Tris, pH 8.0, 1% Triton X-100, 0.1% DOC) containing protease inhibitor and RNase inhibitor and incubated overnight with anti-NELF-E (H-140; Santa Cruz) or anti-normal rabbit IgG (Santa Cruz), and then the lysate was incubated with Protein A/G agarose beads for 2 h at 4℃. Subsequently, the agarose beads were washed with ChIP washing buffers. Bound proteins were eluted by ChIP elution buffer (10 mM Tris-HCl, 1 mM EDTA and 1% SDS) containing RNase inhibitor for 10 min at 65℃. Samples were treated with Proteinase K and DNase I (Roche) for post-immunoprecipitation and then the RNA was extracted by phenol/chloroform and ethanol precipitation. The extracted RNA samples were reverse transcribed into cDNA and used as a qPCR template. Primers employed were: TBP-5’ forward, 5’-GGTTTCTGCGGTCGCGTC-3’; TBP-5’ reverse, 5’-GCAAACTCCGGGGACCCG-3’;

TBP-3' forward, 5'-GTTCTCCTTATTTTTGTTTCTGG-3'; TBP-3' reverse, 5'-GTTCTAACACAGAAAATGCCAC-3'.

Western blot analysis. Protein extracts from cultured cortical neurons (DIV 6-7) were prepared with sample buffer (60 mM Tris-HCl, pH 6.8, 2% sodium dodecyl sulfate, 10% glycerol), and before loading mixed with loading buffer (5% 2-mercaptoethanol, 0.1% bromophenol blue) and boiled for denaturation. Proteins were separated by SDS-PAGE and analyzed by Western blot with anti-Arc (Synaptic Systems, 1:1000), anti-Gadd45b (H-70; SantaCruz, 1:500), anti-β-actin (Sigma-Aldrich, 1:5000), or anti-NELF-E (Abcam, 1:1000). Images were acquired by Odyssey (LI-COR) and quantified using ImageJ.

***Nelf-e* Constructs.** The open reading frame of mouse NELF-E (Origene) was cloned into p3XFLAG-CMV. The RNA recognition motif (RRM), consisting of amino acids 254 to 328, was deleted in the ΔRRM mutant. For replacement experiments, FLAG-tagged wildtype or ΔRRM NELF-E was also cloned into the pLLX vector containing a short hairpin RNA against NELF-E, as described previously (Zhou, et al. 2006), inserting FLAG-NELF-E after the Ubiquitin promoter followed by an IRES and GFP to monitor expression. To obtain maximum knockdown while maintaining levels of overexpression similar to endogenous, cells were infected with both shNELF-E alone as well as the overexpression constructs. The shNELF-E targeting sequence is 5'-CTGGATTCCTTGTGCCTCATA-3'.

Biotinylated RNA Pull-down. The minus *Arc* eRNA sequence was amplified from a BAC clone containing the *Arc* gene and cloned into the pBluescript SK(-) vector. The *Arc* minus strand was

transcribed from the T7 promoter using a commercial *in vitro* transcription kit (MegaScript; Ambion), supplementing the dUTP with 25% bio-16-UTP to produce biotinylated transcripts. The pull-down was performed as described previously (Tsai et al., 2010), with the following modifications. 10 ug of biotinylated *Arc* eRNA was heated to 85°C for 2 min, and then placed on ice for 2 min and supplemented with RNA structure buffer (10 mM Tris pH 7, 0.1 M KCl, 10 mM $MgCl_2$), and incubated at room temperature for 20 min. HEK293T cells were transfected with constructs containing FLAG-tagged wildtype or ΔRRM NELF-E and harvested using lysis buffer (150 mM NaCl, 1% TX-100, 2mM EDTA, 50 mM Tris pH 7.5). 500 µg of lysate were diluted with Pull-down buffer (100 mM KCl, 20 mM Hepes pH 7.5, 1.5 mM $MgCl_2$, 0.2 mM EDTA, 0.5 mM DTT) for a final concentration of 0.1% TX-100. The biotinylated RNA was incubated with the lysate for 1 h at room temperature with rotation. 100 µl of M-280 Streptavidin Dynabeads (Invitrogen) were added to the lysate-RNA mixture and further incubated for 1h at room temperature. Beads were washed with wash buffer (20 mM Hepes pH 7.5, 1.5 mM $MgCl_2$, 0.5 mM DTT, 0.2 mM EDTA, 0.1% TX-100) containing either 300 mM or 600 mM KCl. Protein was eluted using SDS buffer (120 mM Tric-HCl pH 6.8, 20% glycerol, 4% SDS) at 100°C for 10 min. Lysate was run alongside 1/40 input on a 10% SDS-PAGE gel, transferred using the Trans-blot Turbo (Biorad), and probed with anti-NELF-E (Abcam; 1:1000).

CHAPTER 3

A transcriptional program underlying homeostatic scaling

3.1 Introduction

3.1.1 AMPA receptor trafficking as a mechanism to regulate homeostatic scaling

In order to maintain an optimal level of firing, neurons employ homeostatic scaling to globally change their synaptic strength in response to differing activity levels. One way in which neurons regulated their synaptic strength is by regulating the amount of AMPA receptors (AMPARs) that are expressed on the surface of the synapse (Turrigiano, 2011; Turrigiano et al., 1998). AMPARs are ionic glutamate receptors that are sensitive to sodium, potassium, and, depending on the subunit composition, calcium. When they are activated, the influx of cations causes a depolarization of the cell, and as such, AMPARs are the main determinant of synaptic strength. The more AMPARs a synapse has, the greater a depolarization will be achieved, therefore representing a stronger synapse. When activity levels are low, neurons will increase the numbers of AMPARs at the surface, while the numbers of AMPARs will decrease when activity levels are high (Figure 3.1). This can be measured by labeling surface AMPARs or measuring the amplitudes of AMPAR-mediated current during miniature-excitatory post-synaptic events (mEPSCs). By both measures, treatment with the sodium channel blocker TTX causes an increase in AMPARs at the synapse, while the GABAA receptor blocker, bicuculline, which blocks all of the inhibitory input in the cultures, causes a decrease in AMPARs at the synapse (Ibata et al., 2008).

3.1.2 Local translational mechanisms

Many of the studies on mechanisms of homeostatic scaling have identified genes that are increased in response to neuronal activity, such as *Arc*, or local translational mechanisms to control the response, such as those by retinoic acid. *Arc* is locally translated at the synapse, and has been shown to play a role there by regulating AMPAR trafficking (Waung et al., 2008). In neurons from mice that lack *Arc*, scaling is disrupted as the basal levels of AMPARs are higher than normal, and the neurons are unable to dynamically regulate the amount of AMPARs at the surface (Shepherd et al., 2006). *Arc* is increased in response to activity, and actually promotes the endocytosis of AMPARs, suggesting that its main role may actually be in decreasing synaptic strength in response to an increase in activity. Retinoic acid (RA) was also shown to be necessary for scaling, but specifically in a manner that was dependent on local translation and independent of the transcriptional activity of the RA receptor (Aoto et al., 2008). RA synthesis was induced during multiple activity-blockade protocols that decreased the entry of postsynaptic Ca^{2+}, such as NMDAR and L-VGCC blockade (Wang et al., 2011b). This suggests that basal Ca^{2+} entry may be able to repress RA synthesis, but that low levels of Ca^{2+} trigger a derepression of RA that upregulates synaptic strength locally where activity levels are low.

3.1.3. A role for transcription and CaMKIV activity

Although increases in AMPA receptor levels can be seen as early as 4 – 6 h of activity silencing, this increase in synaptic strength can continue for up to 24 h or 48 h (Ibata et al., 2008). This time window of synaptic up-scaling suggests that nuclear signaling and transcription processes might be involved. Consistently, addition of the transcription inhibitor, ActD in cortical neuronal cultures blocked the TTX-induced increase in mEPSC amplitude. The group

went on to show that when activity is suppressed, CaMKIV phosphorylation is decreased, and that blocking CaMKIV, either with a blocker for the upstream CaMKK, STO-609, or a dominant negative version of CaMKIV, could mimic scaling (Ibata et al., 2008). This suggests that blocking CaMKIV may lead to a derepression of genes that are necessary for scaling. Another group also showed that CaMKIV played a role in scaling, but during the scaling that occurs in response to an increase in activity (Goold and Nicoll, 2010). Blocking CaMKIV in this scenario was able to block the decrease that is normally seen in AMPAR-mediated current, suggesting that CaMKIV is necessary for this direction of scaling, presumably through the genes that it is activates.

A recent study looked at genes that were regulated after 48 h of TTX or Bic, and focused on genes that were downregulated in response to TTX. Potassium channel genes, K_v1 and K_v7, were identified as downregulated genes, which could explain the increase in intrinsic excitability that occurs during homeostatic plasticity (Lee et al., 2015). Another study showed that DNA methylation played a role in regulating gene transcription in response to scaling, as knockdown of Tet3 disrupted the bidirectional changes in gene expression (Yu et al., 2015). However, how this enzyme specifically alters the sets of genes related to synaptic scaling has not been well explored.

3.1.4. The T-type voltage gated calcium channel in neurons

There are many sources of Ca^{2+} entry that a neuron can use. The GluA2-lacking AMPARs are permeable to Ca^{2+}, and the NMDAR and L-type voltage gated calcium channel (VGCC) allow Ca^{2+} entry as well. The NMDAR and L-VGCC have both been well documented to be critically important for mediating the gene induction resulting from an increase in activity

(Dolmetsch et al., 2001). However there are additional VGCCs present within the cell as well. While the L-, N-, P/Q-, and R-type channels are all high voltage activated channels (HVA), there is another type of VGCC, the T-type VGCC (T-VGCC) that is low voltage activated (LVA), meaning that it can be activated in response to lower membrane potentials (Iftinca and Zamponi, 2009). There are three subtypes of this channel, CaV3.1, CaV3.2, and CaV3.3, encoded by three separate genes, *Cacna1g*, *Cacna1h*, and *Cacna1i*, respectively. The T-VGCC has been implicated in regulating sleep behavior and pain, as well as seizure activity, and it is thought that it is important for these behavioral effects through the proper maintenance of the resting membrane potential of the cell (Cheong and Shin, 2013).

3.2 Results

3.2.1 Genome-wide identification of genes that are upregulated in response to TTX

In our effort to identify the transcription program that specifically mediates TTX-induced homeostatic scaling, we performed RNA-seq analysis from neuron cultures treated with TTX for 2 h or 6 h at days *in vitro* (DIV) 12. We reasoned that, since ActD blocked TTX-induced homeostatic up-scaling (Ibata et al., 2008), genes whose expression is increased upon activity suppression might be functionally implicated in the process. As a control, we also treated neurons with bicuculline (Bic) for the same time periods to ensure the neurons are transcriptionally responsive to bi-directional activity manipulations (Figure 3.2 A). We took the data from two biological replicates and identified differentially regulated genes at FDR < 0.05 and a fold change cutoff of 1.25. Although the magnitudes of the changes seen with TTX were much smaller than Bic-induced changes, there are a substantial number of genes that are reproducibly upregulated in response to TTX. A total of 73 genes were reproducibly induced by TTX whereas the Bic-mediated synaptic activity burst induced 888 genes at either time point.

These two gene sets showed little overlap, suggesting that gene induction in response to TTX and Bic are mediated by distinct pathways. (Figure 3.2 B). However, a large fraction of each gene set showed bi-directional changes, such that genes induced by TTX tend to be downregulated by Bic and vice versa (Figure 3.2 C). Under our filtering criteria, 28 out of 73 TTX-induced genes are significantly down-regulated by Bic (Figure 3.3 C). If TTX-induced genes were to actively mediate synaptic up-scaling through promoting AMPA receptor expression and/or trafficking to the surface, their expression should be decreased when neuronal activity is chronically increased, otherwise their gene products would functionally interfere with the synaptic down-scaling process. In principle, gene expression changes in any direction could be functionally relevant to homeostatic plasticity. Our data identifies members of the cadherin family, such as *Chd10* and *Pcdh20*, to be bidirectionally regulated, with their expression decreasing in response to TTX and increasing in response to bicuculline, and cell adhesion molecules, including N-cadherin (*Chd2*), have been previously implicated in scaling (Fernandes and Carvalho, 2016). Stargazin (*Cacng2*), a gene that is downregulated in response to bicuculline, has previously been identified as having a role in scaling in the visual cortex (Louros et al., 2014).

Gene ontology analysis of TTX-induced genes did not show strong enrichment of any particular functional category, but instead distributed throughout diverse functional categories such as MAPK signaling, RNA metabolism, and transcription (Figure 3.2 D). Notably, when compared to a well-curated list of Autism susceptibility genes, 7 out of the 73 TTX-induced genes have been implicated in ASDs: *Auts2, Cacna1h, Bbs4, Fan1, Ogt, Smg6, and Upf2*, and previously published studies identified associations of another 5 genes, including *Nptx1*, with disorders like schizophrenia and bipolar disorder (Table 3.1) (Fernandez-Enright et al., 2014;

Girirajan et al., 2013; Howerton et al., 2013; Ionita-Laza et al., 2014; Kalscheuer et al., 2007; Nguyen et al., 2013; Rajkumar et al., 2015; Sanders et al., 2013; Shinkai et al., 2002; Splawski et al., 2006; Sultana et al., 2002). The observed association of TTX-induced genes with psychiatric disorders suggests that activity suppression-induced gene expression might be important for proper cognitive function.

Among the 73 TTX-induced genes, we have chosen 8 candidate genes, (*Auts2, Cacna1h, Rps6ka5, Nos1, Elk1, Mical3, Txnip,* and *Nptx1*) for further analysis, in parallel with traditional immediate early genes like *Arc* and *c-fos* that show strong induction in response to Bic (Figure 3.2 E-G). Manual reverse transcription qPCR (RT-qPCR) was able to confirm the changes seen in the genome-wide data (Figure 3.3 A and B). A more extensive time course experiment revealed that there are roughly two groups of genes based on their induction kinetics, with one group peaking at about 6 h of TTX treatment, while another increases until 24 h (Figure 3.4). While the significance of the different kinetics of the two groups is unknown, this is reminiscent of the transcription induction profiles in response to an increase in neuronal activity (e.g., Bic or KCl treated condition), where rapid induction of immediate early genes is followed by a second wave of transcription of slowly induced genes (Flavell and Greenberg, 2008). The slower overall expression kinetics of TTX-induced genes also fit nicely with the previously shown time window for TTX-induced scaling of 4 - 48 h.

To examine the transcriptional response to activity suppression more directly, we used GRO-seq to globally measure actively transcribed genes in response to TTX treatment. For the 73 genes that we identified as TTX-inducible based on mRNA-seq, we find that most of them also show a similar increase in transcription levels determined by GRO-seq (Figure 3.5 A and 2B). As GRO-seq only detects nascent transcription activity of RNAPIIs during the nuclear run-

on (NRO) procedure, it generally shows faster expression kinetics than mRNA-seq. Of note, several genes identified in our list are extremely long genes with multiple isoforms. One such gene, *Auts2*, showed only a slight increase by GRO-seq when looking at the longest isoform, but in looking more closely, two of the shorter isoforms (uc008zut.1 and uc008zuu.1) showed much higher induction (Figure 3.5 C), suggesting isoform specific changes in expression in response to activity suppression. Additionally, by using primers targeting intronic regions to detect nascent transcripts, we measured the levels of *Nptx1, Auts2,* and *Txnip* pre-mRNAs and saw induction upon treatment with TTX (Figure 3.5 D). In parallel, we examined whether changes in mRNA stability would also contribute to the TTX-induced increase in mRNA levels (Figure 3.5 E). We blocked RNAPII transcription in TTX-pretreated or untreated control neurons by adding ActD, and monitored the decay rate of several candidate RNAs. Among tested genes, *Elk1* and *Mical3* showed a noticeable increase in mRNA stability when neurons were treated with TTX, but the rest of the tested genes showed little change in their mRNA stability. Taken together, our combined analysis of RNA-seq and GRO-seq strongly suggest that neurons have an intrinsic transcription network that can be induced in the absence of action potentials.

3.2.2 *Nptx1* is necessary for homeostatic upregulation of synaptic strength

To evaluate the functional significance of the transcriptional response in neurons under activity blockade, we tested one of our candidate genes, *Nptx1* for its role in synaptic up-scaling. *Nptx1* encodes a protein, NP1, which plays a role in clustering AMPA receptors at the cell surface, which may imply its function in synaptic scaling. In addition to an increase in RNA levels, there was also an increase in the total protein level of NP1 in response to TTX, that increased over time, but peaked at about 24 h of TTX treatment (Figure 3.6 A), supporting the

idea that this protein could be playing a role in increasing synaptic strength. We further observed an increase in surface expression of NP1 protein in neurons treated with TTX for 24 h (Figure 3.6 B). To directly test the functional role of NP1 in homeostatic scaling, we measured AMPA receptor mEPSC amplitudes and frequencies in dissociated hippocampal cultures infected with lentiviruses containing a short hairpin RNA (shRNA) targeting *Nptx1* or a scrambled control shRNA. While TTX treatment of neurons with the scrambled control for 24 h significantly increased AMPA-mediated mEPSC amplitude without a significant change in mEPSC frequency (Scr, veh: 6.04 ± 1.41; Scr, TTX: 8.83 ± 2.60; n.s. via Tukey's multiple comparisons test), knockdown of *Nptx1* blocked this increase in mEPSC amplitude (Figure 3.6 C and D). However, there was no difference in the cumulative distributions of mEPSC amplitude between neurons infected with the scrambled control and *Nptx1* knockdown in the vehicle condition, illustrating that the knockdown does not change baseline AMPA receptor surface expression (Figure 3.6 E and F, $p = 0.17$ via K-S test. $D = 0.4$). Conversely, sustained over-expression of NP1 protein alone caused a significant increase in AMPA receptor amplitude, occluding the effect of TTX treatment (Figure 3.6 F and G). There were no significant changes in mEPSC frequency when NP1 was knocked down or overexpressed (Scr, vehicle: 6.04 ± 1.41; KD, veh: 7.72 ± 2.37; OE, veh: 9.88 ± 1.36; n.s. via Tukey's multiple comparisons test). These results suggest that the TTX-induced increase in NP1 is functionally important for the homeostatic synaptic up-scaling process and also that the precise level of NP1 within the cell is critical for maintaining proper AMPA receptor levels at the surface.

3.2.3 SRF and ELK1 mediate TTX-dependent *Nptx1* induction

To further characterize the activity suppression induced transcription program, we conducted a screen of several activity-regulated transcription factors to see if any were necessary for *Nptx1* induction. Cortical neurons were infected with a lentivirus containing a scrambled control shRNA or an shRNA targeting one of the following transcription factors: SRF, CREB, MEF2A, or MEF2D. While knocking down CREB and MEF2A individually showed a slight decrease in the TTX-dependent induction of *Nptx1*, MEF2D knockdown had no effect (Figure 3.7 A and B). Notably, knockdown of SRF (Serum Response Factor) had a significant impact on *Nptx1* induction, reducing *Nptx1* levels during basal conditions as well as blocking the increase usually seen after TTX treatment (Figure 3.8 A). SRF knockdown also affected induction of *Rps6ka5* and *Auts2*. These activity-regulated transcription factors have been extensively characterized for their roles in transcription when neural activity is increased (Flavell and Greenberg, 2008). Their activities are tightly regulated by various calcium-dependent signaling pathways triggered by influx of extracellular calcium through the NMDA receptor and/or L-VGCC. However our finding suggests that at least some of these transcription factors might also promote transcription under the opposite condition when neural activity is chronically suppressed.

SRF has been known to work with other co-factors to convert specific signal inputs into differential gene activation (Knoll and Nordheim, 2009). Therefore, depending on its co-factor partners, SRF-dependent transcription is subject to various signaling pathways. The two best characterized co-factor families are the ternary complex factors (TCFs) and members of the myocardin family (MRTF). Both mitogen-activated protein kinase (MAPK) and Ca^{2+} signaling have been shown to regulate the activity of TCFs through extensive phosphorylation. Actin

signaling dynamically controls MRTF trafficking in which monomeric G-actins sequester them in the cytoplasm whereas filamentous F-actins trigger translocation of MRTFs into the nucleus to drive transcription with SRF. MRTFs are mainly composed of MRTF-A and MRTF-B, and Ternary complex factors (TCFs) are made up of ELK family members. Based on our RNA-Seq data, MRTF-A (*Mkl-1*), MRTF-B (*Mkl-2*), ELK1 (*Elk1*), and ELK4 (*Elk4*) are highly expressed in cortical neurons, while ELK-3 (*Elk3*) is expressed at an extremely low level (Figure 3.8 B). In order to determine which co-factor(s) is required for SRF-mediated transcription of the *Nptx1* gene, knockdown of both MRTF-A and MRTF-B with an shRNA targeting a common region between the two genes, and knockdown of ELK1 or ELK4 was performed in cortical cultures. Despite similar knockdown efficiency of each of the factors (Figure 3.8 C), only knockdown of ELK1 impaired the TTX-mediated induction of *Nptx1*, suggesting that the activating signal to increase *Nptx1* expression works through the SRF cofactor ELK1 (Figure 3.8 D). Interestingly, *Elk1* is the only co-factor gene that shows increased expression in response to TTX, which might be due to an increase in mRNA stability (Figure 3.2 G, 3.5 E, and 3.8 C). ELK1 knockdown also blocked induction of *Auts2* and *Cacna1h*. Therefore, ELK1 also participates in the TTX-dependent transcriptional induction possibly in conjunction with SRF.

In order to determine if the *Nptx1* gene is a direct target of SRF, we examined the promoter and enhancer regions of the *Nptx1* gene for SRF binding. We used the histone H3 lysine 27 acetylation (H3K27Ac) profiles recently determined for neuron cultures treated with 55 mM KCl or TTX to identify potential enhancer regions near the *Nptx1* gene, as H3K27Ac is a marker for active enhancers (Malik et al., 2014). Based on these profiles, we identified one potential enhancer downstream of *Nptx1* (E1; Figure 3.9 A). An interesting feature of this enhancer is that the H3K27Ac level was high under TTX-mediated activity suppression

(overnight treatment of TTX) but then decreased when neurons were depolarized by KCl. While the conditions in this experiment are opposite to ours, it would imply that the enhancer became activated by activity blockade. Further supporting this idea, qRT-PCR primers directed against this region detected enhancer RNAs (eRNAs) that were induced in response to TTX (Figure 3.9 B). As eRNAs have been shown to be a reliable marker of active enhancers within a given cell type (Kim and Shiekhattar, 2015), this also suggests that this region is an enhancer that is activated in response to activity suppression. To address whether this was a feature common to enhancers of TTX-induced genes, we compared the peaks that decreased in response to KCl genome-wide with our list of TTX-induced genes. Out of ~2000 H3K27Ac peaks that decreased in response to KCl, 600 genes were found within 10 kb of a peak, including 12 of our TTX upregulated genes (Figure 3.9 C, *left*). Expanding the distance to within 50 kb of an H3K27Ac peak, there were 2130 genes identified, 22 of which overlapped with our 73 TTX-upregulated genes (Figure 3.9 C, *right*), including *Txnip*, *Nos1,* and *Syt13* (Figure 3.10 A). The overlaps at both distances are significant (p=0.0001689 and p=0.0031693, respectively). This analysis suggests that there might be a genome-wide epigenetic mechanism to regulate the activity of a large number of enhancers, which in turn promotes transcriptional induction of specific gene sets in response to low activity levels.

We also looked for Serum Response Elements (SREs) containing the motif of $CC(A/T)_6GG$ in the genomic regions surrounding the *Nptx1* locus, using the Regulatory Sequence Analysis Tool (RSAT) (Miano, 2003; Thomas-Chollier et al., 2011). There are two canonical SRE sites, the first is ~20 kb downstream of *Nptx1* (SRE1), and the second ~10 kb upstream of *Nptx1* within an H3K27Ac peak present in the forebrain early in development (SRE2) (Figure 3.9 A and 3.10 B) (Nord et al., 2013). When allowing for 1 mismatch in the

motif, there is another potential SRE found within an intron (Intron; Figure 3.9 A) of *Nptx1* that is highly conserved evolutionarily. Our ChIP analysis with an antibody against SRF revealed that the SRF binding level increases ~ 2 fold in response to TTX at the site within the intron of *Nptx1*, while no such enrichment was seen at the upstream or downstream putative enhancer regions (Figure 3.9 D). These results suggest that SRF is directly regulating the transcriptional induction of *Nptx1* in response to activity suppression. We also observed TTX-induced ELK1 binding at the potential downstream enhancer (E1), suggesting that this cofactor is also directly affecting *Nptx1* transcription (Figure 3.9 E). The TTX-dependent increase in their binding levels at the *Nptx1* gene are much smaller than those at the *c-fos* gene promoter, which may simply reflect the smaller induction level of *Nptx1* mRNA.

3.2.4 Calcium-mediated signaling through T-type VGCC is critical for TTX-induced transcription

Previous studies suggested that TTX-induced synaptic up-scaling can be mimicked by a reduction in calcium (Ca^{2+}) influx through the L-type channel or by reduced activity of CaMKK and CaMKIV (Ibata et al., 2008; Turrigiano et al., 1998). However, having seen a role of SRF and ELK1 in *Nptx1* induction, we next investigated whether the activity suppression-induced transcription program would require a particular calcium-dependent signaling pathway. We first found that influx of extracellular calcium is necessary to activate the TTX-specific nuclear signaling. Pre-treatment of neurons with the calcium chelator, EGTA, or a cell permeable form of the compound, EGTA-AM, that only becomes active once inside the cell, was able to block the induction of *Nptx1* in response to TTX (Figure 3.11 A).

To determine the source of calcium entry, we then tested inhibitors of calcium channels important for nuclear gene expression upon an increase in neural activity: NBQX, a selective inhibitor of AMPARs, AP-5, an inhibitor of NMDARs, and nimodipine, a blocker of the L-type VGCC. Interestingly, none of these compounds were able to block TTX-mediated *Nptx1* induction, even though they were all, to varying degrees, able to block *Arc* induction by Bic (Figure 3.11 B). Next, we pretreated neurons with cadmium (Cd^{2+}), a general VGCC blocker, before addition of TTX, and observed a dose-dependent decrease in *Nptx1* induction (Figure 3.11 C). These results suggest that although the L-VGCC has been well documented as the major VGCC responsible for the activity-dependent transcription program, a different type of VGCC mediates TTX-induced transcription under activity suppression. To elucidate which VGCC is regulating the induction of genes during TTX treatment, we tested inhibitors of all known VGCCs (L-, N-, P/Q-, R-, and T-type VGCCs), and found that only T-Type VGCC blockers, NNC 55-0396 dihydrochloride, Mibefradil, and TTA-A2 significantly inhibited the *Nptx1* induction in response to TTX (Figure 3.11 D and E). All three subtypes of the T-VGCC are expressed in our cortical neuronal culture: CaV3.1 (*Cacna1g*), CaV3.2 (*Cacna1h*), and CaV3.3 (*Cacna1i*). One in particular, *Cacna1h* is also induced in response to TTX, and has been implicated in ASD (Figures 3.2, 3.3, and 3.12 A, and Table 3.1). Knockdown of *Cacna1h* was also able to block *Nptx1* induction, as well as a subset of the other TTX-induced genes we tested (*Auts2, Nos1, Rps6ka5*) (Figure 3.11 F and 3.12 B). Similarly, in addition to blocking the increase in *Nptx1*, treatment with the T-type blocker TTA-A2 was able to block the induction of other TTX-induced genes: *Cacna1h*, *Auts2*, and *Mical3* (Figure 3.12 C).

Furthermore, TTA-A2 blocked the TTX-induced increase in AMPA-mediated current, suggesting that in addition to being necessary for the regulation of a subset of TTX-induced

genes, the T-VGCC is also functionally required for homeostatic synaptic up-scaling (Figure 3.13 A). Unlike other VGCCs (L-, R-, N-, P/Q-types), the T-VGCC is a low-voltage activated (LVA) channel that can operate even when Na^+ channels are blocked by TTX (Iftinca and Zamponi, 2009). Due to their distinctive electrophysiological properties, the T-VGCC only opens within a small voltage window near resting membrane potential (Iftinca and Zamponi, 2009; Tsien, 1998). If the T-VGCC activity is required for mediating gene induction in the TTX treated condition, mild depolarization of neurons to potentials past the channel's window current should be able to block the induction seen with TTX. To test this idea, neurons were pretreated with 6 mM KCl before the addition of TTX, and we found that indeed, this was able to completely block the induction of *Nptx1* and *Auts2,* while there was no effect with pretreatment of 6 mM NaCl (Figure 3.13 B). This result is consistent with the premise that T-VGCC channels are responsible for this induction. To further characterize how this channel might be acting under TTX treatment, a time course experiment was performed to determine when the activity of the T-VGCC is necessary. Neurons were treated with the T-VGCC blocker NNC 55-0396 before or at increasing time points after TTX incubation. Measurements of *Nptx1* and *Auts2* induction revealed that the inhibitory effects of T-VGCC block decrease with greater delay in drug treatment (Figure 3.13 C). This suggests that prolonged channel activity throughout the duration of activity suppression mediates the upregulation of TTX-induced genes. This is in contrast to the gene induction in response to an increase in activity, in which an immediate early phase of calcium signaling through the L-VGCC and/or NMDAR following the activity increase seems critical for ensuring late long-term potentiation (LTP) (Deisseroth et al., 1996; Saha et al., 2011; West et al., 2002).

Despite the identification of the source of calcium, how this is able to signal to the nucleus is still unknown. We began by testing the necessity of components of the MAPK signaling pathways, as MAPK signaling is known to regulate ELK1/SRF transcription (Hill et al., 1993), and components of this pathway were identified in our GO analysis (Figure 3.2 D). However, different inhibitors of this pathway did not show significant effects on *Nptx1* induction (Figure 3.14 A). A previous study had shown that inhibition of CaMKIV, through blocking its upstream kinase CaMKK with STO-609, or a drop in somatic calcium influx through the L-VGCC, was sufficient to induce synaptic up-scaling in a manner similar to TTX (Ibata et al., 2008). We treated cells with STO-609 to determine whether CaMKIV could regulate the expression of TTX-induced genes in the same way. When cortical neurons were treated with STO-609, there was no significant difference in the TTX-dependent increase in *Nptx1* expression, and when cells were treated with STO-609 alone, there was no increase in *Nptx1*, and no change in the other TTX-induced genes (Figure 3.14 B). On the other hand, treatment of neurons with the CaMKII inhibitor KN-62 alone was sufficient to cause *Nptx1* induction to a level similar to TTX and also occluded the effect of TTX (Figure 3.14 C). Three additional genes showed a similar increase in their mRNA levels by KN-62 alone. Therefore, KN-62 alone seems to be sufficient to mimic the TTX-induced transcriptional changes of several genes. Blocking the L-VGCC and NMDAR individually, with nimodipine and AP5, respectively, induces *Nptx1* and *Auts2* expression as well, similar to when activity is suppressed by TTX (Figure 3.13 D). The gene expression driven by these treatments is also commonly inhibited by blocking the T-VGCC, which suggests a common mechanism (Figure 3.13 E). Therefore, the TTX-induced transcription program we have defined is related to the signaling pathway previously characterized for

synaptic up-scaling (Ibata et al., 2008; Turrigiano et al., 1998) and that the T-VGCC activity is required for this TTX-induced transcription program.

3.2.5 Gene induction occurs during activity suppression *in vivo*

Homeostatic scaling has been shown to occur in layer 2/3 (L2/3) pyramidal neurons of the visual cortex upon visual deprivation (Goel and Lee, 2007; Lambo and Turrigiano, 2013; Maffei and Turrigiano, 2008). In order to see whether the synaptic up-scaling observed in the visual cortex is accompanied by a transcriptional response during dark rearing (DR), we housed mice in the dark for 24 h and then measured RNA levels in the visual cortex compared to mice that were housed in a normal 12 h light/dark cycle (Figure 3.15 A). Our DR condition led to a significant decrease in the expression of activity-induced genes such as *c-fos* and *Arc*, which is also similar to what occurs during TTX treatment in cortical neuron cultures. Under this condition, we found that a subset of TTX-induced genes, including *Nptx1*, were upregulated (Figure 3.15 B). However, we should note that not all tested genes were induced by DR, which is possibly due to an issue with detection sensitivity resulting from tissue heterogeneity. Alternatively some homeostatic plasticity genes might exhibit developmental stage- or brain region-specific expression patterns. In addition to an increase in RNA levels, we also observed an increase in NP1 protein levels by both western blot and immunohistochemistry in the visual cortex following 3 d of DR (Figure 3.15 C and D). Though dark rearing represents a physiological method to induce synaptic scaling, it does not suppress all spontaneous action potentials in the retina (Hengen et al., 2016). In order to better reproduce the *in vitro* findings, we performed intraocular injections of TTX, which silence all activity coming from the retina, and has previously been shown to trigger scaling up of AMPAR activity in the visual cortex (Desai et

al., 2002; Frenkel and Bear, 2004) This alternative visual deprivation protocol was also able to show an increase in most of the tested TTX-induced genes in a more reliable manner than the dark-rearing paradigm. Taken together, these results indicate the existence of an intrinsic transcription program that can induce expression of specific genes in response to activity suppression *in vivo*.

3.3 Conclusions

Together this study has identified the genes that are upregulated in response to activity suppression that make up an intrinsic transcriptional program that is activated in response to an absence of activity. One such gene, *Nptx1*, also plays a functional role in regulating the up-scaling of synaptic strength. Interestingly, a transcription factor known to be regulated by an increase in activity, SRF, was identified as being necessary for gene induction in this opposite condition. One of its known co-factors ELK1, was also necessary, and showed inducible binding at a region that is expected to be an enhancer based on H3K27Ac profile surrounding *Nptx1*. The region showed high levels of acetylation during the quiescent condition (TTX overnight) and expressed eRNAs in response to TTX, suggesting that this enhancer might be more active when activity levels are low. This appeared to be a genome-wide mechanism for many genes, as this pattern was seen surrounding other TTX-induced genes as well.

Even though TTX suppresses activity, and presumably most of the Ca^{2+} entry that would occur in response to activity, this gene induction was Ca^{2+} dependent, suggesting that there is still an active pathway control this response. The source of the calcium, surprisingly, was not through channels known to be important for transcription induced by an increase in activity, such as the NMDAR and L-VGCC, but instead appeared to be through the T-VGCC, a unique channel

based on its being a LVA VGCC. Three different blockers of this channel were able to inhibit *Nptx1* induction, while knocking down CaV3.2 (*Cacna1h*) also blocked induction. Additionally, blocking the T-VGCC blocked TTX-induced scaling. The fact that a slight depolarization of the cell with 6 mM KCl could block induction further suggested that it was the T-VGCC mediating this response, as the T-VGCC is inactivated at higher membrane potentials. Together this provides evidence for a novel role of the T-VGCC in regulating the activity-suppression induced transcription program that promotes the increase in synaptic strength during scaling (Figure 3.16).

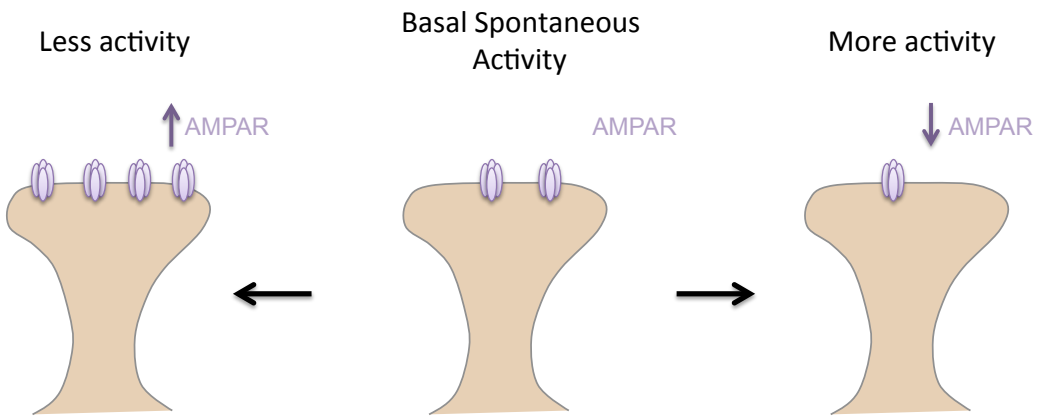

Figure 3.1 AMPAR trafficking as a mechanism to regulate homeostatic plasticity. Under basal conditions, neurons maintain a population of AMPARs at the surface of the synapse, which is a major determinant of synaptic strength (*center*). In response to a decrease in activity, neurons increase the number of AMPARs at the surface, leading to an increase in synaptic strength (*left*), while in response to an increase in activity, neurons decrease the number of AMPARs at the surface, leading to a decrease in synaptic strength (*right*). These mechanisms ensure that the neuron is able to maintain a stable firing pattern.

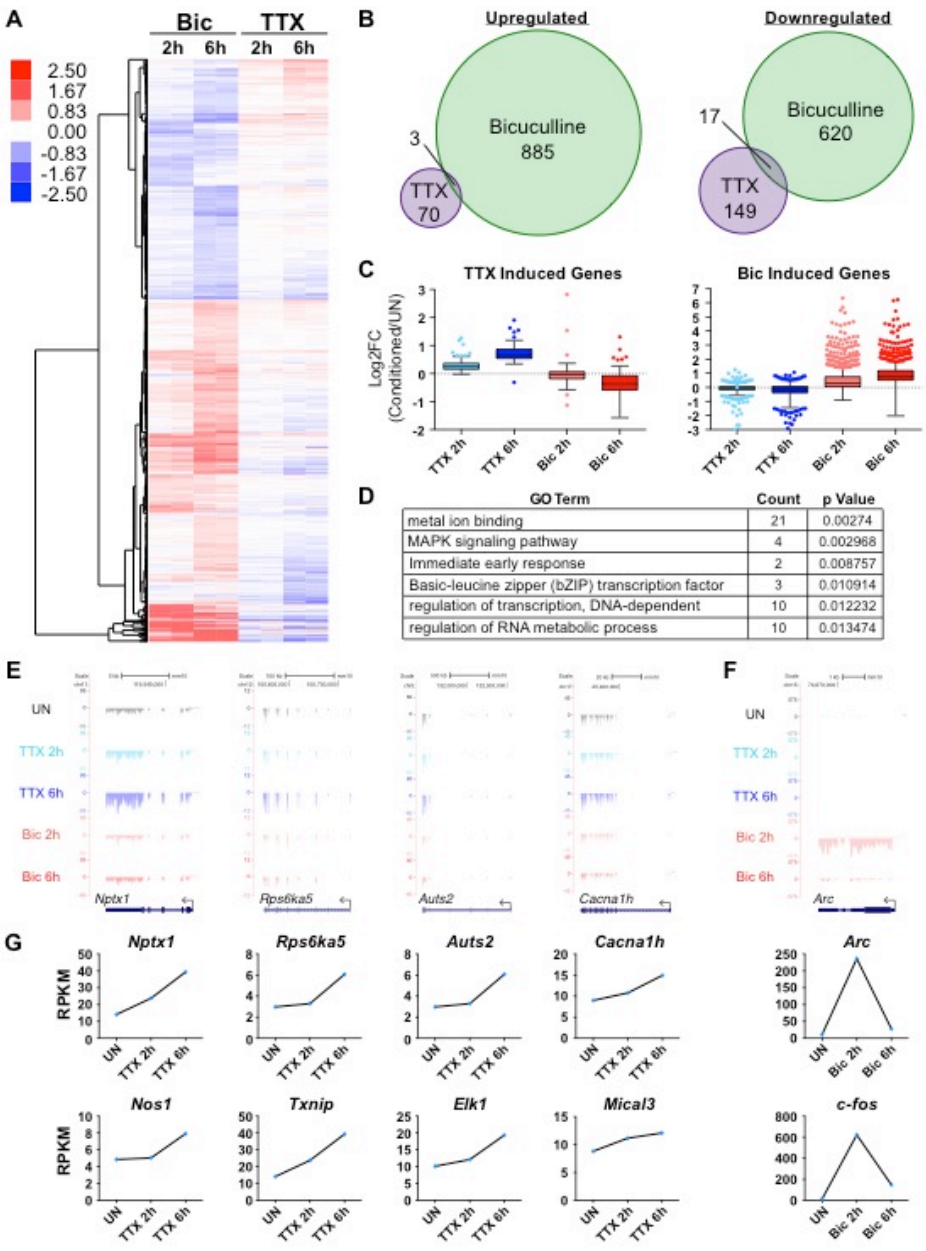

Figure 3.2 RNA-Seq identifies a subset of genes upregulated in response to TTX (A) A heatmap demonstrating the expression of genes that are regulated by either TTX or Bic at 2 h or 6 h of indicated treatments in cortical neurons. The 2 h and 6 h columns each contain two lanes showing replicates of the indicated treatments. **(B)** Venn diagram showing the overlap between TTX and Bic upregulated (left) and downregulated (right) genes. **(C)** Box plots of the Log2 values for TTX upregulated genes (left) or Bic upregulated genes (right) in each different condition normalized to the unstimulated (UN) condition. A grey dotted line is present at 0 to represent no change. **(D)** Select GO terms identified for the TTX upregulated genes. **(E)** Genome browser views of example genes that are upregulated by TTX: *Nptx1*, *Rps6ka5*, *Auts2*, *Cacna1h*. **(F)** Genome browser views of an example gene that is upregulated in response to Bic: *Arc*. **(G)** Graphs displaying the reads per kilobase of transcript per million mapped reads (RPKM) values of the genes for the indicated conditions. **** Note: bioinformatics performed by Gokhul Kilaru.***

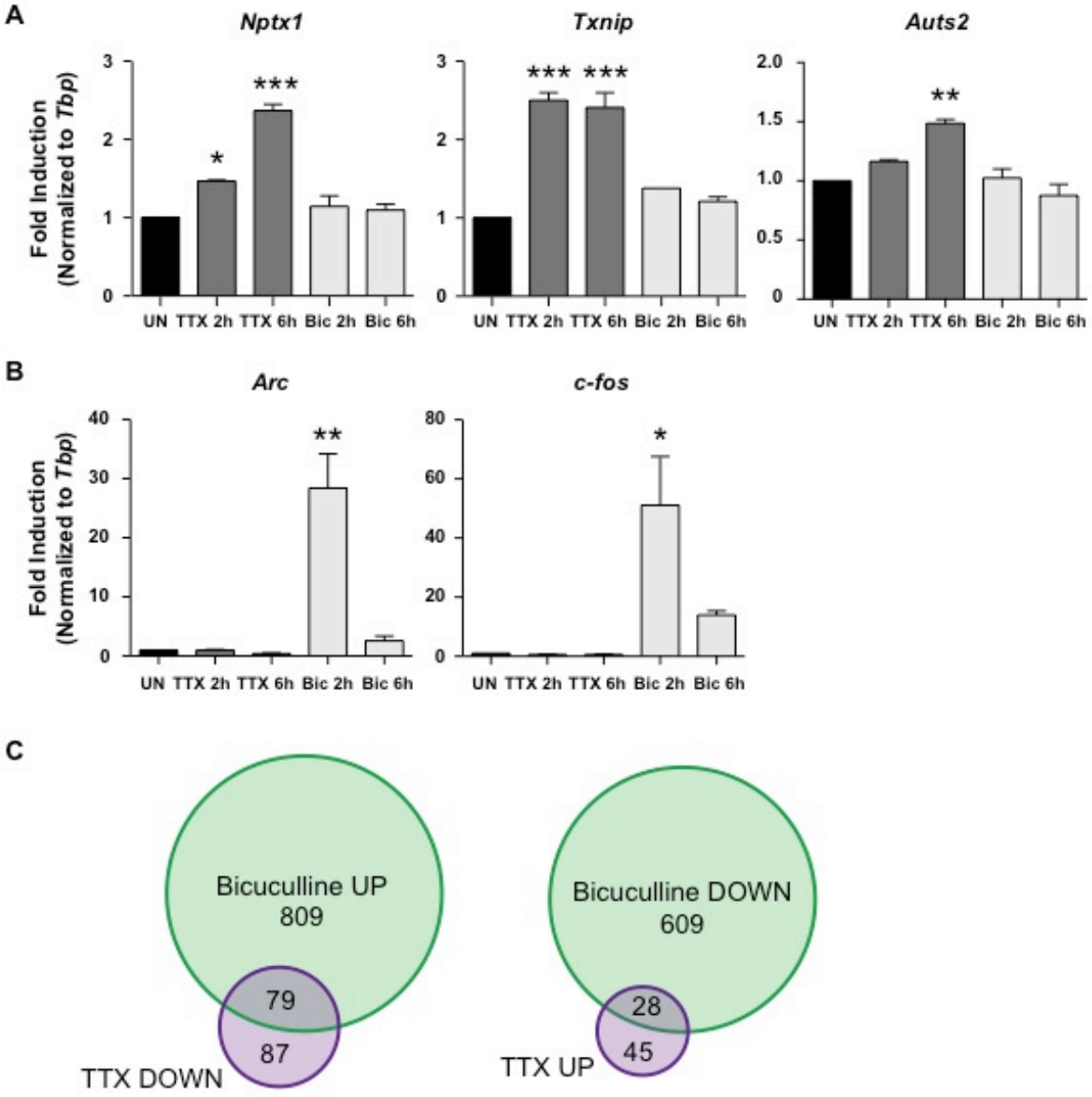

Figure 3.3 Confirmation of genome-wide data with qRT-PCR, qRT-PCR results of TTX induced genes **(A)** and Bic induced genes **(B)** from cells that were treated with TTX or Bic for the indicated time points. n = 2 biological replicates. **(C)** Venn diagrams of bidirectional genes, comparing genes upregulated by bicuculline and downregulated by TTX (left) or genes downregulated by bicuculline and upregulated by TTX. *, $p < 0.05$; **, $p < 0.01$; ***, $p < 0.001$. p values determined by a one-way ANOVA using Dunnett's multiple comparisons test.

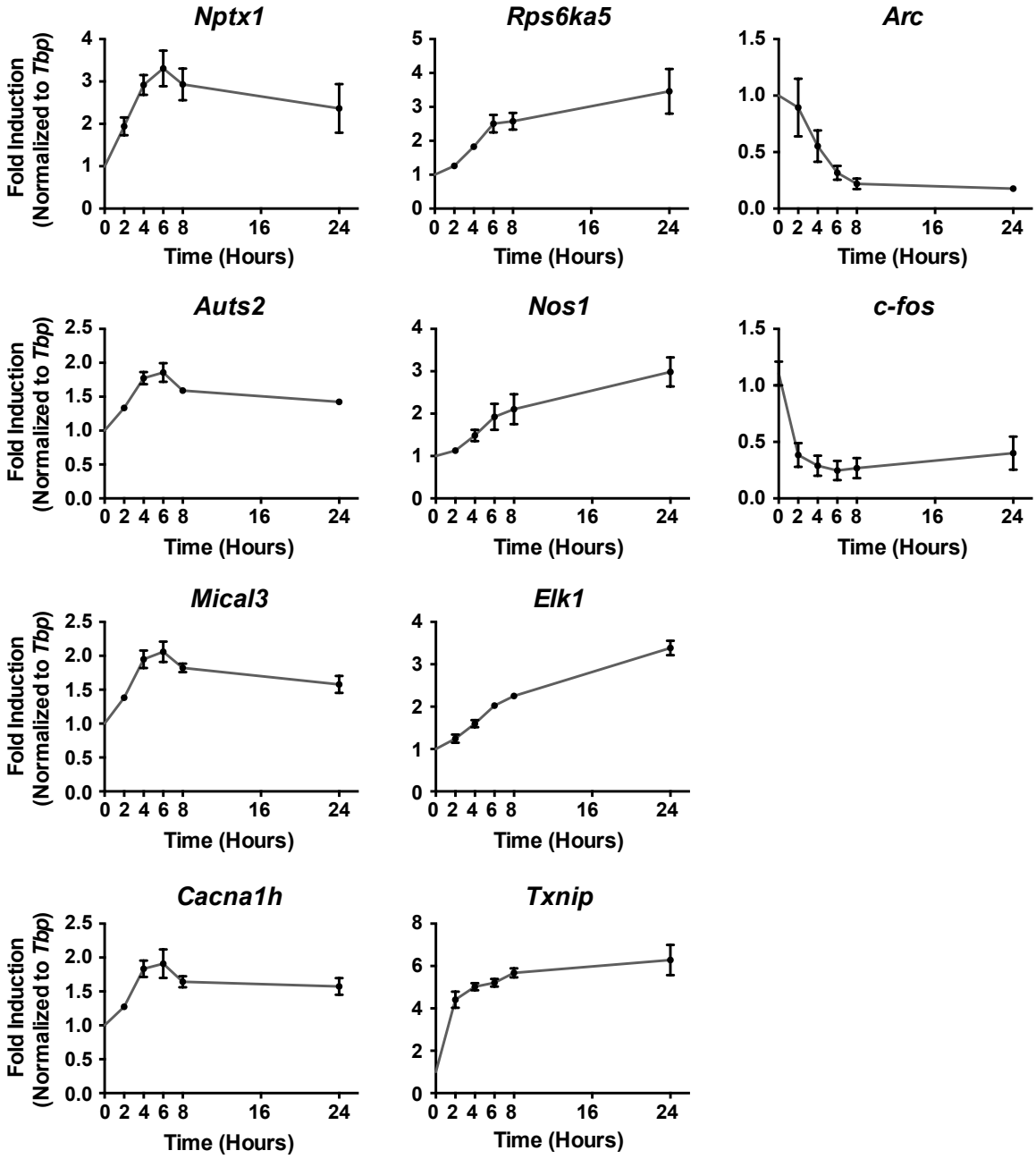

Figure 3.4 There are two waves of TTX-dependent gene induction. qRT-PCR results from cells that were treated with TTX for the indicated time points. RNA levels were measured for the indicated genes. The columns represent distinct classes of genes based on their induction patterns. The left column contains genes that peak around 6 h of TTX treatment, while the middle column contains genes that continue to rise until 24 h. The right column contains immediate early genes that are induced in response to Bic, and decrease with TTX treatment. n = 3 biological replicates. Error bars represent SEM.

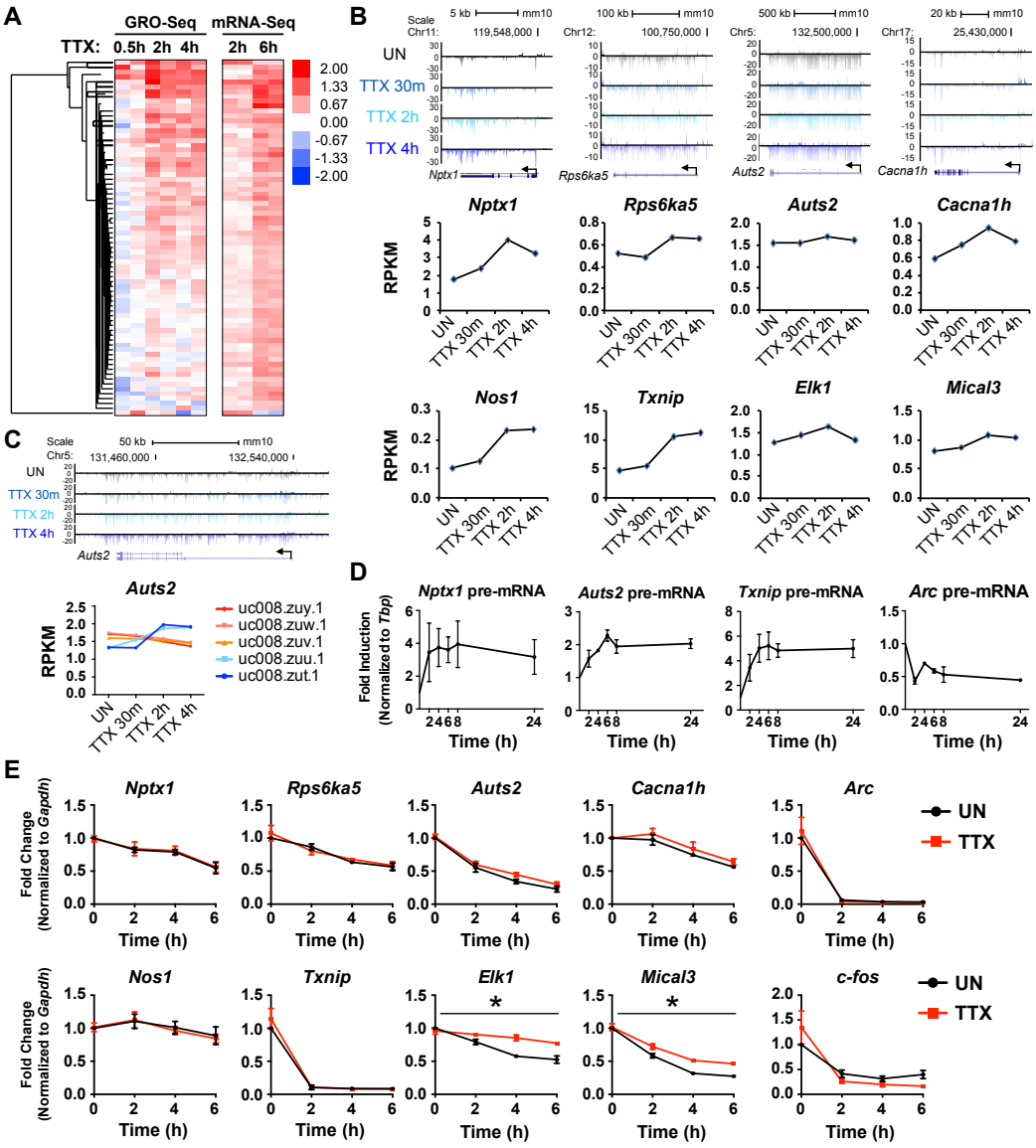

Figure 3.5 GRO-Seq confirms an active transcription program in response to activity-suppression. (A) Heatmap of the 73 TTX-upregulated genes identified by mRNA-seq, showing their expression normalized to unstimulated. Each time point shows the data of two biological replicates. **(B)** Genome browser views showing the global nuclear run-on sequencing (GRO-Seq) tracks aligned with 4 of the candidate genes in response to 30 min, 2h, or 4h TTX treatment. Below the tracks are graphs displaying the RPKM values for each condition. **(C)** A genome browser view of the shorter isoforms of *Auts2* (top), along with isoform specific RPKM values for the indicated time points (bottom). **(D)** qRT-PCR results from cells that were treated with TTX for the indicated time points. pre-mRNA levels were measured for the indicated genes. n = 3 biological replicates. **(E)** RNA levels of the indicated genes after treatment with Actinomycin D (Act D) for the indicated time points, with or without a 15 min pretreatment with TTX. n = 3 biological replicates. Error bars represent SEM. *, $p<0.05$. p values were determined by a two-way ANOVA. ***Note: GRO-Seq performed by Seung-Kyoon Kim.***

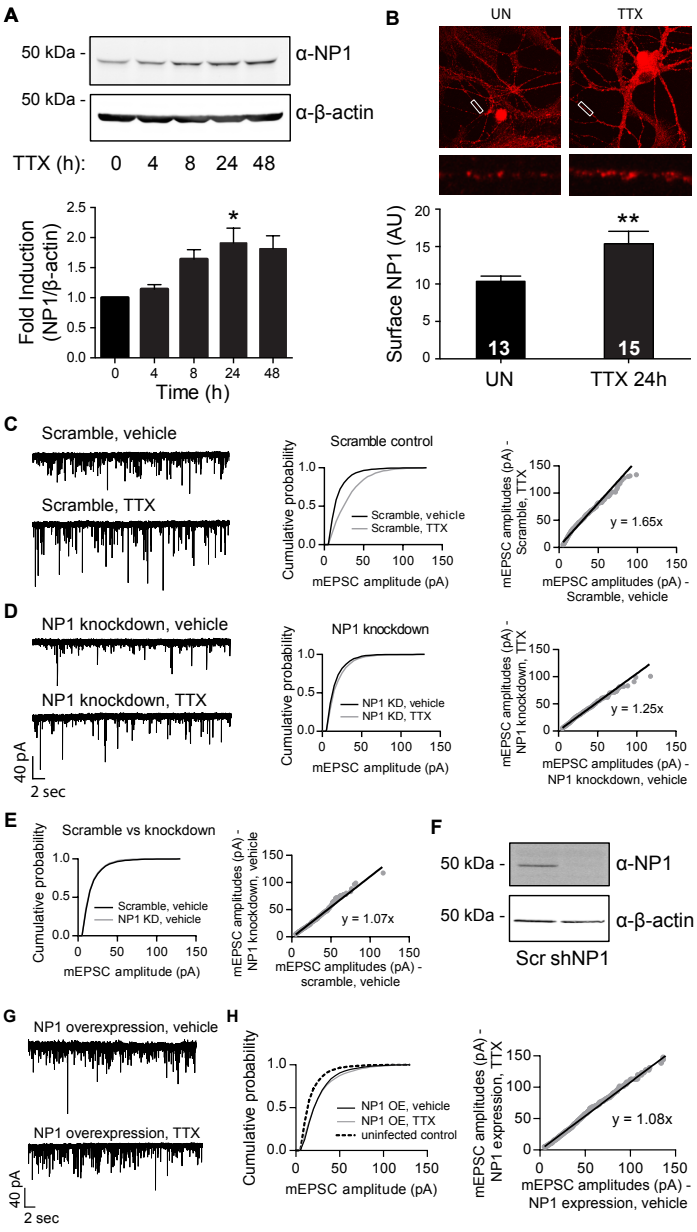

Figure 3.6 *Nptx1* is functionally important for homeostatic scaling. (A) Western blot of NP1 and β-actin expression in cortical neurons that were treated with TTX for the indicated time points (top) and the quantification of the induction (Bottom). n = 3 biological replicates. **(B)** Staining of surface NP1 levels on neuronal dendrites in unstimulated (UN) or TTX treated (24h) conditions, with the quantification below. n = 13 and 15 dendrites for UN and TTX conditions, respectively. **(C, D)** Example traces, cumulative probability histograms, and rank order plots of AMPA-mediated mEPSC amplitudes from cells treated with either vehicle or TTX after infection with the scrambled control **(C)** or NP1 knockdown **(D)**. Scramble vehicle (n = 9) vs Scramble TTX (n = 8) p = 1.5x10-74, D = 0.31. Knockdown vehicle (n = 7) vs Knockdown TTX (n = 8) p = 7.3x10-5, D = 0.08. **(E)** The cumulative probability histograms from vehicle-treated conditions of either the scrambled or knockdown cells from **(C)** and **(D)** overlaid. p = 0.03, D = 0.17. **(F)** Representative western blot of the efficiency of NP1 knockdown in the scaling

experiments. **(G)** Example traces of AMPA-mediated mEPSCs from either vehicle or TTX treated cells when NP1 is overexpressed. **(H)** Cumulative probability histograms of AMPA-mediated mEPSC amplitudes from cells overexpressing NP1 in either vehicle or TTX treated conditions indicate that TTX-induced scaling is occluded by high NP1 levels. NP1/TTX ($n = 11$) vs NP1/veh ($n = 10$), $p = 0.005$, $D = 0.055$. *, $p < 0.05$; **, $p < 0.01$. p values determined by an unpaired Student's t-test. Statistical significance between cumulative probability graphs was determined by the Kolmogorov-Smirnov test. Error bars represent SEM.
Note: electrophysiology performed by Austin Reese.

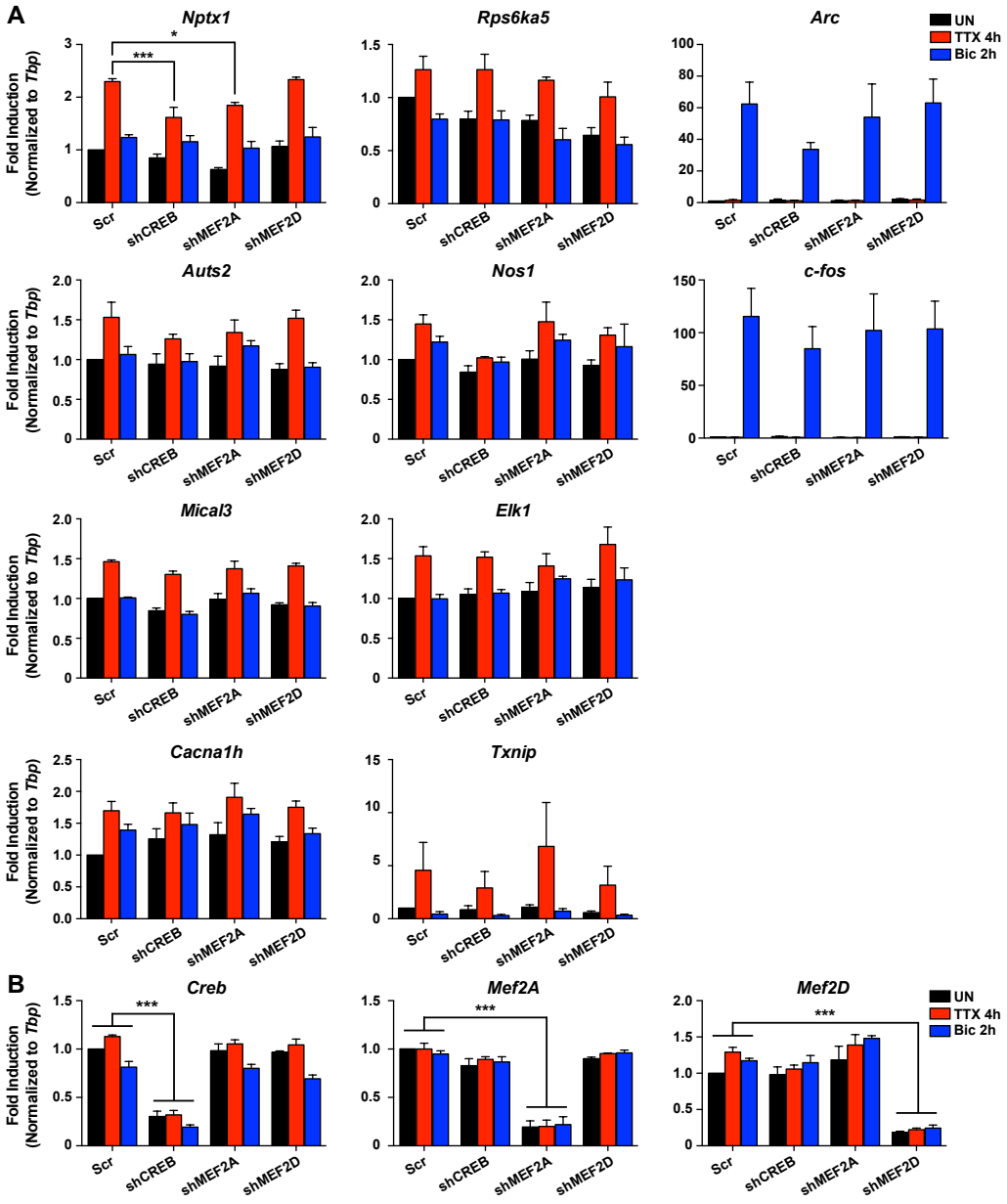

Figure 3.7 Effects of activity-regulated transcription factors in TTX-dependent induction. Cortical neurons were infected with lentiviruses containing a scrambled shRNA control or an shRNA targeting CREB, MEF2A, or MEF2D. **(A)** RNA levels of the indicated TTX or Bic induced genes were measured with qRT-PCR. **(B)** RNA levels of the indicated transcription factor genes were measured with qRT-PCR to test knockdown efficiency. n = 3 biological replicates. *, $p < 0.05$; **, $p < 0.01$; ***, $p<0.001$. p values determined by a two-way ANOVA with Tukey's multiple comparisons test. Error bars represent SEM.

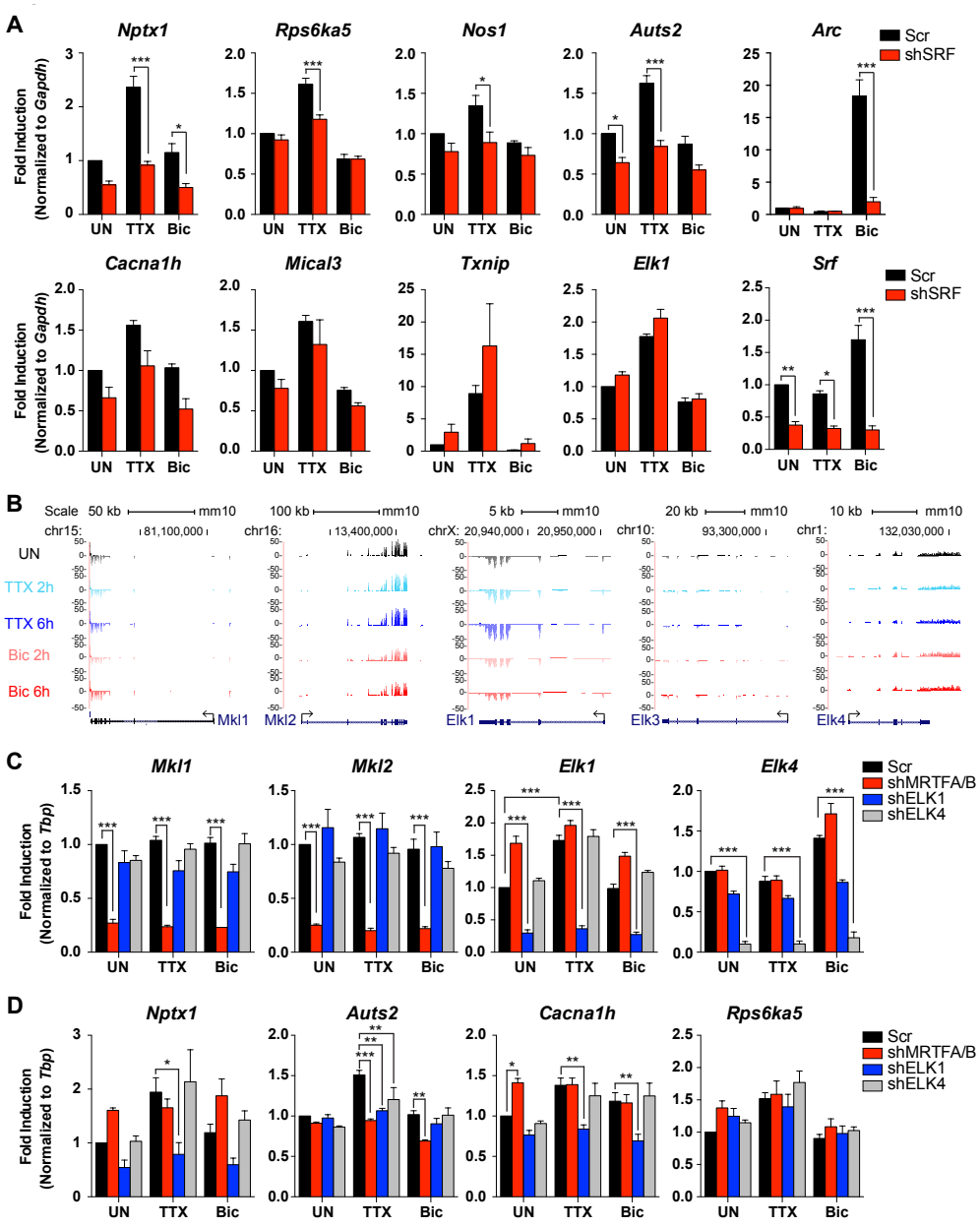

Figure 3.8 SRF and its cofactor ELK1 regulate the expression of *Nptx1*. (A) qRT-PCR results of TTX-induced genes from cells that were infected with the scrambled control or shSRF knockdown. Cells were left untreated (UN) or treated with TTX or Bic. n = 3 biological replicates. The Bic induced gene *Arc* and the transcription factor gene *Srf* were tested as controls of knockdown efficiency. **(B)** UCSC genome browser views of the SRF cofactor family members: *Mkl1*, *Mkl2*, *Elk1*, *Elk3*, and *Elk4* (left to right). **(C)** qRT-PCR results of the cofactor family members after knockdown of the indicated family member (shMRTFA/B, shElk1, or shElk4) compared to a scrambled control. Cells were either left untreated or treated with TTX or Bic. **(D)** qRT-PCR results of TTX-induced genes after the indicated cofactor knockdown. n = 3 biological replicates. *, $p < 0.05$; **, $p < 0.01$; ***, $p < 0.001$. p values determined by a two-way ANOVA with Tukey's multiple comparisons test. Error bars represent SEM.

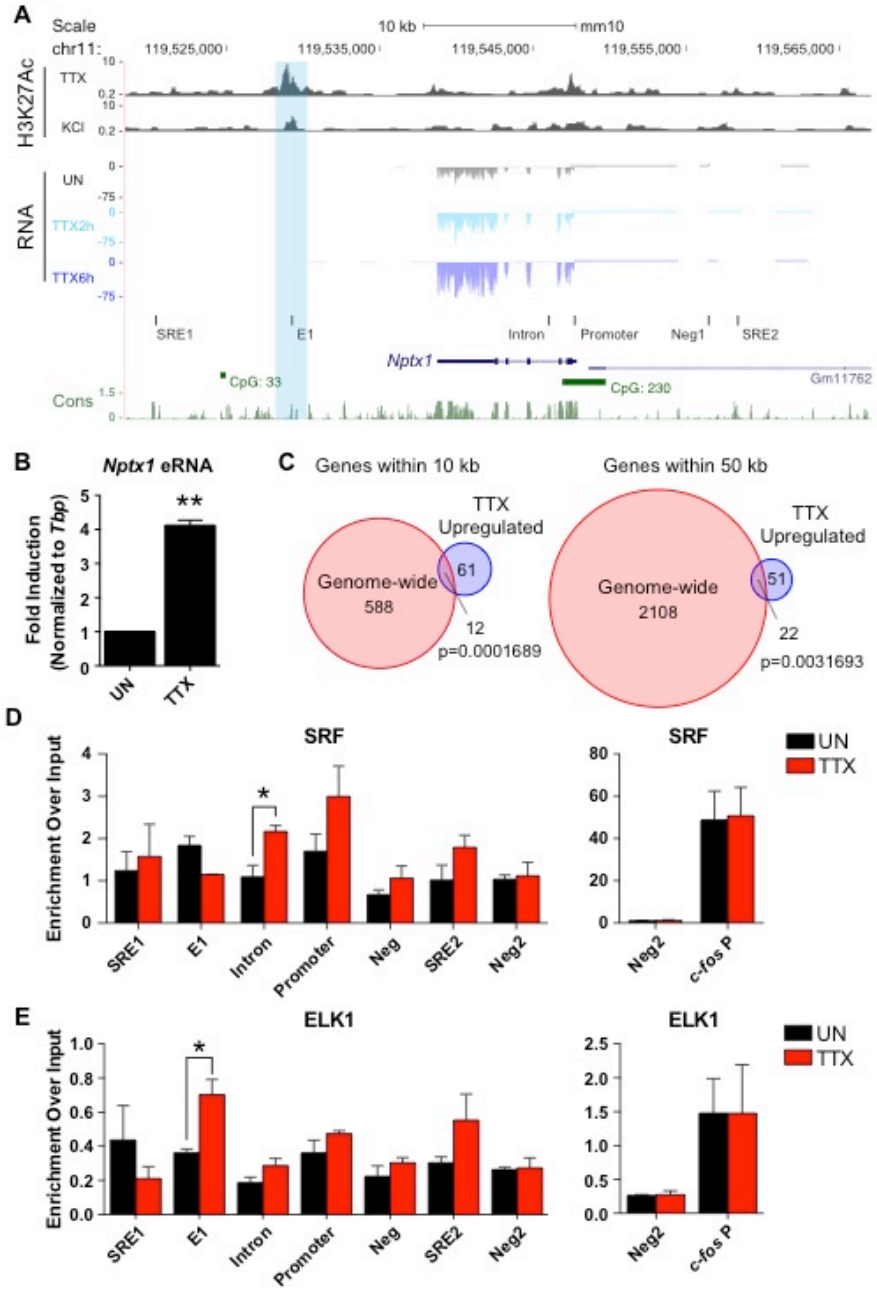

Figure 3.9 SRF and ELK1 directly regulate *Nptx1* expression. (A) A UCSC genome browser view of the *Nptx1* locus aligned with H3K27Ac ChIP-seq from Malik et al., 2014 and the RNA-Seq data from TTX treated cells. The qPCR primer sets used in the ChIP experiments below are labeled with black bars. SRE1 and 4 are potential Serum Response Elements (SREs) based on SRF's consensus sequence. E1 aligns with the H3K27Ac peak, with the blue bar highlighting the decreasing peak. Intron amplifies an intronic conserved region. Neg1 is a negative control region upstream of *Nptx1*, while Neg2 is a negative control on another chromosome. **(B)** qRT-PCR results of an eRNA expressed from the potential enhancer region of *Nptx1* in response to 6 h TTX treatment. n = 3 biological replicates. **(C)** Venn diagrams demonstrating the overlap of genes throughout the genome that were within 10 kb (left) or 50 kb (right) of a H3K27Ac peak

that decreased in response to KCl and the 73 genes found to be significantly upregulated in response to TTX. p values determined by the hypergeometric test. **(D and E)** ChIP results of SRF binding **(C)** or ELK1 binding **(D)** at the indicated loci around the *Nptx1* gene. n = 4 biological replicates for the SRF ChIP, n = 3 biological replicates for the ELK ChIP. *, $p < 0.05$. p values determined by a two-way ANOVA with Tukey's multiple comparisons test, comparing the primer set of interest with the negative region (Neg2). Error bars represent SEM.

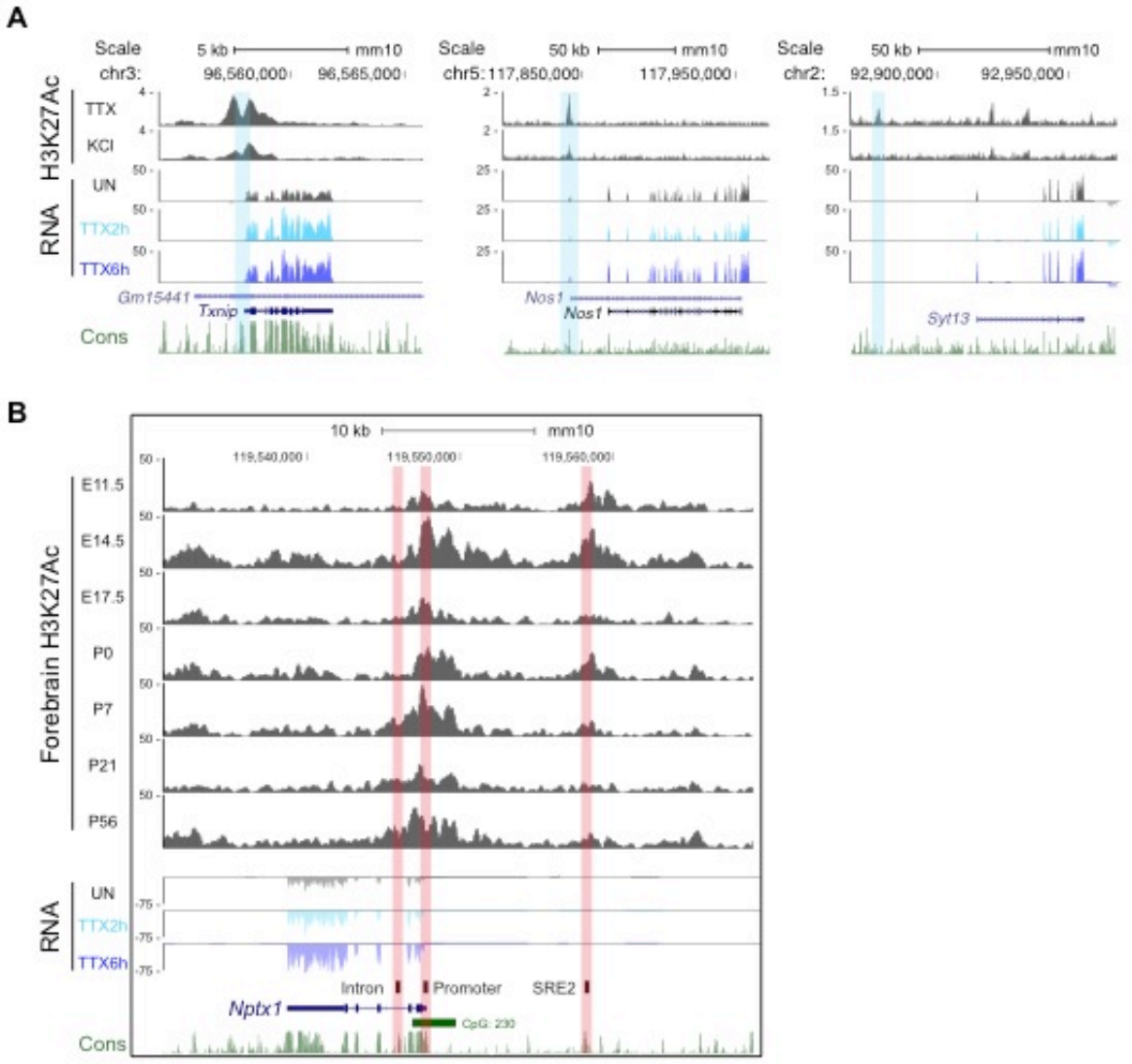

Figure 3.10 H3K27Ac peaks surround TTX upregulated genes. (A) UCSC genome browser views of genes with a decreasing H3K27Ac peak nearby: *Txnip*, *Nos1*, and *Syt13*. The H3K27Ac data from Malik et al., 2014 is aligned with the RNA-seq data for the indicated conditions. Blue bars represent the decreasing H3K27Ac peaks. **(B)** A UCSC genome browser view of the Nptx1 gene aligned with RNA-seq data from the indicated conditions and H3K27Ac ChIP data from Nord et al., 2013. The H3K27Ac ChIP was performed with forebrain tissue at the indicated time points throughout development. A potential SRE (SRE2) is located within a peak that decreases throughout development, while the peak around the promoter expands into the intronic region (Intron) as development progresses. Red bars highlight the regions amplified in ChIP experiments.

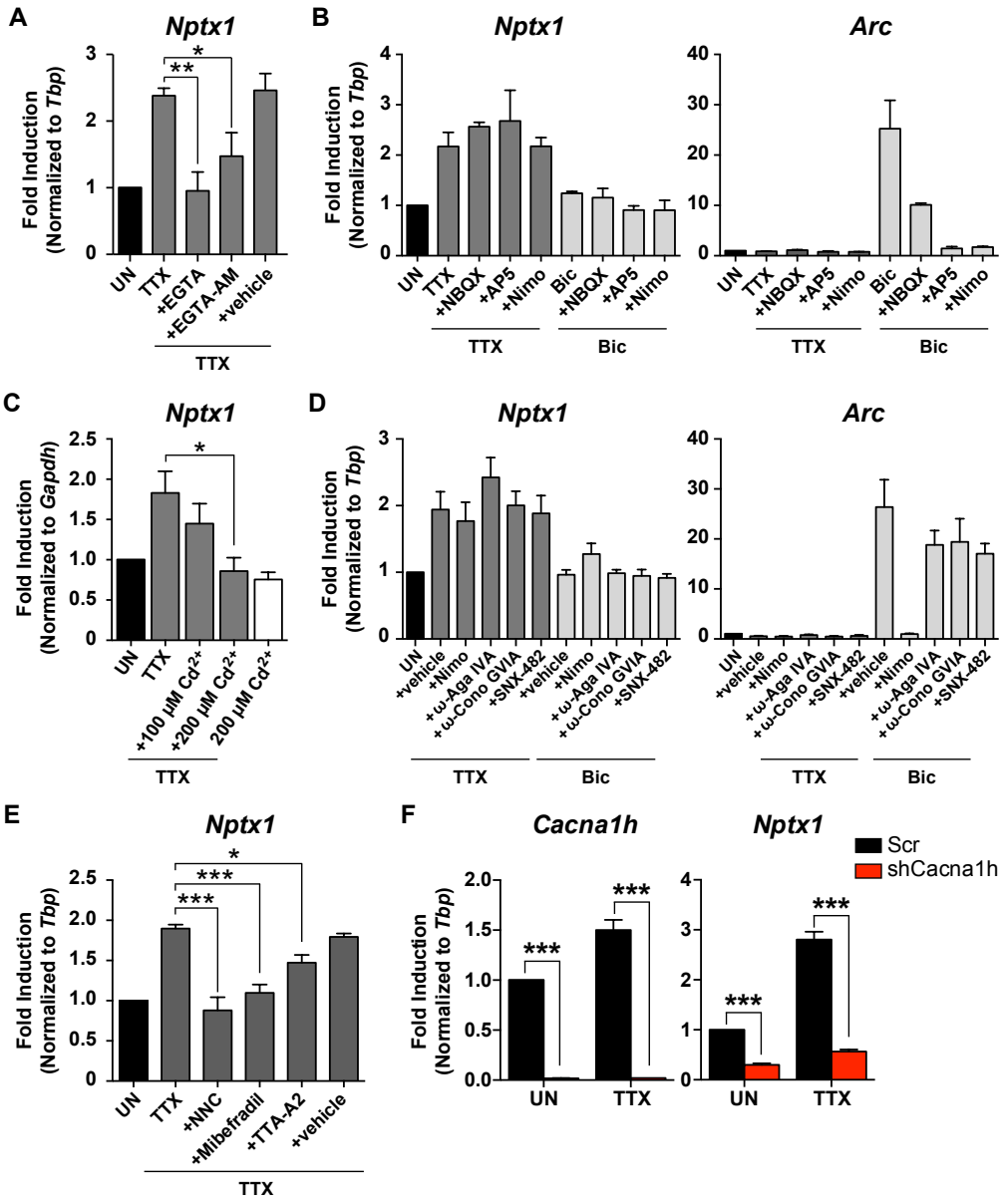

Figure 3.11 The T-type VGCC mediates *Nptx1* induction in response to TTX treatment (A) DIV14 cortical neurons were pretreated with EGTA or EGTA-AM before being treated with TTX for 4 h. Levels of *Nptx1* were measured by qRT-PCR. The vehicle control for EGTA-AM is DMSO. **(B)** Expression levels of *Nptx1* and *Arc* were measured with qRT-PCR from cortical neurons that were pretreated with NBQX, AP-V, or Nimodipine (Nimo) before treatment with TTX or Bic. **(C)** Cortical neurons were pretreated with 100 μM or 200 μM Cadmium (Cd2+) before treatment with TTX, or treated with 200 μM Cd2+ alone. n = 3 biological replicates. **(D)** Cortical neurons were pretreated with Nimodipine (Nimo), ω-Agatoxin IVA (ω-Aga IVA), ω-Conotoxin GVIA (ω-Cono GVIA), or SNX-482 before treatment with TTX or Bic. Vehicle is DMSO. n = 3 biological replicates. **(E)** Blockers of the T-VGCC, NNC 55-0396 (NNC), Mibefradil, or TTA-A2, were used to pretreat cortical neurons for 15 min before treatment with TTX. n = 5 biological replicates. In all of the above bar graphs, black bars represent untreated

cells. Dark grey bars represent cells treated with TTX and pretreated with the indicated compounds. Light grey bars represent cells treated with Bic and pretreated with the indicated compounds. **(F)** Cells were infected with a lentivirus containing either an shRNA targeting the CaV3.2 gene (shCacna1h) or a scrambled control. The levels of the indicated genes were measured by qRT-PCR. n = 3 biological replicates. *, $p < 0.05$; **, $p< 0.01$; ***, $p < 0.001$. p values determined by a one-way ANOVA using Dunnett's multiple comparisons test, except for **(F)** where multiple t tests were performed and statistical significance was determined using the Holm-Sidak multiple comparison test.

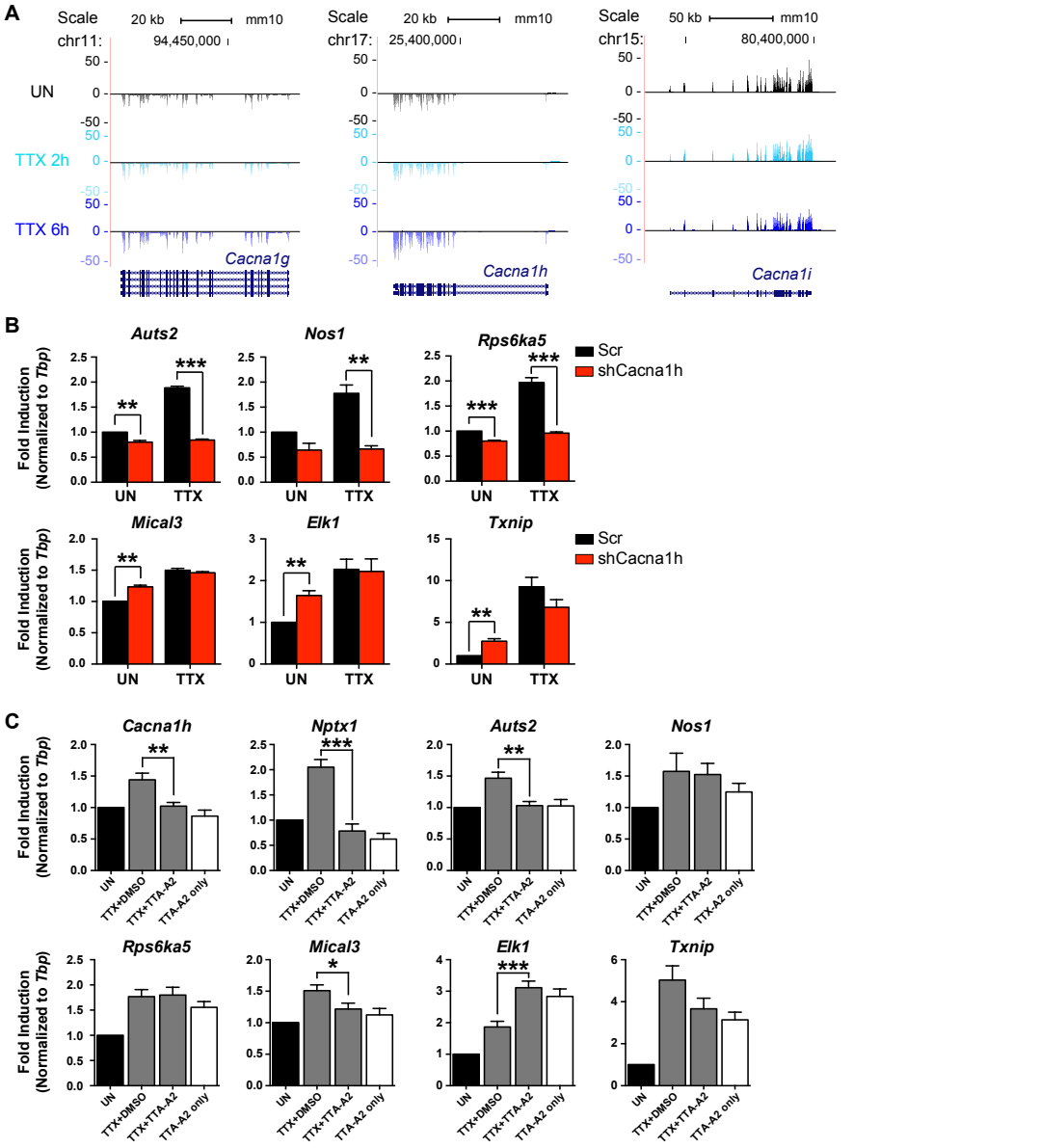

Figure 3.12 Cortical neurons express all three isoforms of the T-VGCC. (A) UCSC genome browser views of the RNA-seq data from cells treated with TTX for 2 or 6 h, aligned with the genomic loci of the three T-VGCC genes: Cacna1g, Cacna1h, and Cacna1i. These genes encode the CaV3.1, CaV3.2, and CaV3.3 subtypes, respectively. **(B)** RNA expression levels of the indicated genes after knockdown of Cacna1h (CaV3.2) or infection with a scrambled control, in either untreated or TTX-treated conditions. n = 3 biological replicates. **(C)** RNA expression levels of the indicated genes in response to TTA-A2 treatment. Cells were either untreated (UN), treated with TTX for 6 h pretreated with DMSO or TTA-A2, or treated with TTA-A2 alone. n = 7 biological replicates. *, $p < 0.05$; **, $p < 0.01$; ***, $p < 0.001$. p values for **(B)** were determined by multiple t tests, as performed, where statistical significance was determined using the Holm-Sidak method. p values for **(C)** were determined using a one-way ANOVA using Dunnett's multiple comparisons test. Error bars represent SEM.

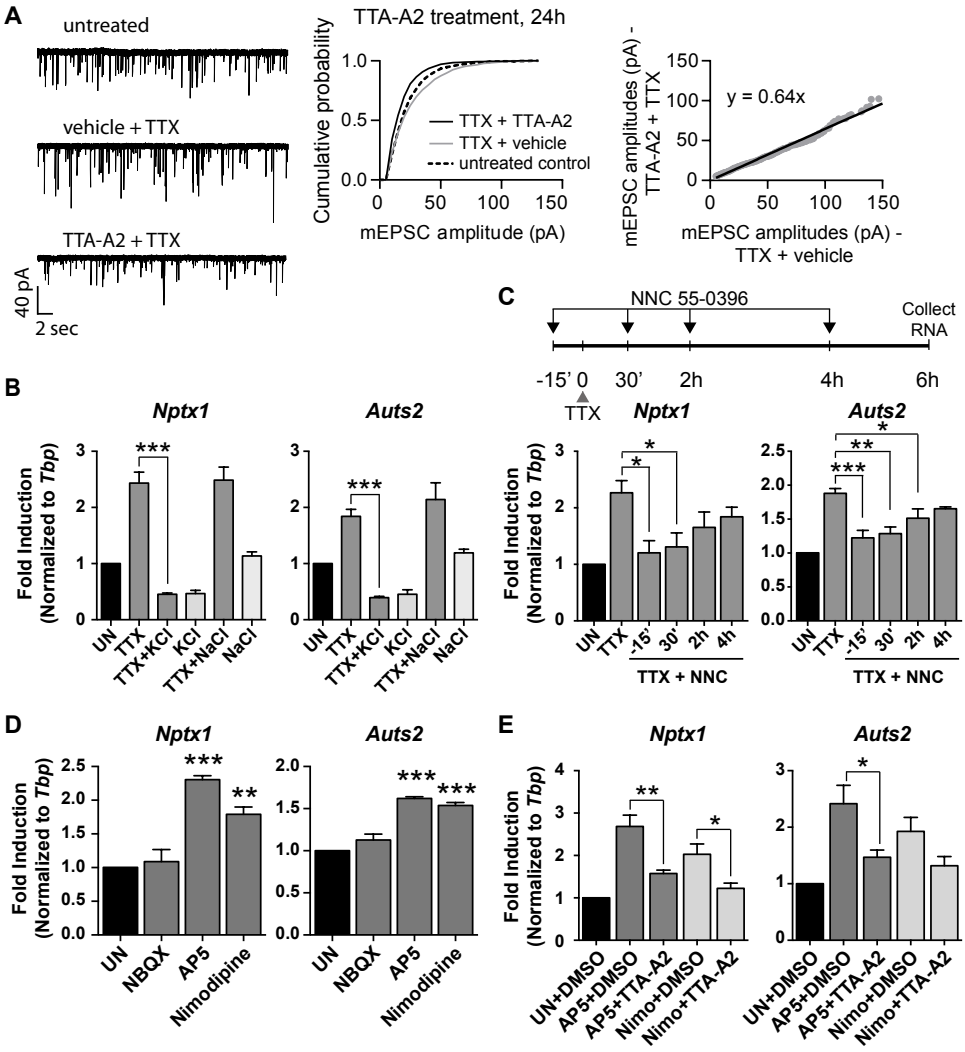

Figure 3.13 The T-VGCC is necessary for scaling. (A) Example traces, cumulative probability histograms, and rank order plots of cells that were pretreated with either TTA-A2 or vehicle, and then treated with TTX for 24 h. n = 9 cells for the untreated condition, n = 10 cells for both TTX treated conditions. TTA-A2/TTX vs vehicle/TTX (n = 10 cells each) p = 2.11x10-27, D = 0.185. Vehicle/TTX vs untreated (n = 9 cells) p = 4.79x10-6, D = 0.08. Statistical significance between cumulative probability graphs was determined by the Kolmogorov-Smirnov test. **(B)** Cells were pretreated with 6 mM KCl or 6 mM NaCl for before the addition of TTX for 6 h. **(C)** The T-VGCC blocker was added either 15 min before the addition of TTX, or 30 min, 2 h, or 4 h after the addition of TTX. The total time of TTX treatment was 6 h. *Nptx1* and *Auts2* RNA levels were measured with qRT-PCR. **(D)** Neurons were treated with the indicated blockers for 6 h, and the RNA levels of the indicated genes were measured with qRT-PCR. **(E)** Cells were pretreated with the VGCC blocker TTA-A2, before the addition of the NMDAR or L-VGCC blocker. RNA levels of the indicated genes were measured with qRT-PCR. For bar graphs, *, $p < 0.05$; **, $p < 0.01$; ***, $p<0.001$. p values determined by a one-way ANOVA using Dunnett's multiple comparisons test. Error bars represent SEM.

Note: electrophysiology performed by Austin Reese.

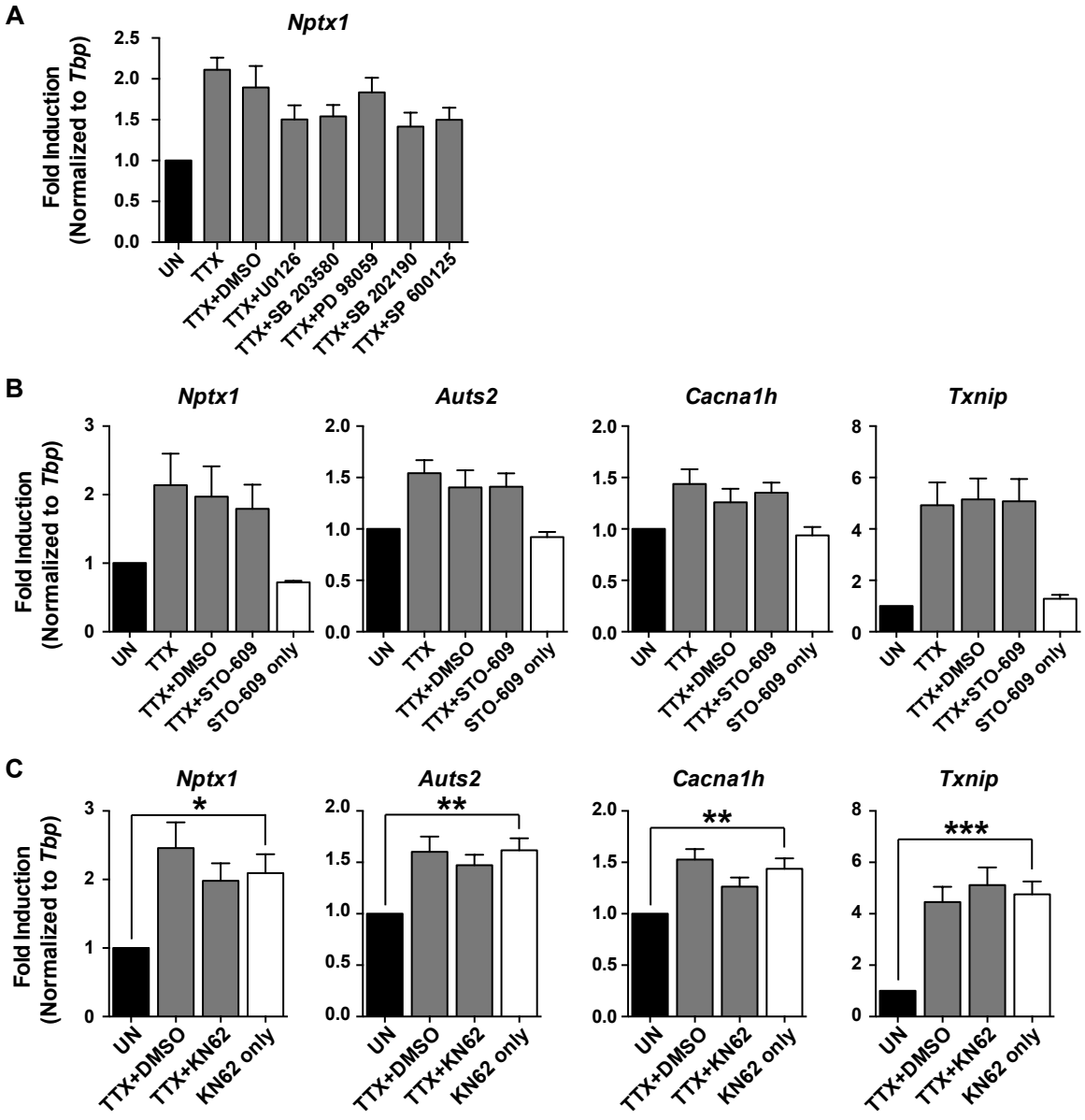

Figure 3.14 Calcium signaling pathways mediating induction. (A) qRT-PCR results of cells treated with TTX for 6 h and pretreated with the indicated blockers of components of the MAPK signaling pathway. n = 5 biological replicates. **(B)** qRT-PCR results of cells treated with TTX and/or STO-609. n = 4 biological replicates. **(C)** qRT-PCR results of cells treated with TTX and/or KN-62. DMSO was used as a vehicle when indicated. n = 5 biological replicates. In the above bar graphs, black bars represent untreated cells. Grey bars represent cells treated with TTX and pretreated with the indicated compounds. White bars represent cells treated only with the indicated compound. *, $p < 0.05$; **, $p < 0.01$; ***, $p < 0.001$. p values determined by a one-way ANOVA using Dunnett's multiple comparisons test. Error bars represent SEM.

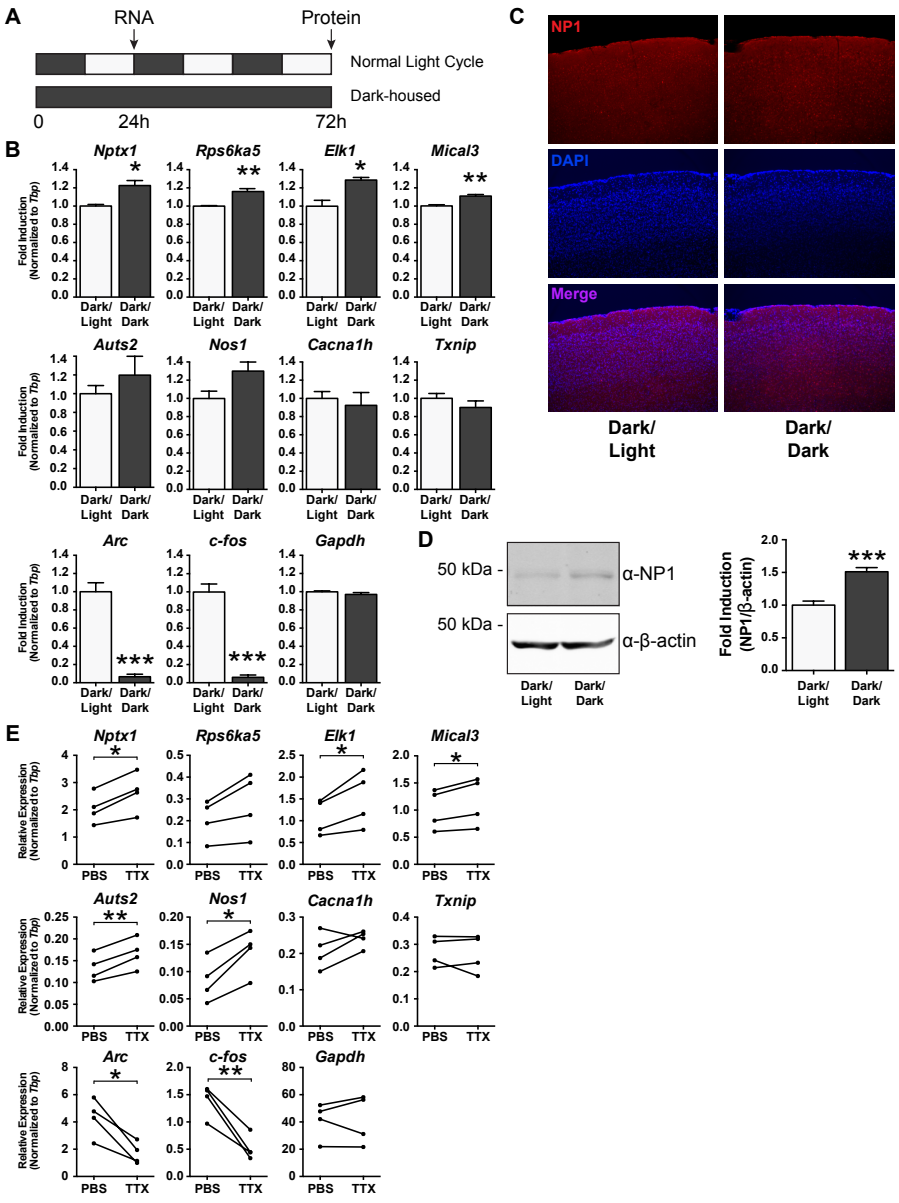

Figure 3.15 ***Nptx1*** **is induced** ***in vivo*** **(A)** A schematic timeline of the dark rearing behavior experiment. Mice were either housed in normal 12 h dark-light cycle or placed in a completely dark chamber for 24 h. **(B)** qRT-PCR results of the indicated genes that are induced in the visual cortex in response to dark housing for 24 h. n = 3 biological replicates. **(C)** Staining of the visual cortex with an antibody against NP1, costained with the nuclear marker, DAPI. Images taken at 10X magnification. **(D)** Western blot results from the visual cortices of mice that were dark reared for 3 d compared to those reared in a normal light/dark cycle. Quantification of the western blot results of NP1 normalized to β-actin. n = 5 biological replicates. **(E)** qRT-PCR results of the visual cortices of mice that were injected intraocularly with either PBS or TTX. n = 4 biological replicates. *, $p < 0.05$; **, $p < 0.01$; ***, $p < 0.001$. p values were determined with an unpaired Student's t-test for dark rearing experiments. p values for the intraocular injections were determined using a paired t-test. Error bars represent SEM.
Note: Intraocular injections performed by Jae-Yeol Joo.

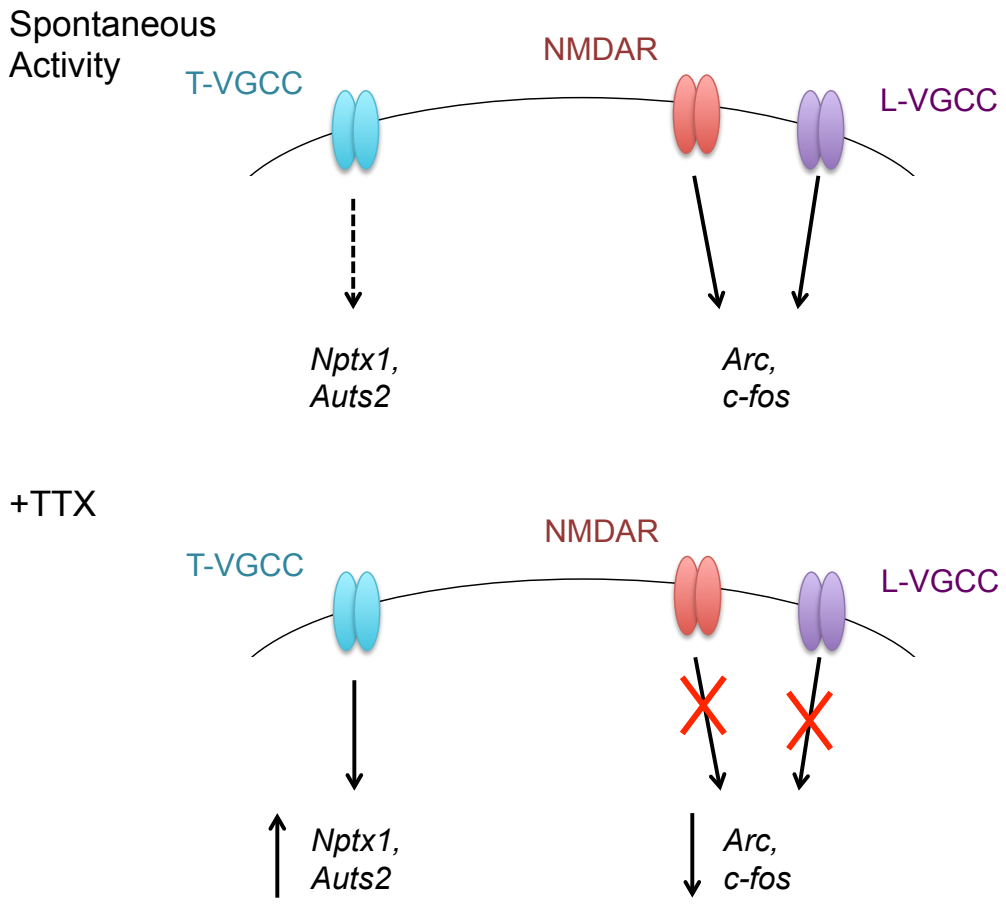

Figure 3.16 Working model of activity-suppression induced transcription Under basal conditions when neurons are experiencing spontaneous activity, the NMDAR and L-VGCC are activated to induce transcription of genes such as *Arc* and *c-fos*, while suppressing the pathway activated by the T-VGCC. When neuronal activity is suppressed by TTX, the pathways normally activated by NMDARs and L-VGCCs are blocked, and the T-VGCC signaling is unmasked and able to be activated at voltages close to the resting membrane potential, and genes such as *Nptx1* and *Auts2* are upregulated.

Gene ID	Gene Name	Associated Disorder	Reference
Auts2	*Autism susceptibility candidate 2*	ASD, ADHD, epilepsy	Sultana et al., 2002; Kalscheuer et al., 2007
Cacna1h	*Calcium channel, voltage-dependent, alpha 1H subunit*	ASD	Splawski et al., 2006
Bbs4	*Bardet-Biedl syndrome 4*	Bardet-Biedl syndrome, ASD	Girirajan et al., 2013
Fan1	*FANCD2/FANCI-associated nuclease 1*	ASD and schizophrenia	Ionita-Laza et al., 2013
Ogt	*O-linked N-acetylglucosamine (GlcNAc) transferase*	Maternal stress marker	Howerton et al., 2013
Smg6	*Smg-6 homolog, nonsense mediated mRNA decay factor (C. elegans)*	ASD, neurodevelopmental disorders	Nguyen et al., 2013
Upf2	*UPF2 regulator of nonsense transcripts homolog (yeast)*	ASD, neurodevelopmental disorders	Nguyen et al., 2013
Nos1	*Nitric Oxide Synthase 1*	Schizophrenia	Shinkai et al., 2002
Elk1	*Elk1, member of ETS oncogene category*	Schizophrenia	Sanders et al., 2013
Nptx1	*Neuronal pentraxin 1*	Bipolar disorder	Rajkumar et al., 2015
Myt1	*Myelin transcription factor 1*	Schizophrenia	Fernandez-Enright et al., 2013
Dbp	*D site of albumin promoter binding protein1*	Schizophrenia	Sanders et al., 2013

Table 3.1 TTX-induced genes have been associated with neurodevelopmental disorders. Gene information from SFARI and other published sources.

3.4 Materials and Methods

Cell culture, transfections, and lentiviral infections

All experiments carried out with the use of animals were reviewed and approved by the IACUC committee at University of Texas, Southwestern Medical Center. Primary cortical cultures were made from embryonic day 16-18 (E16/18) mice, and they were grown in Neurobasal media supplemented with B-27 and Glutamax. AraC was added at DIV6 to prevent glial proliferation. Cells were used in experiments on days *in vitro* (DIV) 12-15, as indicated. Hippocampal cultures were made from postnatal day 1-3 (P1-3) rat pups, and cultured as described previously (Kavalali et al., 1999). Lentiviral constructs containing the indicated shRNAs in the pLLX vector were transfected into HEK293T cells with the helper plasmids Δ8.9 and VsVg using Fugene HD (Promega) before incubating for 48-72 h. Viral supernatant was then added directly to the cultures to infect the neurons. shRNA sequences were designed using GE Dharmacon siDesign Center or as previously described (Abad et al., 2006; Joo et al., 2015; Lee et al., 2010; Rodriguez-Gomez et al., 2012). The shRNA sequences used are: *Scrambled,* 5'-GCCCTGCCACCGTAATTTA-3'; *shNP1*, 5'-GTACAGCCGCCTCAATTCT-3'; *shSRF*, 5'-AAGATGGAGTTCATCGACAAC-3'; *shCREB*, 5'-GGAGTCTGTGGATAGTGTA-3'; *shMEF2A*, 5'-GTTATCTCAGGGTTCAAAT-3'; *shMEF2D*, 5'-GTAGCTCTCTGGTCACTCC-3'; *shMRTFA/B*, 5'-CATGGAGCTGGTGGAGAAGAA-3'; *shELK1*, 5'-GGGATGGTGGTGAGTTCAAGT-3'; *shELK4*, 5'-GCAACGAGCCCTAGTCTTTCT-3'; *shCacna1h*, 5'-GGGCTTCCTTTAGTAGCAA-3'.

Pharmacological Inhibitors

To induce scaling, 1 μM TTX (Tocris) or 50 μM bicuculline (Sigma) was used. Cells were also pretreated with the following inhibitors at the indicated concentrations: 5 μM NBQX (Tocris), 100 μM AP-5 (Tocris), 10 μM Nimodipine (Tocris), 5 mM EGTA (Bio-world), 10 μM EGTA-AM (Life Technologies), 2 μM ω-Conotoxin GVIA (Alomone labs), 2 μM ω-Agatoxin IVA (Alomone labs), 2 μM SNX-482 (Alomone labs), 10 μM NNC 55-0396 dihydrochloride (Alomone labs), 1 μM Mibefradil (Alomone labs), 50 μM TTA-A2 (Alomone labs), 10 μM KN-62 (Tocris), 3 μM STO-609 (Tocris), and 10 μM each of the MAPK inhibitors: U0126, SB 203580, PD 98059, SB 202190, SP 600125 (Tocris). 5 μg/mL Actinomycin D was added to block transcription. EGTA-AM, Nimodipine, TTA-A2, STO-609, KN-62, Actinomycin D, and the MAPK inhibitors were dissolved in DMSO to make stock solutions. Cells were pretreated with EGTA-AM for 30 min before exchanging the media and being stimulated with TTX. Cells were pretreated with EGTA for 5 min before stimulation, and for all other inhibitors, cells were pretreated for 15 min before stimulation by either TTX or bicuculline.

Whole cell voltage clamp recordings

At DIV14-18, dissociated hippocampal cultures were voltage-clamped at -70 mV, as previously described (Reese and Kavalali, 2015), using an Axon Instruments Axopatch 200B amplifier. Access resistance was less than 25MΩ for each recording. The internal pipette solution contained (in mM): 120 K-Gluconate, 20 KCl, 10 NaCl, 10 HEPES, 0.6 EGTA, 4 Mg-ATP and 0.3 Na-GTP at pH 7.3. In order to isolate AMPA-mEPSCs, the extracellular solution contained 1 μM TTX, 50 μM picrotoxin (to block mIPSCs), 50 μM (2R)-amino-5-phosphonovaleric acid (AP5), 2 mM Ca^{2+} and 1.25 mM Mg^{2+}. All recordings were performed under continuous perfusion, and

cells were perfused for 3 min before recording to achieve stable baselines. The AMPA-mEPSCs were quantified with Synaptosoft MiniAnalysis software. 4 minutes were analyzed per recording. To ensure that high frequency cells did not skew the amplitude comparisons by being overrepresented, 200 mEPSC amplitudes were randomly selected from each recording to generate the cumulative probability histograms and rank order plots. Significance was determined using the Kolmogorov-Smirnov test, which was performed using PAST 3.1 (http://folk.uio.no/ohammer/past/).

Chromatin Immunoprecipitation (ChIP)

ChIP was performed as previously described (Joo et al., 2015; Kim et al., 2010; Schaukowitch et al., 2014). Briefly, neurons were crosslinked with 1% formaldehyde for 10 min before quenching with 2M glycine (125 mM final concentration). Cells were washed with cold PBS and harvested in PBS with proteinase inhibitors (Roche). Cells were lysed with Buffer I (50 mM Hepes KOH, pH 7.5, 140 mM NaCl, 1 mM EDTA, pH 8.0, 10 % Glycerol, 0.5% NP-40, protease inhibitors) and nuclei were resuspended in Buffer II (300 mM NaCl, 1 % Triton-X 100, 0.1% Sodium deoxycholate, 1 mM EDTA, pH 8.0, 0.5 mM EGTA, pH 8.0, 10 mM Tris, pH 8.0, protease inhibitors) before being sonicated to shear the DNA on a Misonix sonicator. Lysates were incubated with 4 μg of the following antibodies overnight at 4°C: anti-SRF (H-300, Santa Cruz Biotechnology Cat# sc-13029, RRID:AB_2302440), anti-ELK1 (I-20 X, Santa Cruz Biotechnology, Cat# sc-355, RRID:AB_631429). The next day, Protein A/G beads (Santa Cruz) were added for 2 h at 4°C, and then the beads were washed with Low, High, and LiCl buffers. DNA was eluted with Elution buffer (10 mM Tris, pH 8.0, 1 mM EDTA, pH 8.0, 1 % SDS) at 65°C for 10 min, and then reverse crosslinked at 65°C for 5-8 h. DNA was incubated with

RNAse A (Qiagen), followed by Proteinase K (NEB), and purified by Phenol:Chloroform extraction, followed by a commercial DNA purification kit (Qiagen). Regions were amplified using qPCR with the primers listed below.

Immunostaining

Hippocampal neurons from P3 rats were cultured until DIV14-17. Cells were treated with 1 μM TTX overnight. Cells were washed once with PBS before fixation with 4% paraformaldehyde in PBS for 20 min at room temperature. Cells were washed three times with PBS. To stain for surface NP1, neurons were left unpermeabilized, and blocked with 10% Normal Donkey Serum (NDS; Jackson ImmunoResearch Laboratories) in PBS for 1 h at room temperature. Primary antibody incubation was performed for 2 h at room temperature in 2% NDS in PBS at the following dilution: anti-NP1 (BD Biosciences Cat# 610369, RRID:AB_397754, 1:300). Cells were washed three times with PBS before secondary incubation for 1 h at room temperature. The secondary antibody Alexa-Fluor anti-Mouse 555 was diluted 1:1000 in 2% NDS in PBS. Cells were washed three times in PBS, and mounted using hard-set mounting solution (VectaShield). Images were taken on a Zeiss LSM 150 using a 63x objective, and were quantified using ImageJ. For immunohistochemistry, mice were perfused with 4% formaldehyde and brains were incubated in 4% paraformaldehyde overnight. After three washes with PBS, the brains were incubated with 30% sucrose and then mounted in Tissue-tek (Sakura). The brains were sliced at 40 μm, and the slices were incubated with blocking solution (10% NDS in PBS) for 1 h at room temperature. Primary antibody incubation was performed overnight at 4°C in 0.1% TX-100 in PBS at a dilution of 1:50. Cells were washed four times with 0.1% TX-100 in PBS, and incubated with secondary antibody Alexa-Fluor anti-Mouse 555 at a dilution of 1:200 in 0.1%

TX-100 in PBS for 1 h at room temperature. Slices were again washed four times with 0.1% TX-100 and coverslips were applied with hard-set mounting solution (VectaShield).

RNA-seq

Total RNA was extracted using Trizol reagent (Life Technologies) and given to the UT Southwestern Genomics and Microarray core for mRNA library preparation and sequencing. The library was prepared using the TruSeq RNA Library Preparation Kit (Illumina) according to the manufacturer's instructions. The sequencing reads were mapped to the mm10 UCSC annotation using TOPHAT (Trapnell et al., 2009) with the parameters (-a 8 -m 0 -I 500000 -p 8 -g 20 --library-type fr-firststrand --no-novel-indels --segment-mismatches 2). RPKM calculations were done using the HOMER package by normalizing to 10 million reads. Tracks for visualization on UCSC browser are generated using HOMER. Heatmaps were generated in JavaTreeView from log transformed fold change values, normalized to the unstimulated condition, using hierarchical clustering in Cluster. Venn diagrams were created using BioVenn (Hulsen et al., 2008).

ChIP-seq analysis

H3K27Ac ChIP-seq (GSE60192) data was downloaded from GEO. Bowtie2 (Langmead et al., 2009) aligner was used to align the fastq reads to mm10 UCSC annotation. Duplicates were removed using Picard MarkDuplicates (http://broadinstitute.github.io/picard/) and visualization tracks were generated using HOMER. Using MACS, the KCl-K27ac peaks were identified by using the Unstimulated-K27ac samples as control at a p-value of 1E-5. Closest genes were identified near the negative peaks generated for KCl-K27ac through MACS by using in-house downstream scripts.

GRO-seq analysis

GRO-seq was carried out as previously described (Core et al., 2008; Hah et al., 2011) with modifications (Danko et al., 2013; Lam et al., 2013). Briefly, 10 million nuclei per sample were extracted and used for global run-on, and base hydrolysis was performed as previously described (Core et al., 2008). Nascent RNAs were immunoprecipitated with anti-BrdU antibody-conjugated beads (Santa Cruz Biotech) twice. Between two immunoprecipitations, purified run-on RNAs were subjected to polyA tailing by using Poly(A)-polymerase (NEB). Subsequently, RNAs are subjected to first-strand cDNA synthesis using Superscript III Reverse Transcriptase (Invitrogen) with the oNTI223 primer. Extra oNTI223 primers were removed by Exonuclease I (NEB) and cDNAs were size-selected in an 8 % polyacrylamide TBE-urea gel. Purified cDNAs were subsequently circularized using CircLigase (Epicentre) and relinearized with ApeI (NEB). The relinearized DNA template were subjected to PCR amplification by using Phusion High-Fidelity DNA Polymerase (NEB) and Illumina TrueSeq small-RNA sample barcoded primers. Subsequently, PCR products were isolated by 6 % polyacrylamide TBE gel and purified. The final libraries were sequenced using an Illumina HiSeq per the manufacturer's instructions. The raw fastq reads were trimmed using CUTADAPT with parameters -a AAAAAAAAAAAAAAAAAAAA -z -e 0.10 -f fastq -m 32 (Chae et al., 2015). Then the surviving reads were submitted to BWA aligner for mapping to the mm10 UCSC annotation. Samtools and the HOMER package were used to make visualization tracks and RPKM calculations. RPKM was calculated by normalizing to 10 million reads.

qRT-PCR

Total RNA was extracted from neurons using Trizol reagent (Life Technologies) according to the manufacturer's protocol. cDNA made with the high-capacity reverse transcription kit (Life Technologies), and amplification was performed with SybrGreen (Life Technologies) using the primers indicated below.

Western blotting

Protein was extracted from neurons using sample buffer (60 mM Tris-HCl, pH 6.8, 2% SDS, 10% glycerol). Before loading, samples were mixed with loading buffer (5% 2-mercaptoethanol, 0.1% bromophenol blue) and denatured at 95°C. Proteins were run on a 12% SDS-PAGE gel, and analyzed by western blotting with the following antibodies: anti-NP1 (BD Biosciences Cat# 610369, RRID:AB_397754, 1:1000) or anti-β-actin (Sigma-Aldrich Cat#A5441, RRID:AB_476744, 1:5000).

Visual Cortex experiments

For dark rearing experiments, male C57Bl6/J mice were placed into completely dark chambers at P21-25 at the end of their light cycle. The visual cortices were removed, and RNA was extracted in Trizol after 24 h in the dark. For measuring protein levels, mice were taken out of the dark after 3 d. Intraocular injections of TTX were performed as in (Frenkel and Bear, 2004). Briefly, 1 μL of 1 mM TTX or PBS was injected into each eye of the mouse using a glass pipette at a rate of 1 μL/1 min (Joo et al., 2015). RNA was then extracted from visual cortex of the opposite hemisphere with Trizol.

CHAPTER 4

Discussion and Future Directions

Sensory experience is capable of remodeling neuronal circuits throughout development through the activation of specific gene sets by transcription factors and the remodeling of the epigenetic landscape. The studies presented here demonstrate new levels of regulation that the neurons use to respond to the changing activity levels in the environment around them. My first project demonstrated how eRNAs can activate target gene induction in response to neuronal activity, and my second project identified a novel transcriptional program neurons utilize to scale up their synaptic strength when activity levels are low. There is an increasing number of mutations that are found in psychiatric disorders such as ASD that are components of the neuronal activity-dependent signaling pathways (Chahrour et al., 2012; Morrow et al., 2008), including the L-VGCC in Timothy syndrome, MeCP2 in Rhett syndrome, and UBE3A in Angelman syndrome (Ebert and Greenberg, 2013). While there appear to be many mutations that are all able to produce an ASD-like syndrome, a large proportion of these mutations fall into a convergent molecular pathway (Ebert and Greenberg, 2013), suggesting the importance of this pathway in proper neuronal function. Targeting a common pathway, rather than an individual gene, may benefit the discovery of better therapeutics to treat a disease with many different genetic causes.

Future directions aim to understand the role of these pathways *in vivo*. It is still to be seen whether the regulation provided by eRNAs is necessary for the function of their target genes in behaviors such as learning and memory. Ongoing experiments aim to explore whether knockdown of the *Arc* eRNA in the hippocampus will lead to defect in memory, as ARC has been shown to be critically important for this behavior. As more sequencing of patient genomes

become available, it is becoming increasingly evident that many of the mutations found are not within protein coding genes themselves, but many are found within regulatory regions such as enhancers (Kleinjan and Coutinho, 2009). Many diseases that have a strong psychiatric phenotype, such as Rhett syndrome (mutations in MeCP2), or Rubinstein-Taybi syndrome (mutations in CBP), can be caused by haploinsufficiency, suggesting that the precise levels of these proteins are absolutely crucial for maintaining proper neuronal function. In cases of important neuronal genes, mutations in the gene itself might be detrimental to the survival of the organism, but mutations in the regulatory regions may disrupt the expression just enough to throw the neuronal circuit out of balance.

Homeostatic scaling is a process specifically designed to maintain balance within neuronal circuits. It is responsible for maintaining minimum firing patterns, while preventing runaway network activity. Our data suggests that a nuclear transcription program would provide cells with a mechanism to make long-lasting changes in response to information from the environment. Future experiments will aim to understand whether these programs have a functional role *in* vivo. Gaining a better understanding of how neurons can activate distinct gene programs in response to an absence of activity will provide a more complete understanding of how neurons maintain balance and could provide opportunities to discover better treatment options for disorders that could be caused by disruptions in the activity-dependent pathway.

BIBLIOGRAPHY

Abad, M.A., Enguita, M., DeGregorio-Rocasolano, N., Ferrer, I., and Trullas, R. (2006). Neuronal pentraxin 1 contributes to the neuronal damage evoked by amyloid-beta and is overexpressed in dystrophic neurites in Alzheimer's brain. The Journal of neuroscience : the official journal of the Society for Neuroscience *26*, 12735-12747.

Adelman, K., Kennedy, M.A., Nechaev, S., Gilchrist, D.A., Muse, G.W., Chinenov, Y., and Rogatsky, I. (2009). Immediate mediators of the inflammatory response are poised for gene activation through RNA polymerase II stalling. Proceedings of the National Academy of Sciences of the United States of America *106*, 18207-18212.

Adelman, K., and Lis, J.T. (2012). Promoter-proximal pausing of RNA polymerase II: emerging roles in metazoans. Nature reviews Genetics *13*, 720-731.

Aoto, J., Nam, C.I., Poon, M.M., Ting, P., and Chen, L. (2008). Synaptic signaling by all-trans retinoic acid in homeostatic synaptic plasticity. Neuron *60*, 308-320.

Arner, E., Daub, C.O., Vitting-Seerup, K., Andersson, R., Lilje, B., Drablos, F., Lennartsson, A., Ronnerblad, M., Hrydziuszko, O., Vitezic, M.*, et al.* (2015). Transcribed enhancers lead waves of coordinated transcription in transitioning mammalian cells. Science *347*, 1010-1014.

Bading, H., Ginty, D.D., and Greenberg, M.E. (1993). Regulation of gene expression in hippocampal neurons by distinct calcium signaling pathways. Science *260*, 181-186.

Bear, M.F., and Malenka, R.C. (1994). Synaptic plasticity: LTP and LTD. Curr Opin Neurobiol *4*, 389-399.

Chae, M., Danko, C.G., and Kraus, W.L. (2015). groHMM: a computational tool for identifying unannotated and cell type-specific transcription units from global run-on sequencing data. BMC Bioinformatics *16*, 222.

Chahrour, M.H., Yu, T.W., Lim, E.T., Ataman, B., Coulter, M.E., Hill, R.S., Stevens, C.R., Schubert, C.R., Collaboration, A.A.S., Greenberg, M.E.*, et al.* (2012). Whole-exome sequencing and homozygosity analysis implicate depolarization-regulated neuronal genes in autism. PLoS Genet *8*, e1002635.

Cheng, B., and Price, D.H. (2008). Analysis of factor interactions with RNA polymerase II elongation complexes using a new electrophoretic mobility shift assay. Nucleic acids research *36*, e135.

Cheong, E., and Shin, H.S. (2013). T-type Ca2+ channels in normal and abnormal brain functions. Physiol Rev *93*, 961-992.

Chrivia, J.C., Kwok, R.P., Lamb, N., Hagiwara, M., Montminy, M.R., and Goodman, R.H. (1993). Phosphorylated CREB binds specifically to the nuclear protein CBP. Nature *365*, 855-859.

Cole, A.J., Abu-Shakra, S., Saffen, D.W., Baraban, J.M., and Worley, P.F. (1990). Rapid rise in transcription factor mRNAs in rat brain after electroshock-induced seizures. J Neurochem *55*, 1920-1927.

Core, L.J., Waterfall, J.J., Gilchrist, D.A., Fargo, D.C., Kwak, H., Adelman, K., and Lis, J.T. (2012). Defining the status of RNA polymerase at promoters. Cell reports *2*, 1025-1035.

Core, L.J., Waterfall, J.J., and Lis, J.T. (2008). Nascent RNA sequencing reveals widespread pausing and divergent initiation at human promoters. Science *322*, 1845-1848.

Danko, C.G., Hah, N., Luo, X., Martins, A.L., Core, L., Lis, J.T., Siepel, A., and Kraus, W.L. (2013). Signaling pathways differentially affect RNA polymerase II initiation, pausing, and elongation rate in cells. Mol Cell *50*, 212-222.

De Santa, F., Barozzi, I., Mietton, F., Ghisletti, S., Polletti, S., Tusi, B.K., Muller, H., Ragoussis, J., Wei, C.L., and Natoli, G. (2010). A large fraction of extragenic RNA pol II transcription sites overlap enhancers. PLoS biology *8*, e1000384.

Deisseroth, K., Bito, H., and Tsien, R.W. (1996). Signaling from synapse to nucleus: postsynaptic CREB phosphorylation during multiple forms of hippocampal synaptic plasticity. Neuron *16*, 89-101.

Desai, N.S., Cudmore, R.H., Nelson, S.B., and Turrigiano, G.G. (2002). Critical periods for experience-dependent synaptic scaling in visual cortex. Nature neuroscience *5*, 783-789.

Djebali, S., Davis, C.A., Merkel, A., Dobin, A., Lassmann, T., Mortazavi, A., Tanzer, A., Lagarde, J., Lin, W., Schlesinger, F.*, et al.* (2012). Landscape of transcription in human cells. Nature *489*, 101-108.

Dolmetsch, R.E., Pajvani, U., Fife, K., Spotts, J.M., and Greenberg, M.E. (2001). Signaling to the nucleus by an L-type calcium channel-calmodulin complex through the MAP kinase pathway. Science *294*, 333-339.

Ebert, D.H., and Greenberg, M.E. (2013). Activity-dependent neuronal signalling and autism spectrum disorder. Nature *493*, 327-337.

Egloff, S., Dienstbier, M., and Murphy, S. (2012). Updating the RNA polymerase CTD code: adding gene-specific layers. Trends in genetics : TIG *28*, 333-341.

Fernandes, D., and Carvalho, A.L. (2016). Mechanisms of homeostatic plasticity in the excitatory synapse. J Neurochem.

Fernandez-Enright, F., Andrews, J.L., Newell, K.A., Pantelis, C., and Huang, X.F. (2014). Novel implications of Lingo-1 and its signaling partners in schizophrenia. Transl Psychiatry *4*, e348.

Flavell, S.W., Cowan, C.W., Kim, T.K., Greer, P.L., Lin, Y., Paradis, S., Griffith, E.C., Hu, L.S., Chen, C., and Greenberg, M.E. (2006). Activity-dependent regulation of MEF2 transcription factors suppresses excitatory synapse number. Science *311*, 1008-1012.

Flavell, S.W., and Greenberg, M.E. (2008). Signaling mechanisms linking neuronal activity to gene expression and plasticity of the nervous system. Annu Rev Neurosci *31*, 563-590.

Flavell, S.W., Kim, T.K., Gray, J.M., Harmin, D.A., Hemberg, M., Hong, E.J., Markenscoff-Papadimitriou, E., Bear, D.M., and Greenberg, M.E. (2008). Genome-wide analysis of MEF2 transcriptional program reveals synaptic target genes and neuronal activity-dependent polyadenylation site selection. Neuron *60*, 1022-1038.

Frenkel, M.Y., and Bear, M.F. (2004). How monocular deprivation shifts ocular dominance in visual cortex of young mice. Neuron *44*, 917-923.

Gilchrist, D.A., Dos Santos, G., Fargo, D.C., Xie, B., Gao, Y., Li, L., and Adelman, K. (2010). Pausing of RNA polymerase II disrupts DNA-specified nucleosome organization to enable precise gene regulation. Cell *143*, 540-551.

Gilchrist, D.A., Fromm, G., dos Santos, G., Pham, L.N., McDaniel, I.E., Burkholder, A., Fargo, D.C., and Adelman, K. (2012). Regulating the regulators: the pervasive effects of Pol II pausing on stimulus-responsive gene networks. Genes & development *26*, 933-944.

Girirajan, S., Dennis, M.Y., Baker, C., Malig, M., Coe, B.P., Campbell, C.D., Mark, K., Vu, T.H., Alkan, C., Cheng, Z.*, et al.* (2013). Refinement and discovery of new hotspots of copy-number variation associated with autism spectrum disorder. Am J Hum Genet *92*, 221-237.

Goel, A., and Lee, H.K. (2007). Persistence of experience-induced homeostatic synaptic plasticity through adulthood in superficial layers of mouse visual cortex. The Journal of neuroscience : the official journal of the Society for Neuroscience *27*, 6692-6700.

Goold, C.P., and Nicoll, R.A. (2010). Single-cell optogenetic excitation drives homeostatic synaptic depression. Neuron *68*, 512-528.

Gupta, R.A., Shah, N., Wang, K.C., Kim, J., Horlings, H.M., Wong, D.J., Tsai, M.C., Hung, T., Argani, P., Rinn, J.L.*, et al.* (2010). Long non-coding RNA HOTAIR reprograms chromatin state to promote cancer metastasis. Nature *464*, 1071-1076.

Guttman, M., Amit, I., Garber, M., French, C., Lin, M.F., Feldser, D., Huarte, M., Zuk, O., Carey, B.W., Cassady, J.P.*, et al.* (2009). Chromatin signature reveals over a thousand highly conserved large non-coding RNAs in mammals. Nature *458*, 223-227.

Guzowski, J.F., Lyford, G.L., Stevenson, G.D., Houston, F.P., McGaugh, J.L., Worley, P.F., and Barnes, C.A. (2000). Inhibition of activity-dependent arc protein expression in the rat hippocampus impairs the maintenance of long-term potentiation and the consolidation of long-term memory. The Journal of neuroscience : the official journal of the Society for Neuroscience *20*, 3993-4001.

Hah, N., Danko, C.G., Core, L., Waterfall, J.J., Siepel, A., Lis, J.T., and Kraus, W.L. (2011). A rapid, extensive, and transient transcriptional response to estrogen signaling in breast cancer cells. Cell *145*, 622-634.

Hah, N., Murakami, S., Nagari, A., Danko, C.G., and Kraus, W.L. (2013). Enhancer transcripts mark active estrogen receptor binding sites. Genome research *23*, 1210-1223.

Hardingham, G.E., Arnold, F.J., and Bading, H. (2001). Nuclear calcium signaling controls CREB-mediated gene expression triggered by synaptic activity. Nature neuroscience *4*, 261-267.

Heintzman, N.D., Stuart, R.K., Hon, G., Fu, Y., Ching, C.W., Hawkins, R.D., Barrera, L.O., Van Calcar, S., Qu, C., Ching, K.A.*, et al.* (2007). Distinct and predictive chromatin signatures of transcriptional promoters and enhancers in the human genome. Nature genetics *39*, 311-318.

Hengen, K.B., Torrado Pacheco, A., McGregor, J.N., Van Hooser, S.D., and Turrigiano, G.G. (2016). Neuronal Firing Rate Homeostasis Is Inhibited by Sleep and Promoted by Wake. Cell *165*, 180-191.

Hevroni, D., Rattner, A., Bundman, M., Lederfein, D., Gabarah, A., Mangelus, M., Silverman, M.A., Kedar, H., Naor, C., Kornuc, M.*, et al.* (1998). Hippocampal plasticity involves extensive gene induction and multiple cellular mechanisms. J Mol Neurosci *10*, 75-98.

Hill, C.S., Marais, R., John, S., Wynne, J., Dalton, S., and Treisman, R. (1993). Functional analysis of a growth factor-responsive transcription factor complex. Cell *73*, 395-406.

Howerton, C.L., Morgan, C.P., Fischer, D.B., and Bale, T.L. (2013). O-GlcNAc transferase (OGT) as a placental biomarker of maternal stress and reprogramming of CNS gene transcription in development. Proceedings of the National Academy of Sciences of the United States of America *110*, 5169-5174.

Hsieh, C.L., Fei, T., Chen, Y., Li, T., Gao, Y., Wang, X., Sun, T., Sweeney, C.J., Lee, G.S., Chen, S.*, et al.* (2014). Enhancer RNAs participate in androgen receptor-driven looping that selectively enhances gene activation. Proceedings of the National Academy of Sciences of the United States of America *111*, 7319-7324.

Hulsen, T., de Vlieg, J., and Alkema, W. (2008). BioVenn - a web application for the comparison and visualization of biological lists using area-proportional Venn diagrams. BMC Genomics *9*, 488.

Ibata, K., Sun, Q., and Turrigiano, G.G. (2008). Rapid synaptic scaling induced by changes in postsynaptic firing. Neuron *57*, 819-826.

Iftinca, M.C., and Zamponi, G.W. (2009). Regulation of neuronal T-type calcium channels. Trends Pharmacol Sci *30*, 32-40.

IIott, N.E., Heward, J.A., Roux, B., Tsitsiou, E., Fenwick, P.S., Lenzi, L., Goodhead, I., Hertz-Fowler, C., Heger, A., Hall, N.*, et al.* (2014). Long non-coding RNAs and enhancer RNAs regulate the lipopolysaccharide-induced inflammatory response in human monocytes. Nature communications *5*, 3979.

Ionita-Laza, I., Xu, B., Makarov, V., Buxbaum, J.D., Roos, J.L., Gogos, J.A., and Karayiorgou, M. (2014). Scan statistic-based analysis of exome sequencing data identifies FAN1 at 15q13.3 as a susceptibility gene for schizophrenia and autism. Proceedings of the National Academy of Sciences of the United States of America *111*, 343-348.

Jones, J.C., Phatnani, H.P., Haystead, T.A., MacDonald, J.A., Alam, S.M., and Greenleaf, A.L. (2004). C-terminal repeat domain kinase I phosphorylates Ser2 and Ser5 of RNA polymerase II C-terminal domain repeats. The Journal of biological chemistry *279*, 24957-24964.

Joo, J.Y., Schaukowitch, K., Farbiak, L., Kilaru, G., and Kim, T.K. (2015). Stimulus-specific combinatorial functionality of neuronal c-fos enhancers. Nature neuroscience.

Kagey, M.H., Newman, J.J., Bilodeau, S., Zhan, Y., Orlando, D.A., van Berkum, N.L., Ebmeier, C.C., Goossens, J., Rahl, P.B., Levine, S.S., *et al.* (2010). Mediator and cohesin connect gene expression and chromatin architecture. Nature *467*, 430-435.

Kaikkonen, M.U., Spann, N.J., Heinz, S., Romanoski, C.E., Allison, K.A., Stender, J.D., Chun, H.B., Tough, D.F., Prinjha, R.K., Benner, C., *et al.* (2013). Remodeling of the enhancer landscape during macrophage activation is coupled to enhancer transcription. Mol Cell *51*, 310-325.

Kalscheuer, V.M., FitzPatrick, D., Tommerup, N., Bugge, M., Niebuhr, E., Neumann, L.M., Tzschach, A., Shoichet, S.A., Menzel, C., Erdogan, F., *et al.* (2007). Mutations in autism susceptibility candidate 2 (AUTS2) in patients with mental retardation. Hum Genet *121*, 501-509.

Kandel, E.R. (2001). The molecular biology of memory storage: a dialogue between genes and synapses. Science *294*, 1030-1038.

Kavalali, E.T., Klingauf, J., and Tsien, R.W. (1999). Activity-dependent regulation of synaptic clustering in a hippocampal culture system. Proceedings of the National Academy of Sciences of the United States of America *96*, 12893-12900.

Kawashima, T., Okuno, H., Nonaka, M., Adachi-Morishima, A., Kyo, N., Okamura, M., Takemoto-Kimura, S., Worley, P.F., and Bito, H. (2009). Synaptic activity-responsive element in the Arc/Arg3.1 promoter essential for synapse-to-nucleus signaling in activated neurons. Proceedings of the National Academy of Sciences of the United States of America *106*, 316-321.

Kim, T.K., Hemberg, M., Gray, J.M., Costa, A.M., Bear, D.M., Wu, J., Harmin, D.A., Laptewicz, M., Barbara-Haley, K., Kuersten, S., *et al.* (2010). Widespread transcription at neuronal activity-regulated enhancers. Nature *465*, 182-187.

Kim, T.K., and Shiekhattar, R. (2015). Architectural and Functional Commonalities between Enhancers and Promoters. Cell *162*, 948-959.

Kleinjan, D.J., and Coutinho, P. (2009). Cis-ruption mechanisms: disruption of cis-regulatory control as a cause of human genetic disease. Brief Funct Genomic Proteomic *8*, 317-332.

Knoll, B., and Nordheim, A. (2009). Functional versatility of transcription factors in the nervous system: the SRF paradigm. Trends in neurosciences *32*, 432-442.

Korb, E., and Finkbeiner, S. (2011). Arc in synaptic plasticity: from gene to behavior. Trends in neurosciences *34*, 591-598.

Lai, F., Orom, U.A., Cesaroni, M., Beringer, M., Taatjes, D.J., Blobel, G.A., and Shiekhattar, R. (2013). Activating RNAs associate with Mediator to enhance chromatin architecture and transcription. Nature *494*, 497-501.

Lam, M.T., Cho, H., Lesch, H.P., Gosselin, D., Heinz, S., Tanaka-Oishi, Y., Benner, C., Kaikkonen, M.U., Kim, A.S., Kosaka, M.*, et al.* (2013). Rev-Erbs repress macrophage gene expression by inhibiting enhancer-directed transcription. Nature *498*, 511-515.

Lambo, M.E., and Turrigiano, G.G. (2013). Synaptic and intrinsic homeostatic mechanisms cooperate to increase L2/3 pyramidal neuron excitability during a late phase of critical period plasticity. The Journal of neuroscience : the official journal of the Society for Neuroscience *33*, 8810-8819.

Langmead, B., Trapnell, C., Pop, M., and Salzberg, S.L. (2009). Ultrafast and memory-efficient alignment of short DNA sequences to the human genome. Genome Biol *10*, R25.

Latos, P.A., Pauler, F.M., Koerner, M.V., Senergin, H.B., Hudson, Q.J., Stocsits, R.R., Allhoff, W., Stricker, S.H., Klement, R.M., Warczok, K.E.*, et al.* (2012). Airn transcriptional overlap, but not its lncRNA products, induces imprinted Igf2r silencing. Science *338*, 1469-1472.

Lee, K.Y., Royston, S.E., Vest, M.O., Ley, D.J., Lee, S., Bolton, E.C., and Chung, H.J. (2015). N-methyl-D-aspartate receptors mediate activity-dependent down-regulation of potassium channel genes during the expression of homeostatic intrinsic plasticity. Mol Brain *8*, 4.

Lee, S.M., Vasishtha, M., and Prywes, R. (2010). Activation and repression of cellular immediate early genes by serum response factor cofactors. The Journal of biological chemistry *285*, 22036-22049.

Li, W., Notani, D., Ma, Q., Tanasa, B., Nunez, E., Chen, A.Y., Merkurjev, D., Zhang, J., Ohgi, K., Song, X.*, et al.* (2013). Functional roles of enhancer RNAs for oestrogen-dependent transcriptional activation. Nature *498*, 516-520.

Louros, S.R., Hooks, B.M., Litvina, L., Carvalho, A.L., and Chen, C. (2014). A role for stargazin in experience-dependent plasticity. Cell reports *7*, 1614-1625.

Luscher, C., and Malenka, R.C. (2012). NMDA receptor-dependent long-term potentiation and long-term depression (LTP/LTD). Cold Spring Harbor perspectives in biology *4*.

Lyon, M.F. (1961). Gene action in the X-chromosome of the mouse (Mus musculus L.). Nature *190*, 372-373.

Lyons, M.R., and West, A.E. (2011). Mechanisms of specificity in neuronal activity-regulated gene transcription. Prog Neurobiol *94*, 259-295.

Ma, D.K., Jang, M.H., Guo, J.U., Kitabatake, Y., Chang, M.L., Pow-Anpongkul, N., Flavell, R.A., Lu, B., Ming, G.L., and Song, H. (2009). Neuronal activity-induced Gadd45b promotes epigenetic DNA demethylation and adult neurogenesis. Science *323*, 1074-1077.

Maffei, A., and Turrigiano, G.G. (2008). Multiple modes of network homeostasis in visual cortical layer 2/3. The Journal of neuroscience : the official journal of the Society for Neuroscience *28*, 4377-4384.

Malik, A.N., Vierbuchen, T., Hemberg, M., Rubin, A.A., Ling, E., Couch, C.H., Stroud, H., Spiegel, I., Farh, K.K., Harmin, D.A., *et al.* (2014). Genome-wide identification and characterization of functional neuronal activity-dependent enhancers. Nature neuroscience *17*, 1330-1339.

Melo, C.A., Drost, J., Wijchers, P.J., van de Werken, H., de Wit, E., Oude Vrielink, J.A., Elkon, R., Melo, S.A., Leveille, N., Kalluri, R., *et al.* (2013). eRNAs are required for p53-dependent enhancer activity and gene transcription. Mol Cell *49*, 524-535.

Miano, J.M. (2003). Serum response factor: toggling between disparate programs of gene expression. J Mol Cell Cardiol *35*, 577-593.

Missra, A., and Gilmour, D.S. (2010). Interactions between DSIF (DRB sensitivity inducing factor), NELF (negative elongation factor), and the Drosophila RNA polymerase II transcription elongation complex. Proceedings of the National Academy of Sciences of the United States of America *107*, 11301-11306.

Morrow, E.M., Yoo, S.Y., Flavell, S.W., Kim, T.K., Lin, Y., Hill, R.S., Mukaddes, N.M., Balkhy, S., Gascon, G., Hashmi, A., *et al.* (2008). Identifying autism loci and genes by tracing recent shared ancestry. Science *321*, 218-223.

Mousavi, K., Zare, H., Dell'orso, S., Grontved, L., Gutierrez-Cruz, G., Derfoul, A., Hager, G.L., and Sartorelli, V. (2013). eRNAs Promote Transcription by Establishing Chromatin Accessibility at Defined Genomic Loci. Mol Cell.

Nagano, T., Mitchell, J.A., Sanz, L.A., Pauler, F.M., Ferguson-Smith, A.C., Feil, R., and Fraser, P. (2008). The Air noncoding RNA epigenetically silences transcription by targeting G9a to chromatin. Science *322*, 1717-1720.

Nedivi, E., Hevroni, D., Naot, D., Israeli, D., and Citri, Y. (1993). Numerous candidate plasticity-related genes revealed by differential cDNA cloning. Nature *363*, 718-722.

Nguyen, L.S., Kim, H.G., Rosenfeld, J.A., Shen, Y., Gusella, J.F., Lacassie, Y., Layman, L.C., Shaffer, L.G., and Gecz, J. (2013). Contribution of copy number variants involving nonsense-mediated mRNA decay pathway genes to neuro-developmental disorders. Hum Mol Genet *22*, 1816-1825.

Nord, A.S., Blow, M.J., Attanasio, C., Akiyama, J.A., Holt, A., Hosseini, R., Phouanenavong, S., Plajzer-Frick, I., Shoukry, M., Afzal, V.*, et al.* (2013). Rapid and pervasive changes in genome-wide enhancer usage during mammalian development. Cell *155*, 1521-1531.

Orom, U.A., Derrien, T., Beringer, M., Gumireddy, K., Gardini, A., Bussotti, G., Lai, F., Zytnicki, M., Notredame, C., Huang, Q.*, et al.* (2010). Long noncoding RNAs with enhancer-like function in human cells. Cell *143*, 46-58.

Paralkar, V.R., Mishra, T., Luan, J., Yao, Y., Kossenkov, A.V., Anderson, S.M., Dunagin, M., Pimkin, M., Gore, M., Sun, D.*, et al.* (2014). Lineage and species-specific long noncoding RNAs during erythro-megakaryocytic development. Blood *123*, 1927-1937.

Paralkar, V.R., Taborda, C.C., Huang, P., Yao, Y., Kossenkov, A.V., Prasad, R., Luan, J., Davies, J.O., Hughes, J.R., Hardison, R.C.*, et al.* (2016). Unlinking an lncRNA from Its Associated cis Element. Mol Cell *62*, 104-110.

Ploski, J.E., Pierre, V.J., Smucny, J., Park, K., Monsey, M.S., Overeem, K.A., and Schafe, G.E. (2008). The activity-regulated cytoskeletal-associated protein (Arc/Arg3.1) is required for memory consolidation of pavlovian fear conditioning in the lateral amygdala. The Journal of neuroscience : the official journal of the Society for Neuroscience *28*, 12383-12395.

Rajkumar, A.P., Christensen, J.H., Mattheisen, M., Jacobsen, I., Bache, I., Pallesen, J., Grove, J., Qvist, P., McQuillin, A., Gurling, H.M.*, et al.* (2015). Analysis of t(9;17)(q33.2;q25.3)

chromosomal breakpoint regions and genetic association reveals novel candidate genes for bipolar disorder. Bipolar Disord *17*, 205-211.

Ramanan, N., Shen, Y., Sarsfield, S., Lemberger, T., Schutz, G., Linden, D.J., and Ginty, D.D. (2005). SRF mediates activity-induced gene expression and synaptic plasticity but not neuronal viability. Nature neuroscience *8*, 759-767.

Rao, J.N., Neumann, L., Wenzel, S., Schweimer, K., Rosch, P., and Wohrl, B.M. (2006). Structural studies on the RNA-recognition motif of NELF E, a cellular negative transcription elongation factor involved in the regulation of HIV transcription. The Biochemical journal *400*, 449-456.

Rasmussen, E.B., and Lis, J.T. (1993). In vivo transcriptional pausing and cap formation on three Drosophila heat shock genes. Proceedings of the National Academy of Sciences of the United States of America *90*, 7923-7927.

Reese, A.L., and Kavalali, E.T. (2015). Spontaneous neurotransmission signals through store-driven Ca(2+) transients to maintain synaptic homeostasis. Elife *4*.

Rinn, J.L., Kertesz, M., Wang, J.K., Squazzo, S.L., Xu, X., Brugmann, S.A., Goodnough, L.H., Helms, J.A., Farnham, P.J., Segal, E., *et al.* (2007). Functional demarcation of active and silent chromatin domains in human HOX loci by noncoding RNAs. Cell *129*, 1311-1323.

Rodriguez-Gomez, J.A., Levitsky, K.L., and Lopez-Barneo, J. (2012). T-type Ca2+ channels in mouse embryonic stem cells: modulation during cell cycle and contribution to self-renewal. Am J Physiol Cell Physiol *302*, C494-504.

Rougvie, A.E., and Lis, J.T. (1988). The RNA polymerase II molecule at the 5' end of the uninduced hsp70 gene of D. melanogaster is transcriptionally engaged. Cell *54*, 795-804.

Saha, R.N., Wissink, E.M., Bailey, E.R., Zhao, M., Fargo, D.C., Hwang, J.Y., Daigle, K.R., Fenn, J.D., Adelman, K., and Dudek, S.M. (2011). Rapid activity-induced transcription of Arc and other IEGs relies on poised RNA polymerase II. Nature neuroscience *14*, 848-856.

Sanders, A.R., Goring, H.H., Duan, J., Drigalenko, E.I., Moy, W., Freda, J., He, D., Shi, J., Mgs, and Gejman, P.V. (2013). Transcriptome study of differential expression in schizophrenia. Hum Mol Genet *22*, 5001-5014.

Schaukowitch, K., Joo, J.Y., Liu, X., Watts, J.K., Martinez, C., and Kim, T.K. (2014). Enhancer RNA facilitates NELF release from immediate early genes. Mol Cell *56*, 29-42.

Shepherd, J.D., Rumbaugh, G., Wu, J., Chowdhury, S., Plath, N., Kuhl, D., Huganir, R.L., and Worley, P.F. (2006). Arc/Arg3.1 mediates homeostatic synaptic scaling of AMPA receptors. Neuron *52*, 475-484.

Shinkai, T., Ohmori, O., Hori, H., and Nakamura, J. (2002). Allelic association of the neuronal nitric oxide synthase (NOS1) gene with schizophrenia. Mol Psychiatry *7*, 560-563.

Sleutels, F., Zwart, R., and Barlow, D.P. (2002). The non-coding Air RNA is required for silencing autosomal imprinted genes. Nature *415*, 810-813.

Smallwood, A., and Ren, B. (2013). Genome organization and long-range regulation of gene expression by enhancers. Current opinion in cell biology *25*, 387-394.

Splawski, I., Yoo, D.S., Stotz, S.C., Cherry, A., Clapham, D.E., and Keating, M.T. (2006). CACNA1H mutations in autism spectrum disorders. The Journal of biological chemistry *281*, 22085-22091.

Strahl, B.D., and Allis, C.D. (2000). The language of covalent histone modifications. Nature *403*, 41-45.

Sultan, F.A., Wang, J., Tront, J., Liebermann, D.A., and Sweatt, J.D. (2012). Genetic deletion of Gadd45b, a regulator of active DNA demethylation, enhances long-term memory and synaptic plasticity. The Journal of neuroscience : the official journal of the Society for Neuroscience *32*, 17059-17066.

Sultana, R., Yu, C.E., Yu, J., Munson, J., Chen, D., Hua, W., Estes, A., Cortes, F., de la Barra, F., Yu, D*., et al.* (2002). Identification of a novel gene on chromosome 7q11.2 interrupted by a translocation breakpoint in a pair of autistic twins. Genomics *80*, 129-134.

Sun, S., Del Rosario, B.C., Szanto, A., Ogawa, Y., Jeon, Y., and Lee, J.T. (2013). Jpx RNA activates Xist by evicting CTCF. Cell *153*, 1537-1551.

Thomas-Chollier, M., Defrance, M., Medina-Rivera, A., Sand, O., Herrmann, C., Thieffry, D., and van Helden, J. (2011). RSAT 2011: regulatory sequence analysis tools. Nucleic acids research *39*, W86-91.

Tian, D., Sun, S., and Lee, J.T. (2010). The long noncoding RNA, Jpx, is a molecular switch for X chromosome inactivation. Cell *143*, 390-403.

Tolhuis, B., Palstra, R.J., Splinter, E., Grosveld, F., and de Laat, W. (2002). Looping and interaction between hypersensitive sites in the active beta-globin locus. Mol Cell *10*, 1453-1465.

Trapnell, C., Pachter, L., and Salzberg, S.L. (2009). TopHat: discovering splice junctions with RNA-Seq. Bioinformatics *25*, 1105-1111.

Tsai, M.C., Manor, O., Wan, Y., Mosammaparast, N., Wang, J.K., Lan, F., Shi, Y., Segal, E., and Chang, H.Y. (2010). Long noncoding RNA as modular scaffold of histone modification complexes. Science *329*, 689-693.

Tsien, R.W. (1998). Molecular physiology. Key clockwork component cloned. Nature *391*, 839, 841.

Turrigiano, G. (2011). Too many cooks? Intrinsic and synaptic homeostatic mechanisms in cortical circuit refinement. Annu Rev Neurosci *34*, 89-103.

Turrigiano, G.G., Leslie, K.R., Desai, N.S., Rutherford, L.C., and Nelson, S.B. (1998). Activity-dependent scaling of quantal amplitude in neocortical neurons. Nature *391*, 892-896.

Wang, D., Garcia-Bassets, I., Benner, C., Li, W., Su, X., Zhou, Y., Qiu, J., Liu, W., Kaikkonen, M.U., Ohgi, K.A*., et al.* (2011a). Reprogramming transcription by distinct classes of enhancers functionally defined by eRNA. Nature *474*, 390-394.

Wang, H.L., Zhang, Z., Hintze, M., and Chen, L. (2011b). Decrease in calcium concentration triggers neuronal retinoic acid synthesis during homeostatic synaptic plasticity. The Journal of neuroscience : the official journal of the Society for Neuroscience *31*, 17764-17771.

Wang, K.C., Yang, Y.W., Liu, B., Sanyal, A., Corces-Zimmerman, R., Chen, Y., Lajoie, B.R., Protacio, A., Flynn, R.A., Gupta, R.A*., et al.* (2011c). A long noncoding RNA maintains active chromatin to coordinate homeotic gene expression. Nature *472*, 120-124.

Watts, J.K., and Corey, D.R. (2012). Silencing disease genes in the laboratory and the clinic. The Journal of pathology *226*, 365-379.

Waung, M.W., Pfeiffer, B.E., Nosyreva, E.D., Ronesi, J.A., and Huber, K.M. (2008). Rapid translation of Arc/Arg3.1 selectively mediates mGluR-dependent LTD through persistent increases in AMPAR endocytosis rate. Neuron *59*, 84-97.

West, A.E., Griffith, E.C., and Greenberg, M.E. (2002). Regulation of transcription factors by neuronal activity. Nat Rev Neurosci *3*, 921-931.

Wondolowski, J., and Dickman, D. (2013). Emerging links between homeostatic synaptic plasticity and neurological disease. Frontiers in cellular neuroscience *7*, 223.

Wysocka, J., Swigut, T., Milne, T.A., Dou, Y., Zhang, X., Burlingame, A.L., Roeder, R.G., Brivanlou, A.H., and Allis, C.D. (2005). WDR5 associates with histone H3 methylated at K4 and is essential for H3 K4 methylation and vertebrate development. Cell *121*, 859-872.

Yamaguchi, Y., Inukai, N., Narita, T., Wada, T., and Handa, H. (2002). Evidence that negative elongation factor represses transcription elongation through binding to a DRB sensitivity-inducing factor/RNA polymerase II complex and RNA. Molecular and cellular biology *22*, 2918-2927.

Yu, H., Su, Y., Shin, J., Zhong, C., Guo, J.U., Weng, Y.L., Gao, F., Geschwind, D.H., Coppola, G., Ming, G.L.*, et al.* (2015). Tet3 regulates synaptic transmission and homeostatic plasticity via DNA oxidation and repair. Nature neuroscience *18*, 836-843.

Zhao, J., Sun, B.K., Erwin, J.A., Song, J.J., and Lee, J.T. (2008). Polycomb proteins targeted by a short repeat RNA to the mouse X chromosome. Science *322*, 750-756.

Zhao, Y., Wang, L., Ren, S., Wang, L., Blackburn, P.R., McNulty, M.S., Gao, X., Qiao, M., Vessella, R.L., Kohli, M.*, et al.* (2016). Activation of P-TEFb by Androgen Receptor-Regulated Enhancer RNAs in Castration-Resistant Prostate Cancer. Cell reports *15*, 599-610.